Journal of Asian Earth Sciences 137 (2017) 109–140

Contents lists available at ScienceDirect

Journal of Asian Earth Sciences

journal homepage: www.elsevier.com/locate/jseaes

Full length article

Genetic types, mineralization styles, and geodynamic settings of Mesozoic tungsten deposits in South China

Wen Winston Zhao [a], Mei-Fu Zhou [a], Yan Hei Martin Li [a], Zheng Zhao [b,*], Jian-Feng Gao [c]

[a] Department of Earth Sciences, The University of Hong Kong, Pokfulam Road, Hong Kong, China
[b] MLR Key Laboratory of Metallogeny and Mineral Assessment, Institute of Mineral Resources, Chinese Academy of Geological Sciences, Beijing 100037, China
[c] State Key Laboratory of Ore Deposit Geochemistry, Institute of Geochemistry, Chinese Academy of Sciences, Guiyang 550081, China

ARTICLE INFO

Article history:
Received 9 September 2016
Received in revised form 28 December 2016
Accepted 29 December 2016
Available online 6 January 2017

Keywords:
South China
Tungsten mineralization
Mesozoic
Paleo-Pacific subduction
Geodynamic model

ABSTRACT

South China hosts the most abundant and largest tungsten (W) deposits in the world, being a famous W metallogenic region. Located at the eastern part of the South China Block, which was formed by amalgamation of the Yangtze and Cathaysia Blocks during the Neoproterozoic, these W deposits were mainly formed during the Mesozoic. The W mineralization is dominanted by greisen, quartz-vein, skarn, and porphyry types, all of which are genetically related to the evolution of highly fractionated granitoids. Four episodes of W mineralization are recognized: (1) Late Triassic (230–210 Ma) in the central and western parts of South China; (2) Middle Jurassic (ca. 170 Ma) to Early Cretaceous (ca. 140 Ma) in the interior of South China, with the mineralization being concentrated in southern Jiangxi Province between 165 and 150 Ma; (3) Early Cretaceous (136–120 Ma) with deposits across South China; and (4) Late Cretaceous (100–80 Ma) mainly in the southwestern parts of South China. These four periods of mineralization are closely related to the closure of paleo-Tethys and subduction of the paleo-Pacific plate. In the Late Triassic, these two events caused local extensional environments, facilitating emplacement of the peraluminous granitoids, and formation of the W deposits. In the Middle Jurassic, break-off of the subducting oceanic plate resulted in emplacement of highly fractionated granites in the Nanling region. Later anticlockwise rotation of the paleo-Pacific plate created widespread S-type granitoids and associated Middle Jurassic to Early Cretaceous W mineralization in the interior of South China. Since 136 Ma, rollback of the subducting Pacific plate resulted in weak W mineralization across South China. Finally, a change of direction in the retreating plate from SE to ESE resulted in intensive mineralization of the southwestern part of South China.

1. Introduction

Tungsten (W) is a rare metal, which is widely used in filaments, electrodes, projectiles, catalysts, and radiation shielding. Important W ore minerals are wolframite and scheelite, which occur in a variety of hydrothermal ore deposits. Globally, every continent in the world has W deposits, but the majority occur on both sides of the Pacific Ocean; for example, Mactung and Cantung in Canada, McCullough Butte in the United States, Chicto Grande in Bolivia, King Island in Australia, Sangdong in Korea and numerous deposits in China (Fig. 1) (Barton, 1987; Bowman et al., 1985; Černý et al., 2005; Dick and Hodgson, 1982; Einaudi et al., 1981; Klepper, 1947; Kwak, 1978; Kwak and Tan, 1981; Meinert et al., 2005; Newberry, 1998; Sheng et al., 2015; Yong, 1963).

According to USGS statistics, the world's W reserves are about 3.1 million tons (Mt), and China contains more than 60% of the total (Sheng et al., 2015). Tungsten resources have been identified in 23 provinces in China, including Northeast China (e.g., the Shilizi and Tiegongshan deposits in Jilin, Gongpengzi, Yangbishan, and Cuihongshan deposits in Heilongjiang, and Wurinitu and Shamai deposits in Inner Mongolia), North China (e.g., the Nannihu, and Yechangping deposits in Henan), West China (e.g., the Taergou deposit in Gansu, Dongqiyishan deposit in Inner Mongolia, Baishitou and Kekekaerde deposits in Xinjiang, and Yulong and Nuri deposits in Tibet), and South China (e.g., the Nanyangtian deposit in Yunnan, Shizhuyuan deposit in Hunan, and Xihuashan deposit in Jiangxi) (Fig. 2) (Chen et al., 2012b; Feng et al., 2013, 2011c; Hu and Zhou, 2012; Jiang et al., 2016; Li et al., 2004b; Liu et al., 2011; Lu et al., 2003; Mao et al., 2011a, 2013a; McKee et al., 1987; Nie and Jiang, 2011; Shao et al., 2011; Sheng et al., 2015; Tang et al., 2009; Zaw et al., 2007; Zhang et al., 2002). Among these

* Corresponding author.
E-mail address: kevin8572@hotmail.com (Z. Zhao).

http://dx.doi.org/10.1016/j.jseaes.2016.12.047
1367-9120/

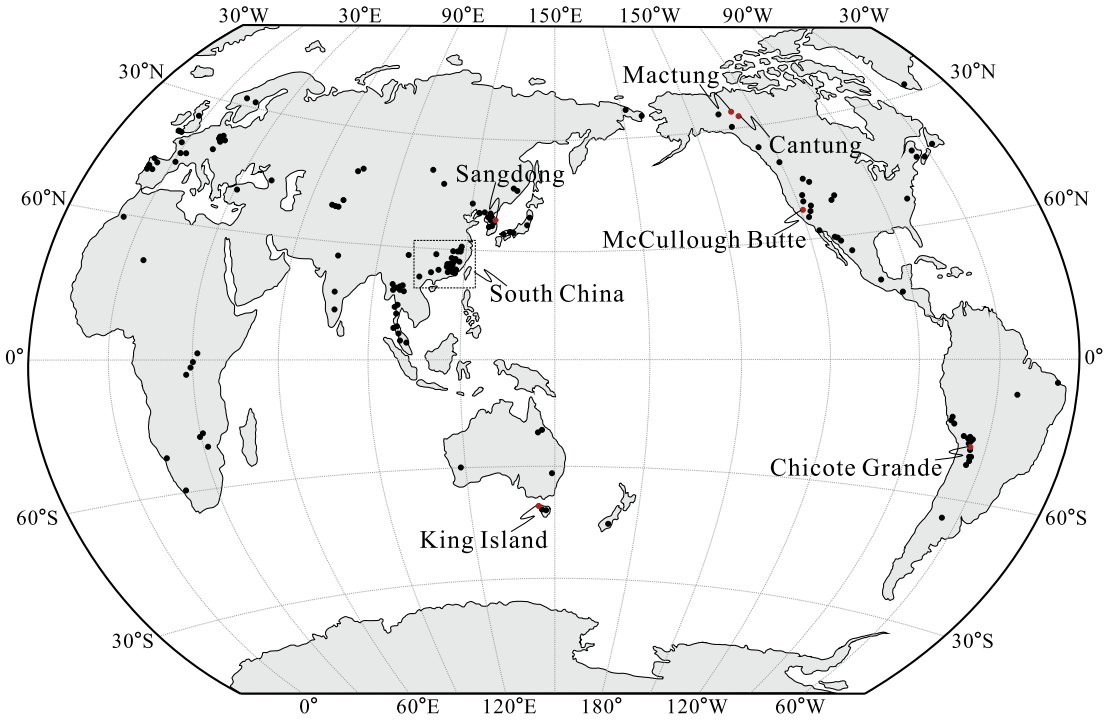

Fig. 1. Distribution of W deposits in the world, modified after Sheng et al. (2015).

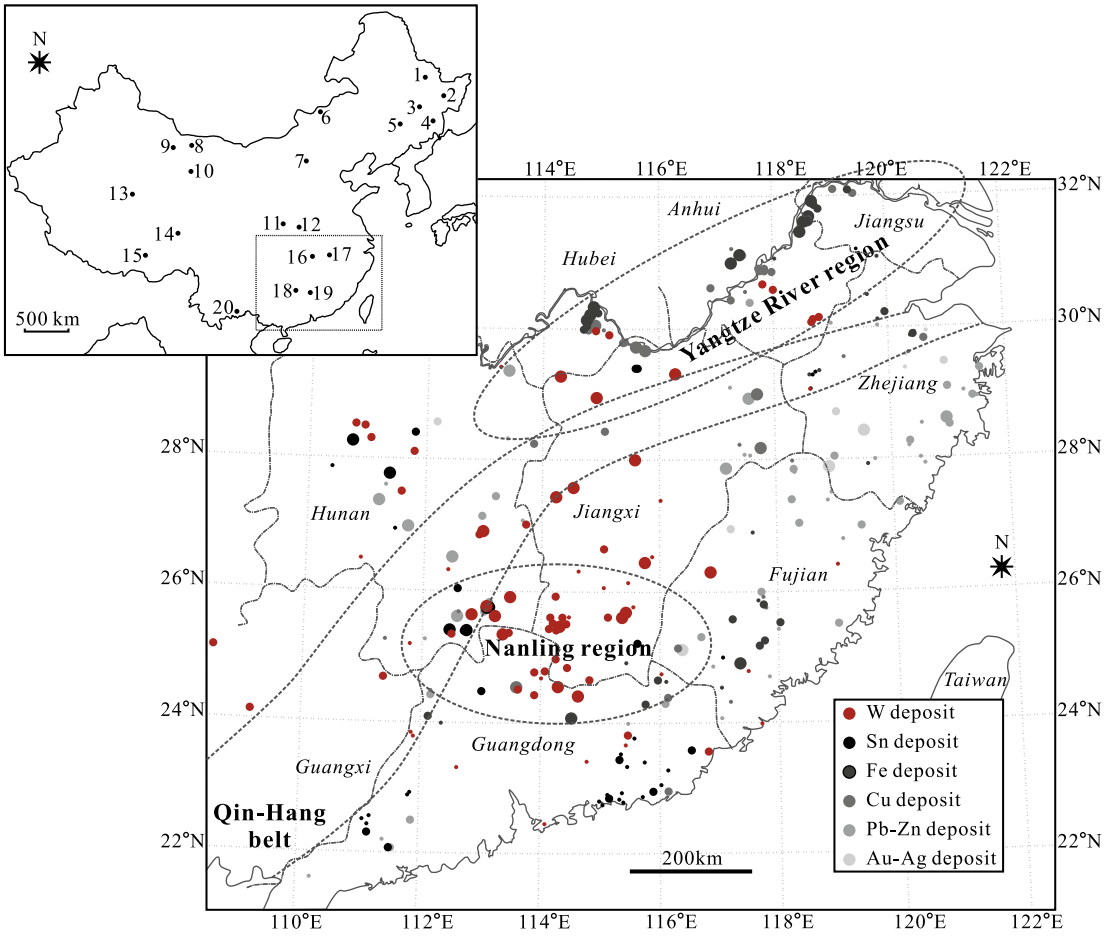

Fig. 2. Simplified map showing the distribution of W deposits and other metal mineralization in South China. The inserted map showing some main tungsten deposits in China. 1-Cuihongshan; 2-Yangbishan; 3-Gongpengzi; 4-Shilizi; 5-Tiegongshan; 6-Shamai; 7-Wurinitu; 8-Dongqiyishan; 9-Baishitou; 10-Taergou; 11-Yechangping; 12-Nannihu; 13-Kekekaerde; 14-Yulong; 15-Nuri; 16-Dahutang; 17-Zhuxi; 18-Shizhuyuan; 19-Xihuashan; 20-Nanyangtian.

districts, the eastern part of South China, including Hunan, Jiangxi, Guangdong, Fujian, Zhejiang, and parts of Guangxi, Anhui, Hubei, and Jiangsu Provinces, accounts for about 70% of the country's total and around 45% of the world's total. It makes South China the world's largest W metallogenic province. Traditionally, the W mineralization was thought to be concentrated in the Nanling region of central South China (Fig. 2). However, recent discoveries of super-large deposits, such as the Dahutang and Zhuxi deposits in northern Jiangxi Province (Chen et al., 2012a; Huang and Jiang, 2014; Mao et al., 2013b, 2015; Yao et al., 2016), have been discovered in the Yangtze River region of northeastern South China (Fig. 2), which has greatly increased the W reserves in the country. It is timely to review the existing literature and to provide a better understanding of the giant mineralization event in this region.

Numerous models have been proposed to relate the giant mineralization event of South China with the collision of the South China and Indochina Blocks in the Triassic and the subduction of the paleo-Pacific plate dominated in the Jurassic (e.g., Cai and Zhang, 2009; Charvet et al., 1994; Chen et al., 2004; Chen et al., 2008a; Chen et al., 2008b; Chu et al., 2012; Cui et al., 2013; Li et al., 2014a; Li et al., 2007; Li et al., 2014b; Li and Li, 2007; Li et al., 2012d, 2014c; Liu et al., 2012a, 2012b; Mao et al., 2013a; Sun et al., 2007; Sun et al., 2012; Wang et al., 2011a; Wang et al., 2013c; Zhou and Li, 2000; Zhou et al., 2006). However, most proposed models fail to explain the vast metallogenesis between the Nanling region and the Yangtze River region, especially W mineralization, in the Mesozoic of South China.

On the basis of field investigations, integrated with published literature and exploration reports, in this paper, we review the genetic types, mineralization styles, and geodynamic settings of the Mesozoic W mineralization in South China. Our ultimate objective is to propose a new geodynamic model in which the giant W metallogenic province was formed.

2. Geological background

The South China Block, separated from the North China Block by the Qinling-Dabie Orogenic Belt, is bounded to the northwest and southwest by the Tibetan Plateau and the Indochina Block (Fig. 3). The South China Block is composed of the Yangtze Block to the northwest and the Cathaysia Block to the southeast, which were welded together along the Jiangnan Orogenic Belt at 880–860 Ma, or ca. 830 Ma, or slightly later (Li et al., 2009b; Wang et al., 2013a, 2012a; Zhang et al., 2012; Zhao, 2015; Zhao et al., 2011).

The basement of the Yangtze Block is represented by the Paleo- to Neoarchean Kongling Complex exposed in the northern part (Gao et al., 2011; Qiu et al., 2000; Zhang et al., 2006a). Subsequently following a regional metamorphism at ca. 2.0–1.8 Ga (Wang et al., 2016b; Yin et al., 2013), rift related magmatism and sedimenation, represented by the Dahongshan, Dongchuan and Hekou groups as well as associated Fe-Cu mineral deposits, were extensive in the southwestern Yangtze Block since ca. 1.7 Ga and then are overlain by the Meosproterozoic volcanic-sedimentary sequences of the Kuiyang, Huili and Julin Groups (Chen et al., 2013b; Wang and Zhou, 2014; Zhao et al., 2010; Zhou et al., 2014). Thick Neoproterozoic sedimentary successions, such as the Sibao Group and its equivalents and the overlying Nanhua sequences, are largely developed along the southeastern margin, while a few outcrops of such units, termed the Yanbian, Xixiang and Machaoyuan Groups, are exposed in the western and northern margins of the Yangtze Block (Sun et al., 2008; Wang and Li, 2003; Wang et al., 2012a; Yan et al., 2015). Neoproterozoic granitoids are widely emplaced and distributed along the margins of the Yangtze Block, whereas the petrogenesis and tectonic affinity of these igneous rocks are highly debated (Li et al., 2003; Wang et al., 2013b; Zhao et al., 2013; Zheng et al., 2008; Zhou et al., 2002, 2014). The sedimentary cover of the Yangtze Block consists mainly of folded Paleozoic and Early Mesozoic strata of shallow marine origin and Jurassic, Cretaceous, and Cenozoic strata of continental facies (Yan et al., 2003).

The Cathaysia Block has a more complicated evolutional history with several separated Proterozoic basement units in the east, west, and south part. The Paleoproterozoic (1890–1830 Ma) granitoids and the Badu Complex in the Wuyishan area, southern Zhejiang and the Fujian Province currently are the oldest rocks exposed in the Cathaysia Block (Liu et al., 2009; Xia et al., 2012; Yu et al., 2009, 2012a; Zhao et al., 2015a). Mesoproterozoic rocks, represented by the volcaniclastic sequences of the Baoban and Shilu Groups (ca. 1.44–1.43 Ga) (Li et al., 2008c; Long et al., 2005; Xu et al., 2007), predominately crop out in the Hainan Island. Neoproterozoic volcano-sedimentary rocks, termed the Mamianshan, Mayuan and Louziba Groups in the Wuyishan area, the Chencai and Longquan Groups in the Chencai-Badu area, and the Yunkai Group in the Yunkai area, are mainly composed of the greenschist facies metamorphosed schist, shale and siltstone (Li et al., 2010b; Shu et al., 2011; Wan et al., 2007).

The Devonian to Early Permian carbonate rocks developed extensively in both the Yangtze and Cathaysia Blocks, indicating a relatively stable environment in the South China Block. Littoral Triassic clastic and carbonatic rocks primarily occur in the western Yangtze Block. In the southeastern coastal region, northwest-trending Middle to Late Jurassic thrust faults, folds, and nappes extensively developed towards the interior of the South China up to several hundred kilometers, together with northwest-trending linear Middle to Late Jurassic volcanic basins (Mao et al., 2013a). Most of these Cretaceous basins, distributed along the southeastern coastal region, are filled with the Late Cretaceous andesitic-dacitic volcanic rocks and red bed strata (Zhou et al., 2006).

A profound feature of South China is the giant Mesozoic igneous province, which forms a swath more than 1300 km wide across the whole Cathaysia Block and the eastern part of the Yangtze Block (Li and Li, 2007). Granitic rocks include I-, S-, and A-types, and the A-type granites generally occur along regional and local fault zones in the eastern part of South China.

Triassic magmatism produced voluminous granitic plutons in South China, particularly in Hunan, Jiangxi, and Guangxi Provinces (Chen and Jahn, 1998) (Fig. 4). The granitic rocks have a wide range of ages from ca. 260 to 200 Ma (Zhou et al., 2006). The Jurassic igneous rocks include 180–170-Ma, bimodal volcanic rocks in southern Hunan, southern Jiangxi, and southwestern Fujian Provinces, aluminous A-type granites in southern Jiangxi Province, and granodiorites in southeastern Hunan and northeastern Jiangxi Provinces (Sun, 2006; Zhou et al., 2006) (Fig. 4). A group of dominantly 165–150-Ma granitic rocks is widespread in the Nanling and adjacent regions. These are biotite and two-mica granites associated with minor amounts of granodiorite, A-type granite and potassic syenite. The Middle-Jurassic A-type granites are constrained by the Shannan-Xunwu fault in southern Hunan and southern Jiangxi Provinces. Basaltic rocks and rhyolites are locally associated with A-type granites (Zhou et al., 2006). Early Cretaceous (145–125 Ma) granitic rocks are widespread in the region around the Middle-Lower Yangtze River region (Fig. 4). They consist of diorite, quartz diorite, monzodiorite, and granodiorite similar to I-type granitoids. The late Cretaceous (110–85 Ma) granitic rocks consist mainly of biotite granite in the western Nanling region and of felsic volcanic rocks in the coastal region of the Cathaysia Block. The Cretaceous A-type granites in Fujian and Zhejiang Provinces were emplaced along the NE-trending Changle-Nan'ao fault zone.

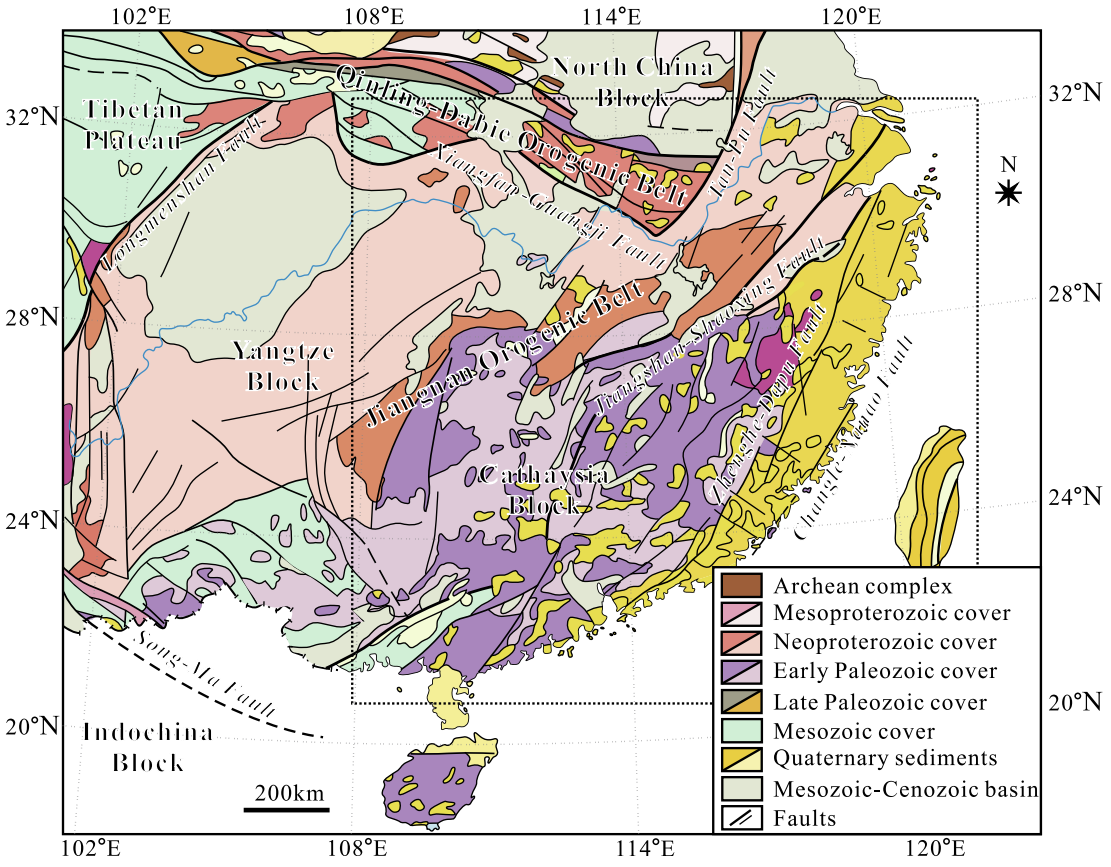

Fig. 3. Simplified geological map showing the cover sequences and basement complexes of South China, modified after Mao et al. (2011a).

3. Deposits in the Nanling and adjacent regions

The Nanling region (110.5–116.5°E, 23.5–26.5°N) includes southern Jiangxi, southern Hunan, northern Guangdong, and eastern Guangxi Provinces (Zhou et al., 2006). The oldest sedimentary rocks are Sinian to Silurian clastic sedimentary and weakly metamorphosed strata that form an abyssal flysch deposit more than 10,000 m thick. The cover sequence is composed of littoral, neritic and terrestrial sedimentary deposits, including carbonates, marls and clastic rocks. Late Jurassic to Cretaceous sedimentary rocks are sandstones and red beds that fill grabens. Granitoid plutons, spatially coexisting with minor gabbrodiorites, are distributed in three E-W-striking belts representing three fault systems (Zhou et al., 2006). Middle Jurassic volcanic rocks with a narrow age range of 180 to 170 Ma are preserved mainly in southern Jiangxi, southern Hunan and southwestern Fujian Provinces, with a few in northern Guangdong Province (Fig. 4) (Chen et al., 2002). These are chiefly basalts and rhyolites that form bimodal magmatic assemblages (Zhou et al., 2006). In this region, the E-W-trending faults and folds are offset by NNW-trending faults.

Closely associated with the vast magmatism, huge numbers of mineral deposits of various metals and generic types have formed during Mesozoic period (Hu and Zhou, 2012; Hua et al., 2005; Mao et al., 2011a, 2013a; Sun et al., 2012; Wang et al., 2011a; Zaw et al., 2007; Zhao and Zhou, 2015). The region serves as one of the most important global W production centres, with numerous super-large and large tungsten deposits across southern Hunan, southern Jiangxi, and northern Guangdong Provinces (Fig. 5). We will hereby present several representative deposits, including the Shizhuyuan skarn W-polymetallic deposit, Tiemuli skarn Fe-W deposit, Baoshan skarn W-polymetallic deposit, Xihuashan quartz-vein W deposit and Xingluokeng porphyry W-Mo deposit, based on a combination of our new results with previous data.

The Shizhuyuan skarn W-polymetallic deposit, in southern Hunan Province, is one of the most famous and significant deposits. It has reserves of 800,000 t WO_3; 486,000 t Sn; 200,000 t Mo and 100,000 t Bi with average grades of 0.35% WO_3, 0.36% Sn, 0.07% Mo, and 0.17% Bi (Lu et al., 2003). The deposit is hosted in the Devonian siliceous limestone and genetically related to Qianlishan granite (Fig. 6). According to Wang et al. (1987) and Lu et al. (2003), four main phases of intrusions have been observed in the Qianlishan granite (Fig. 6): fine-grained porphyritic biotite granite (182–187 Ma, granite 1), medium-grained biotite-K feldspar granite (158–163 Ma, granite 2), fine-grained biotite and K-feldspar granite (granite 3) and granitic porphyry (144–146 Ma, granite 4) (Li et al., 2004a; Liu et al., 1997; Mao et al., 1995; Yin et al., 2002). A late-stage diabase (142 Ma) has also been found in the region (Lu et al., 2003). Major ore minerals in this deposit are scheelite, wolframite, molybdenite, bismuthinite and cassiterite, and gangue minerals are composed of garnet, pyroxene, quartz, wollastonite, idocrase, muscovite, biotite, fluorite, topaz and chlorite. The skarns exhibit mineral zonation, passing outward from garnet, garnet + pyroxene and pyroxene + garnet + idocrase to idocrase + wollastonite (Lu et al., 2003; Yin et al., 2000). Strong greisenization, sericitization, chloritization, silicification, chloritization, carbonatization are observed in both the intrusion and the wall rocks; sericitization is dominant in the upper part of the intrusion. In general, the mineralization is mostly related to granite 1 and 2. Stage 1 mineralization of massive skarn W -Mo-Bi-Sn, massive greisen W-Sn and stockwork Sn-Be is temporally and spatially related to granite 1, whereas stage 2 mineralization of stockwork, vein and greisen W-Sn-Mo-Bi is associated with the intrusion of

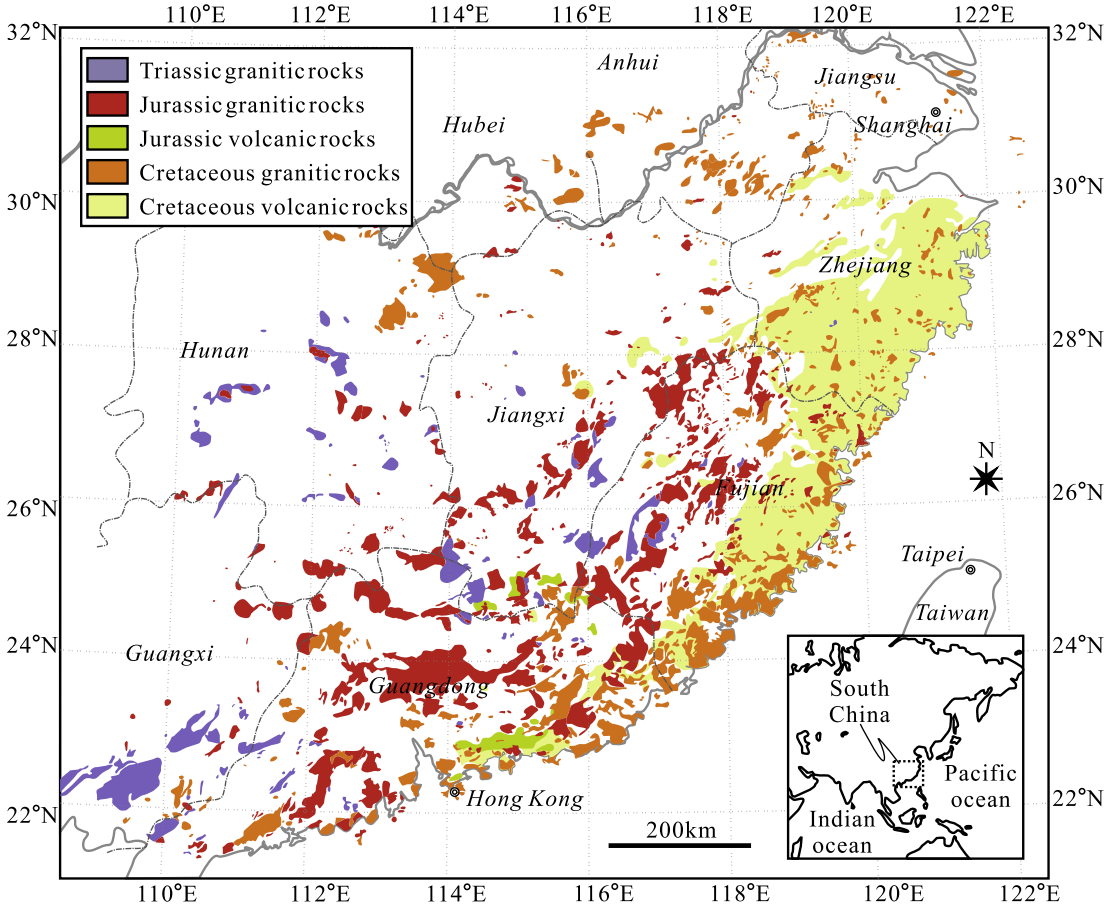

Fig. 4. Simplified map showing the distribution of Mesozoic granite-volcanic rocks in South China, modified after Sun (2006).

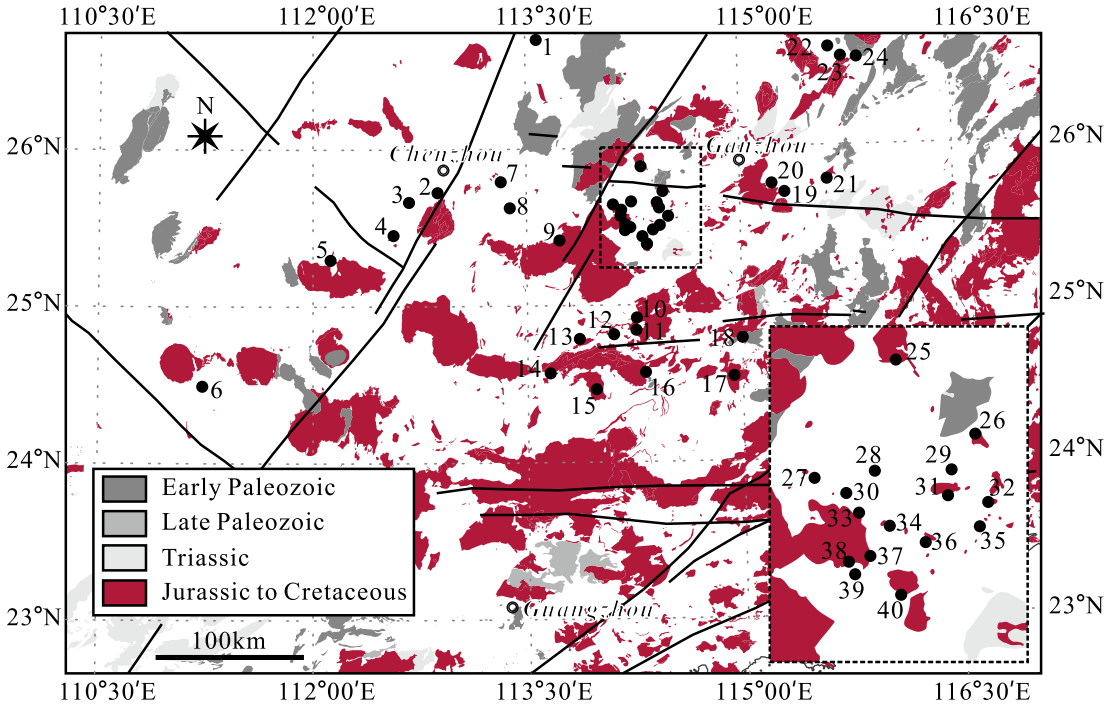

Fig. 5. Geology of the Nanling region and distribution of W deposits. The inserted map shows the W deposits distribution in the Chongyi-Dayu-Shangyou Ore Cluster. 1-Xitian; 2-Xitianling; 3-Huangshaping; 4-Xianghuapu; 5-Da'ao; 6-Shanhu; 7-Shizhuyuang; 8-Yaogangxian; 9-Baiyunxian; 10-Shigushan; 11-Meiziwo; 12-Shirenzheng; 13-Yaoling; 14-Dabaoshan; 15-Hongling; 16-Dajishan; 17-Jubankeng; 18-Guimeishan; 19-Pangushan; 20-Anqiantan; 21-Huangsha; 22-Zhangjiadi; 23-Lijiazhuang; 24-Huameiao; 25-Jiaoli; 26-Yaolanzhai; 27-Xianetang; 28-Taoxikeng; 29-Maoping; 30-Keshuling; 31-Baixiannao; 32-Niuling; 33-Tiemuli; 34-Baoshan; 35-Zhangdou; 36-Piaotang; 37-Hongshuizhai; 38-Jiulongnao; 39-Zhangdongkeng; 40-Xihuashan.

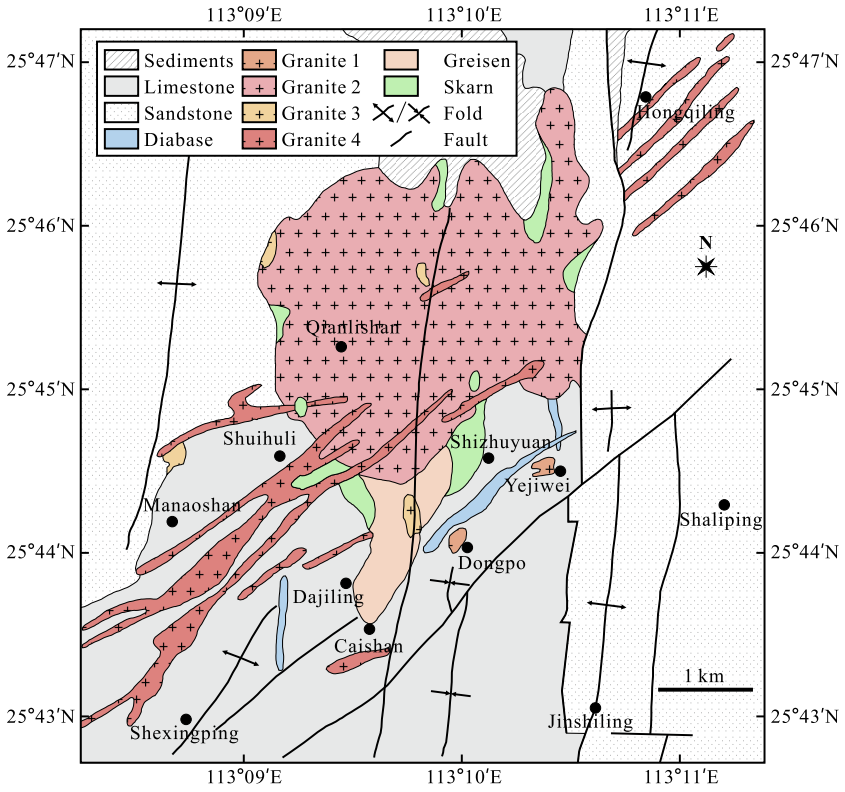

Fig. 6. Geological map of the Shizhuyuan W deposit, modified after Wang et al. (1987) and Lu et al. (2003).

granite 2 (Lu et al., 2003; Mao et al., 1996). Distal Pb-Zn mineralization also occurs in the deposit (Mao et al., 1996, 1998). Homogenization temperatures of fluid inclusions in the skarn minerals range from 350° to 535 °C, whereas the homogenization temperatures of fluid inclusions in greisen and stockwork are lower than those in skarn, ranging from 200° to 360 °C (Lu et al., 2003). The two types of fluids associated with the massive skarn and greisen, have salinities from 26 to 41 wt.% NaCl equiv. and from 1 to 21 wt. % NaCl equiv., respectively (Lu et al., 2003). Helium and Ar isotopic data for pyrite suggest that mantle components contributed to the ore-forming fluids (Wu et al., 2011). Various types of isotopic dating indicate that the deposit was formed at around 150 Ma (Li et al., 1996, 2004a; Wang et al., 2016a; Yin et al., 2002).

The Tiemuli skarn W-Fe deposit is one of numerous bodies in the Congyi-Dayu-Shangyou ore cluster in southern Jiangxi Province. Upper Cambrian to Middle Devonian sedimentary strata are widespread across the area, including Ordovician sandy slate, carboneous slate and siliceous slate and Devonian sandstone and quartz-rich shale that are the dominant host rocks of the deposit. Medium- to fine-grained biotite granite and porphyritic biotite granite are mainly observed northwest of the mine and are believed to be closely associated with the skarn mineralization. Syenite porphyry and volcanic breccia are also present at the mine site. The orebodies generally occur in stratabound, stratiform and lenticular shapes at the contact zone between the porphyritic biotite granite and marble of the exo-skarn. Wallrock alteration, includes silicification, chloritization, carbonatization, sericitization and brecciation. The skarn minerals are garnet, pyroxene, epidote and wollastonite (Fig. 7a), and the ore minerals are magnetite, scheelite, pyrite, pyrrhotite and arsenopyrite (Fig. 7b). Preliminary dating results show that this deposit formed in the Early Cretaceous (ca. 138 Ma; Lu Lin, personal communication).

The Baoshan skarn W-polymetallic deposit is also located in the Congyi-Dayu-Shangyou ore cluster, southern Jiangxi Province. The deposit contains about 40,000 t WO_3 accompanied by economic concentrations of Zn, Cu, and Ag, making it one of the most important polymetallic W skarns in the region (Xu et al., 2008). The orebodies are located along the contacts between the Carboniferous Huanglong and Chuanshan Formations and the Mesozoic Baoshan granites (Fig. 8). These formations are composed mainly of limestone, and sandwiched between sandstone and siltstone of the Lower Carboniferous and Permian. The Baoshan granites, which generally comprise equigranular and porphyritic facies with S-type compositions, were emplaced at ca. 160 Ma (Guo, 2010). The most important fault in the area, the northeastern-trending, strike-slip Tongtianyan Fault, cuts the Carboniferous and Permian strata and the Mesozoic granites. The deposit has been subdivided into four ore zones: the Western, Northern, Eastern, and Southern zones (Fig. 8a). The most important of these zones, the Eastern Ore Zone, is currently the main mining site. In this zone, the mineralized skarns are best developed, both horizontally and vertically, where the contacts between the granites and marble define embayments in the granites; they are most weakly developed where they define salient (Fig. 8b). Skarns in the embayments are usually several meters wide. They are dominated by anhydrous prograde mineral assemblages, and are zoned outwards mineralogically from coarse-grained garnet adjacent to the granite (Fig. 9a), through garnet-pyroxene and fine-grained pyroxene (Fig. 9b), to minor wollastonite (±vesuvianite) adjacent to the marble. Retrograde skarn assemblages, including hydrous silicates, such as amphibole, epidote and chlorite and sulfides, such as chalcopyrite, pyrrhotite, sphalerite and molybdenite, replaced the margins of the prograde skarn minerals, and occur in interstices among these minerals and in veins. Native silver that formed late in the retrograde stage is associated with Bi-bearing minerals. The most scheelite-rich rocks are pyroxene skarns overprinted by retrograde skarns (Fig. 9c). Usually, scheelite is fractured (Fig. 9d), and along the fractures, it is filled by fluid inclusions and molybdenite

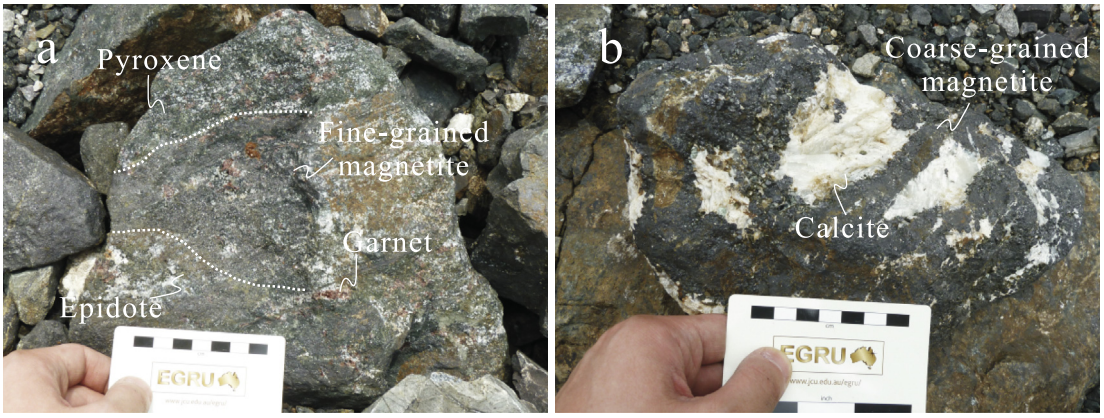

Fig. 7. (a) Scheelite-bearing garnet-pyroxene skarn; (b) Magnetite ores, in the Tengmuli deposit.

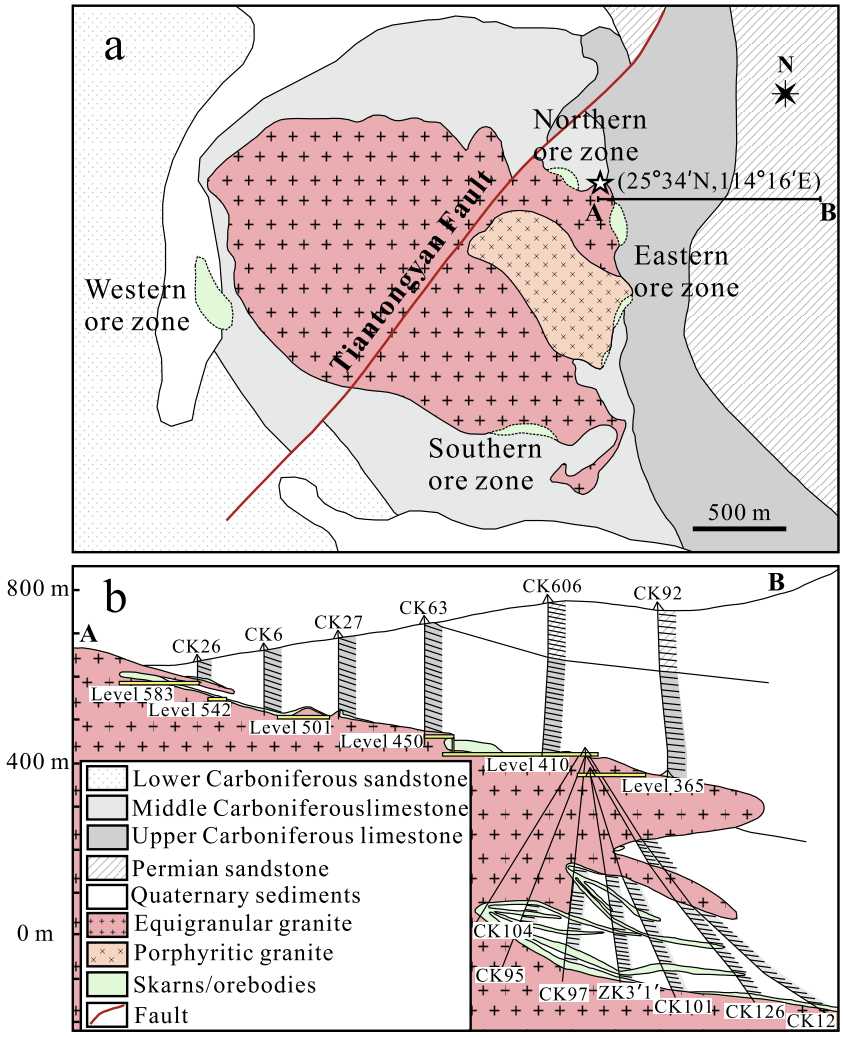

Fig. 8. Geological map of the Baoshan W deposit.

(Fig. 9e). Generally, scheelite shows Mo-poor and Mo-enriched domains under scanning electron microscope (Fig. 9f). Re-Os isochron dating of molybdenite gives an isochron age of 164.2 ± 2.6 Ma (Fig. 10a) and a weighted average age of 163.05 ± 0.93 Ma (Fig. 10b) for the mineralization (Table 1).

The Xihuashan vein-type W deposit is located in the central Nanling region. In the Xihuashan mining district, the Cambrian meta-sandstone and slate are intruded by a Mesozoic granite pluton. This pluton is a polyphase body composed of coarse-grained, medium-grained and medium- to fine-grained porphyritic biotite granites (Fig. 11), with high SiO_2, Al_2O_3 and total alkali contents (Guo et al., 2012; Le Bel et al., 1984; Maruéjol et al., 1990; McKee et al., 1987; Shen et al., 1994; Wang et al., 2003; Xiao et al., 2009; Yang et al., 2012). Accordingly, these granites are

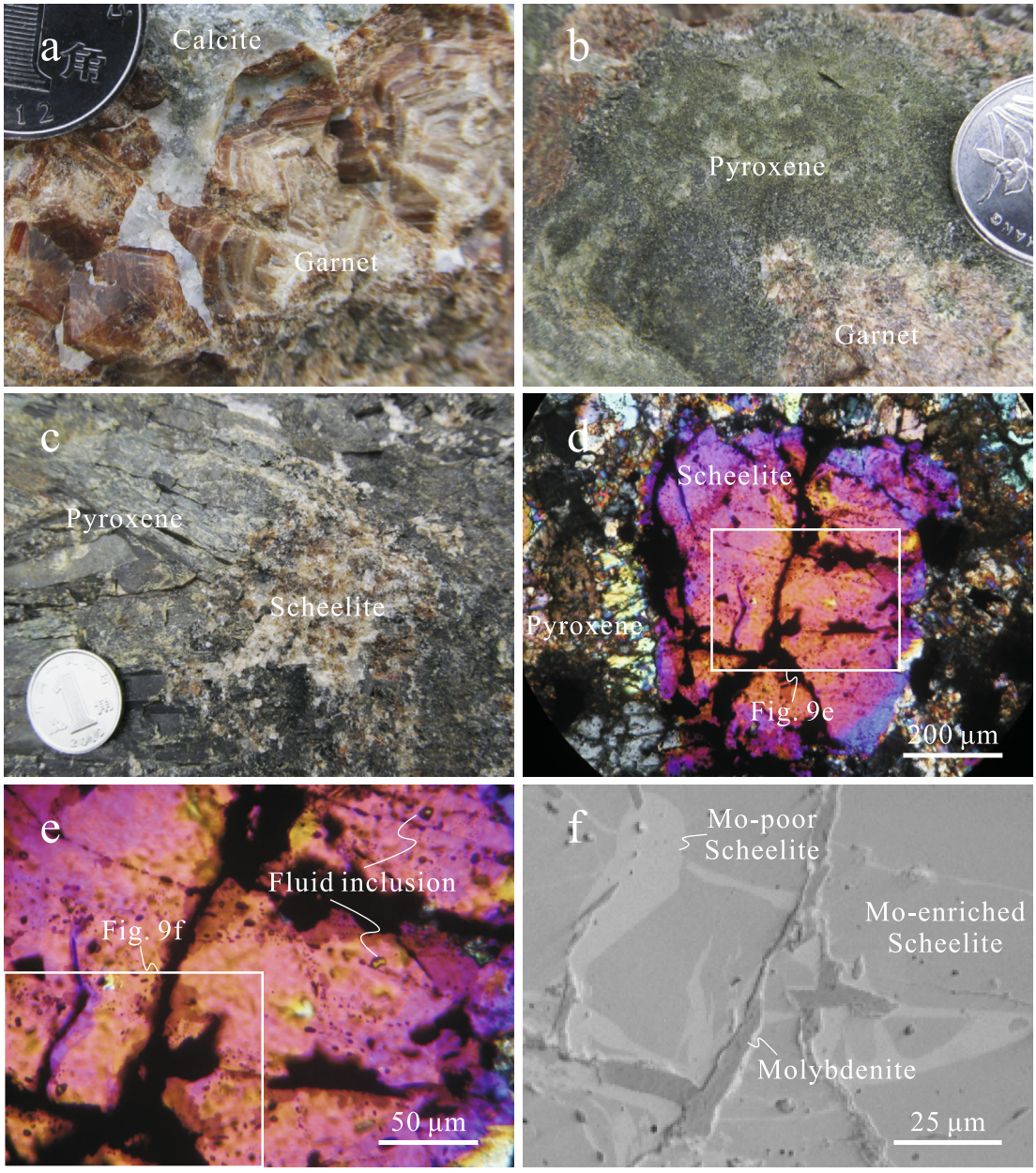

Fig. 9. (a) Coarse-grained zoned granet; **b**: Garnet-pyroxene skarn; **c**: Scheelite-bearing pyroxene skarn; **d**: Scheelite gran in pyroxene skarn under optical microscope; **e**: Fluid inclusions in scheelite; **f**: fractured and zoned scheelites under scanning electron microscope, in the Baoshan deposit.

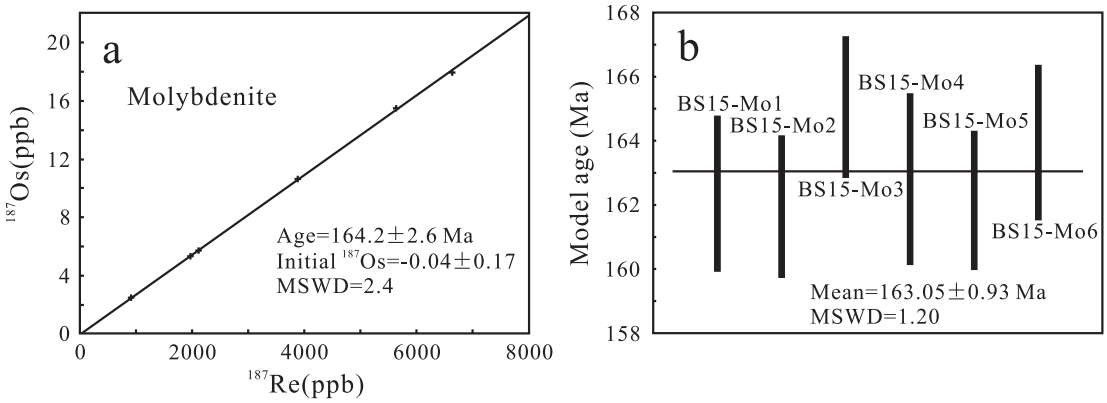

Fig. 10. (a) Molybdenite Re/Os isochron age of the Baoshan deposit; **b**: Molybdenite Re/Os average-weighted age of the Baoshan deposit.

Table 1
Re-Os isotope compositions of molybdenite from the Baoshan W deposit.

Sample no.	Weight (g)	Re (ng/g)		Normal Os (ng/g)		^{187}Re (ng/g)		^{187}Os (ng/g)		Model age (Ma)	
		Measured	2σ	Measured	2σ	Measured	2σ	Measured	2σ	Measured	2σ
BS15-Mo1	0.04001	10,539	95	0.2224	0.0201	6624	59	17.940	0.119	162.4	2.4
BS15-Mo2	0.01510	3128	21	0.0390	0.0099	1966	13	5.312	0.036	161.9	2.2
BS15-Mo3	0.01510	8958	58	1.2316	0.0242	5630	37	15.504	0.094	165.1	2.2
BS15-Mo4	0.01539	1442	16	0.0459	0.0080	906	10	2.462	0.017	162.8	2.7
BS15-Mo5	0.01905	3362	22	0.1923	0.0121	2113	14	5.715	0.035	162.1	2.1
BS15-Mo6	0.01930	6177	53	0.3628	0.0074	3882	33	10.618	0.071	163.9	2.4

Note: Uncertainty for the calculated ages is 1.02% at the 95% confidence level.

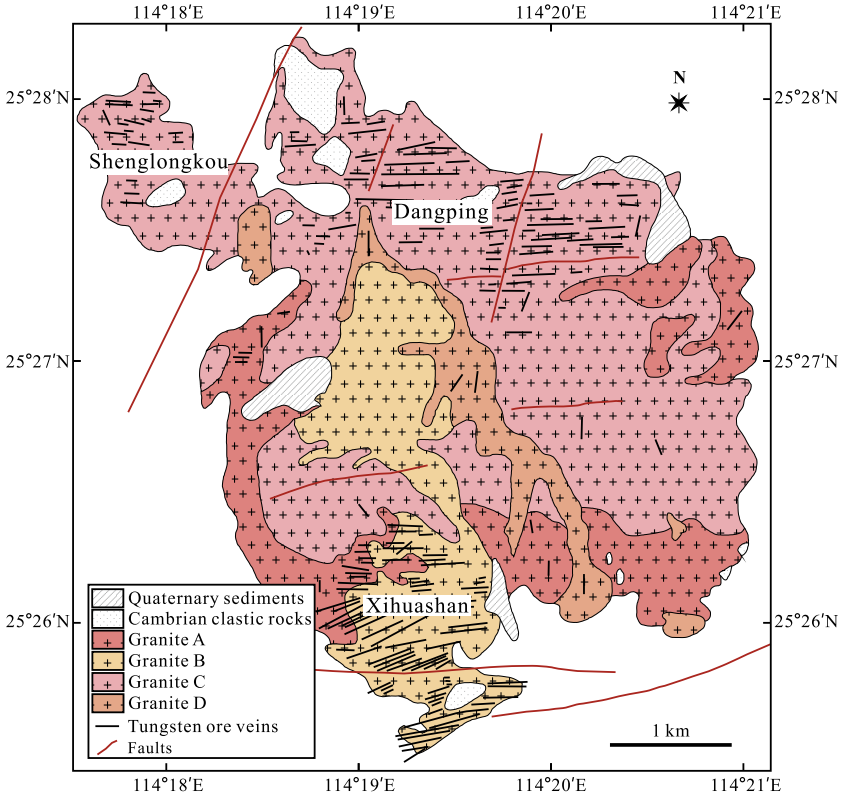

Fig. 11. Geological map of the Xihuashan tungsten mineralization region, modified after Le Bel et al. (1984), Wang et al. (2011b) and (Mao et al., 2013a).

highly evolved, strongly peraluminous, and belong to the calc-alkaline series (Le Bel et al., 1984; Maruéjol et al., 1990; Shen et al., 1994; Wu et al., 1987; Xiao et al., 2009; Zeng et al., 2001). Recent SIMS zircon U-Pb dating shows that these granites range in age from 161 ± 3 Ma to 158 ± 2 Ma (Guo et al., 2012). The Xihuashan deposit is composed of more than 700 ore-bearing veins, which can be divided into two groups on the basis of their orientation and localities. Individual veins are up to 1075 m long, 3.6 m wide, and typically extend for 60 to 200 m downward (Wu et al., 1987). These veins usually show an en echelon structure and occur as clusters (Giuliani et al., 1988). Ore minerals in the veins are mainly wolframite and molybdenite with minor arsenopyrite, cassiterite, chalcopyrite, pyrite and bismuthinite (Fig. 12a). Gangue minerals are predominately quartz with minor mica, feldspar, fluorite, beryl and calcite. Hydrothermal alteration mainly includes greisenization, silicification and sericitization (Wu et al., 1987). Sometimes, in the contact between the carboniferous layer and the grantie, there is weakly skarnization (Fig. 12b). Fluid inclusions in wolframite and quartz show homogenization temperatures of 239°–380 °C and 177°–329 °C and salinity of 3.8–13.7 wt.% NaCl equiv. and 0.9–8.1 wt.% NaCl equiv., respectively (Wei et al., 2012). It is suggested that the W mineralization took place around 155 Ma (Hu et al., 2012).

The Xingluokeng porphyry W-Mo deposit is the largest W deposit in northwestern Fujian Province. It has a reserve of 304,300 t WO_3 with an average grade of 0.23%, and Mo is recovered as a by-product with an average grade of 0.02% in the ore (Mao et al., 2013a). This is a typical porphyry-type deposit with a large tonnage of low-grade ore. The mineralization is generally attributed to the intrusion of two Early Yanshanian granites into the host quartz arenite, silty sandstone and calcareous sandstone lenses of the Sinian Luofengxi Group. The intrusions consist of a coarse- to medium-grained, porphyritic biotite granite stock in the south, which formed earlier than a medium- to fine-grained, two-mica granite in the north with a whole-rock Rb-Sr isochron age of 157 ± 3 Ma (Zhang, 1983). Granitic intrusions appear as small stocks. On the basis of experimental studies, the granites have melting temperatures of 750–780 °C (Cai, 1984). Other late-stage granite porphyries, as well as diabase and lamprophyre dykes, are also present in the mine (Cai, 1984; Zhang, 1983). Mineralization is mainly concentrated in the south granite stock and occurs as disseminated scheelite and wolframite, and molybdenite-bearing

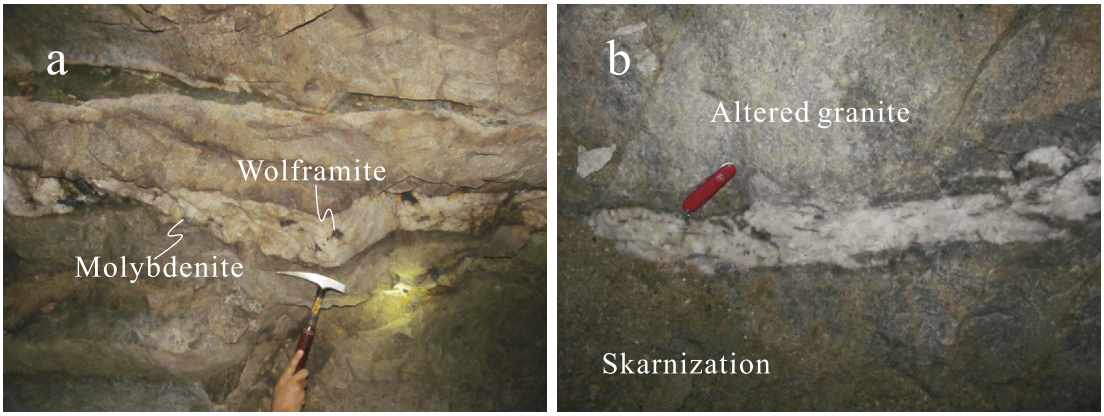

Fig. 12. Ore-bearing quartz vein (a) and ore-barren quartz vein with weakly skarnization (**b**) in the Xihuashan deposit.

quartz veins (Zhang et al., 2008a). Scheelite and wolframite are mainly concentrated at the upper part of the orebody whereas the molybdenite content increases with depth. Major ore minerals include wolframite, scheelite, molybdenite, cassiterite, beryl, sphalerite, chalcopyrite and bismuthinite, and the gangue minerals mainly consist of quartz, biotite, K-feldspar, fluorite, calcite, muscovite, kaolinite and chlorite (Fig. 13). The granitic intrusion and the wall rocks have different styles of alteration, including potassic alteration, greisenization, sericitization, chloritization and silicification (Zhang et al., 2008a). The gangue minerals are zonally distributed with biotite, tourmaline and diopside occurring near the intrusions and actinolite, epidote, chlorite, quartz increasing towards the wall rock. Six stages of hydrothermal activity have been identified (Zhang and Liu, 1993), including the potassic alteration stage, quartz-molybdenite veinlet stage, scheelite-molybdenite-quartz vein stage, beryl-wolframite-feldspar-quartz vein stage, sulfide-carbonate-scheelite-wolframite-quartz vein stage, and barren quartz-carbonate stage. In general, scheelite formed paragenetically earlier while wolframite is usually associated with the later stage quartz vein. Homogenization temperatures of fluid inclusions of quartz in wolframite -quartz vein range from 150° to 310 °C, whereas decrepitation temperature of fluid inclusions hosted within wolframite and scheelite range from 283°–323 °C and 343 °C, respectively (Zhang, 1983). $\delta^{18}O$ of quartz from the W-bearing vein is from +11.0 to +14.2‰, with an average value of +12.8‰, while for $\delta^{34}S$, the results are very diverse. Three peaks at +6.5‰, +1‰ and −3‰, can be observed, respectively, but $\delta^{34}S$ of sulfides from the main mineralization stage concentrate between −0.92 and +2.01‰ (Zhang, 1983). Isochron dating on Re-Os isotopes in molybdenite yield 156.3 ± 4.8 Ma and, on Rb-Sr isotopes in fluid inclusions of quartz yield 147.5 ± 2.9 Ma (Zhang et al., 2008a).

4. Deposits in the Yangtze River and adjacent regions

The Yangtze River region, located at the northern margin of the Yangtze Block, includes the traditionally Middle-Lower Yangtze Valley Metallogenic Belt in the north (Mao et al., 2011b) and the recent-defined North Yangtze Tungsten Belt in the south (Mao et al., 2013b). To the north, the Yangtze River region is bounded to the west by the North China Block and Qinling-Dabie Orogenic Belt (Fig. 14). Its basement is made up of Mesoproterozoic low-grade metamorphic silstone, sandstone, and clastic rocks, intercalated with metaspilite-keratophyre of Shuangqiaoshan and Banxi Groups (Chang et al., 1991; Wang et al., 2008). The basement is discordantly overlain by the Sinian conglomerate, tillite, dolostone, shale, and chert, which are in turn, covered by the Cambrian to

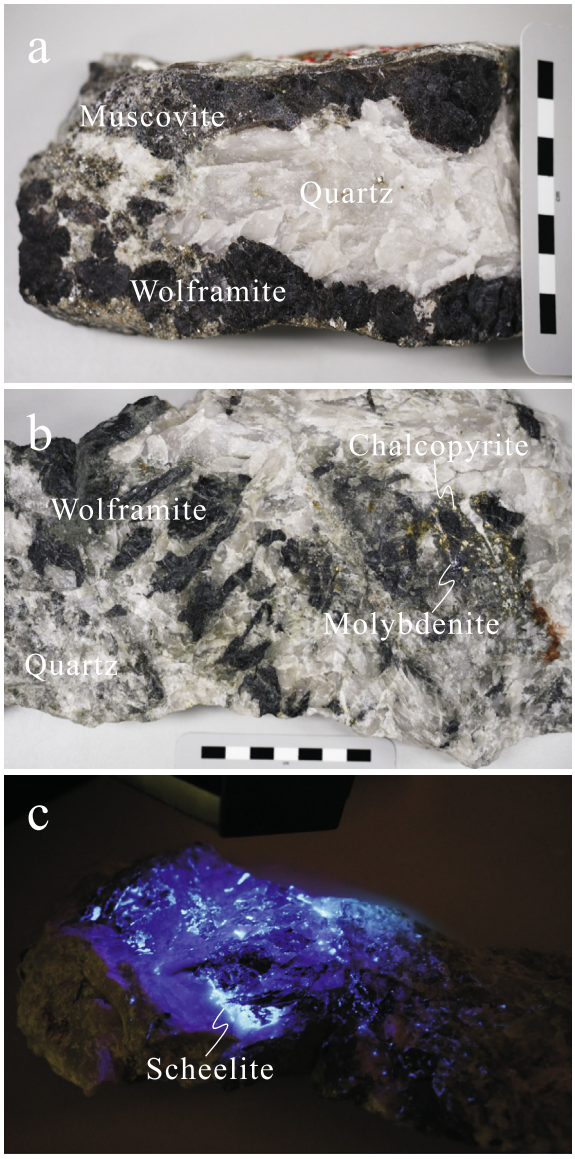

Fig. 13. (a) Wolframite in quartz vein; **b**: Wolframite-molybdenite-chalcopyrite in quartz vein; **c**: Scheelite under fluorescent light.

Early Triassic carbonate and clastic rocks of shallow marine facies (Xu, 1985). Middle Triassic to Early Jurassic strata are marine and terrigenous sedimentary rocks, which are unconformably overlain

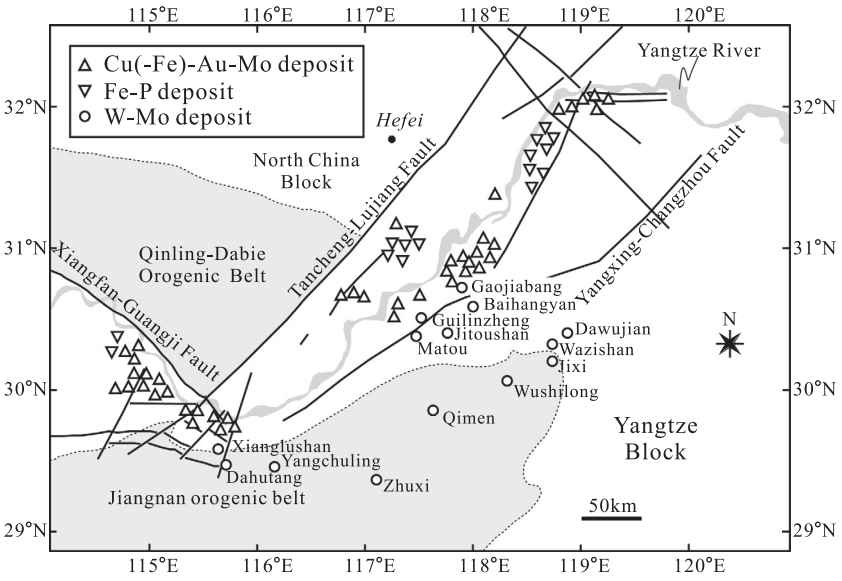

Fig. 14. Geology and distribution of mineral deposits in the Yangtze River region, modified after Mao et al. (2013a).

by the Early Cretaceous volcanic rocks in NE-trending extensional basins. The Neoproterzoic granitoids emplaced in the Jiangnan Orogenic Belt, with an out crop area greater than 2500 km^2 (Zhong et al., 2005), are intruded by multiple phases of Mesozoic granitoids (Di et al., 2005; Li et al., 2009a, 2010a; Wang et al., 2004; Xu et al., 2004; Zhou et al., 2010) that are responsible for the Fe-Cu-W-Mo-Au mineralization (Fig. 14) (Li et al., 2008a; Mao et al., 2006, 2011b; Pan and Dong, 1999; Sun et al., 2003; Xie et al., 2007; Zhou et al., 2015).

Along with the vast mineralization of Cu-(Fe)-Au and Fe-P deposits in the region, numerous W-Mo deposits have been discovered. Selected examples to be elaborated in the following highlight some of the large to super-large deposits in the region, including the Xianglushan skarn deposit and the recently-discovered Zhuxi and Dahutang deposits.

The Zhuxi skarn deposit is a super-large W-Cu deposit located about 20 km SE of Jingdezhen city, northern Jiangxi Province. Originally, exploration was targeted for Cu in the 1980s, but recent exploration discovered more than 1 Mt reserve of WO_3 in this deposit (Hu, 2015). The magmatic intrusions associated with the mineralization are the Late Jurassic to Early Cretaceous biotite granite and granite porphyry dykes that intrude the host rocks of Sinian phyllite, meta-sandstone, slate and Middle Carboniferous to Triassic limestone, dolomite (Fig. 15). The granitic intrusions, dated at 152–148 Ma (Chen et al., 2016), show slight negative Eu anomalies, and display similar geochemical signatures similar to the peraluminous S-type granite (Chen et al., 2016; Hu, 2015). A lamprophyre dated at 160.3 ± 2.1 Ma has also been found in the mine site (Liu et al., 2014). Structural control of the orebodies is obvious with the NE-trending subsidiary fault of the Taqian-Chuntuo fault as the main controlling one (Hu, 2015) at the northwest of the deposit while the southeast of the deposit is bound by an angular unconformity against the Proterozoic basement (Chen et al., 2016). Orebodies are dominantly NE-striking, extending for over 750 m and dipping towards NW for 30–75° (Fig. 15). Two styles of mineralization occur, including skarn type and greisen type with the former contains higher amount of scheelite (Chen et al., 2016). Ore minerals are scheelite, chalcopyrite, sphalerite, pyrrhotite, pyrite, and the gauge minerals are garnet, diopside, wollastonite, quartz, gypsum, calcite and fluorite. Zonation of mineralization is observed in Zhuxi deposit, and in general, dominant

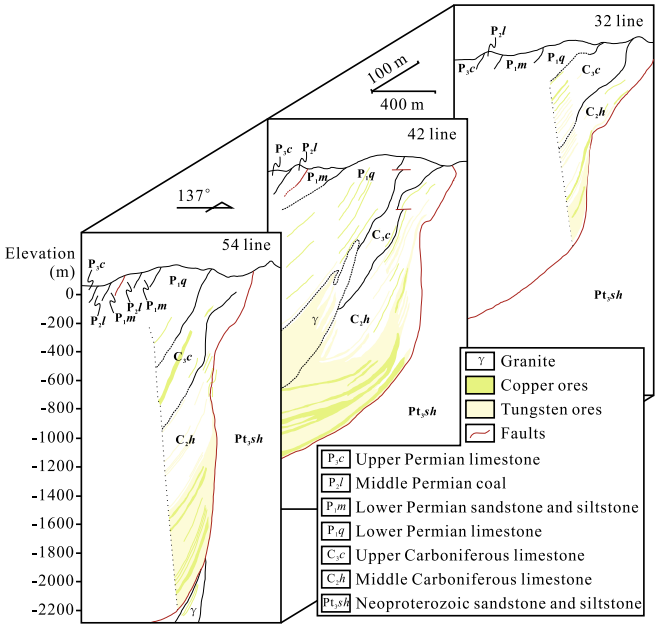

Fig. 15. Profiles of the Zhuxi W deposit from 32 Line, 42 Line, to 54 Line, modified after Hu (2015).

metal assemblages change from W ± Cu to W + Cu ± Zn and to Cu + Zn ± Pb ± W from the intrusion towards the wall rock (Hu, 2015), associating with this are the changes in skarn minerals from garnet + diopside to tremolite + diopside + wollastonite. In viewing at a vertical scale, occurrence of mineralization change from the lower greisen and quartz-vein W ores in the limestone of the Qixia Formation to the middle stratiform and stratabound skarn W-Cu mineralization (Fig. 15). The vein and skarn W-Cu mineralization can be observed in the upper part and the uppermost part of the deposit composes of lenticular skarn Cu-Zn mineralization (Hu, 2015). Six paragenetic stages were determined according to mineral assemblage, intra- and inter-granular texture and structure (Hu, 2015). After the formation of prograde skarns, abundant disseminated scheelite together with pyrrhotite, molybdenite, sphalerite and chalcopyrite form during the retrograde skarn stage.

Subsequently, veinlets, and disseminated scheelite, chalcopyrite and sphalerite were formed, crosscutting the intrusion, skarn and wallrock associated with intense greisenization of the granitic intrusion. Main mineralization stage comes afterwards with abundant quartz veining containing abundant dissemination and aggregation of chalcopyrite with sphalerite, scheelite, pyrrhotite, and subordinate amount of arsenopyrite, stibnite and molybdenite. The later calcite-scheelite stage and the supergene stage further enrich W and Cu in the deposit. Sm-Nd dating of scheelite gives an age of 144 ± 5 Ma (Hu, 2015). Similar age of 145.1 ± 1.5 Ma is also determined by isochron Re-Os dating of molybdenite (Li, 2014).

The Xianglushan skarn W deposit, northwest of Jiangxi, is located between the northern Jiangnan Orogenic Belt and the southern Middle-Lower Yangtze Valley Metallogenic Belt (Fig. 14). In the deposit area, six sedimentary units are exposed (Chen and Zhou, 2012; Chen, 1990): the Late Sinian manganese-bearing argillaceous limestone of Doushantuo Gruop and chert of Dengying Group; the Early Cambrian carbonaceous shale of Wangyinpu Formation and Guangyintang Formation; the Middle Cambrian dark gray to black thin-bedded limestone interbedded with marl and calcareous shale of Yangliugang Formation; the Late Cambrian dark gray to black thin-bedded limestone of Huayansi Formation. These are intruded by biotite granite, aplite veins and diabase veins. The biotite granite is fine-grained near the edges, and the grain size gradually increases to medium-grained towards the centre of the granitic body. The granites are classified as S-type (Tian and Yuan, 2008). Zircon U-Pb dating gives an age of 127.2 ± 0.7 Ma for the biotite granite (Fig. 16; Table 2), consistent with the Rb-Sr age of 126.2 ± 2.6 Ma provided by Zhang et al. (2008b). The NE-trending Xianglushan anticline is the most prominent structure within three groups of faults (i.e., NE-, NEE-, and NW-trending) in this region. The ore-bearing skarns developed mainly in the contact between the Middle Cambrian Yangliugang Formation and the Cretaceous biotite granite (Wu et al., 2014). Scheelite occurs as desimilations or veins. Scheelite-enriched sodic alteration developed along the contact between the skarns (or marble) and granite (Fig. 17a). in the skarn bodies, vein-type scheelite ores crosscut the early skarn assemblages (Fig. 17b). Generally, scheelite-bearing stockworks are the main ore type (Fig. 17c). Studies on fluid inclusions indicate that the fluid temperature decreased from about 450° to 340 °C from the early to the late skarn stages with low to medium salinities (Xiong et al., 2015).

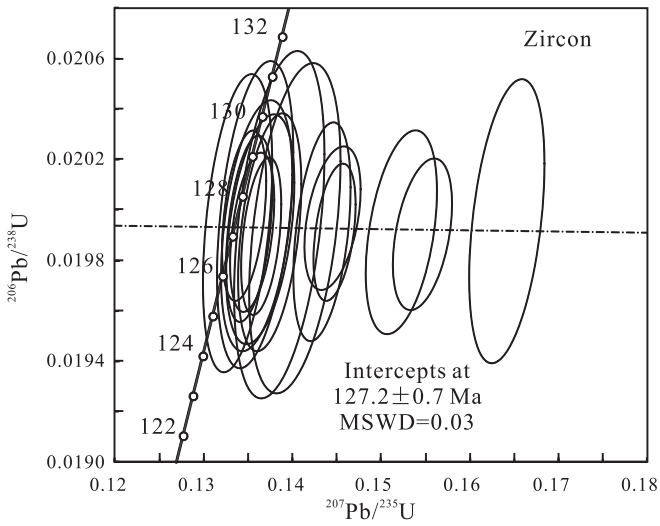

Fig. 16. Zircon U-Pb Concordia age of the granite related to the Xianglushan W mineralization.

The Dahutang W deposit is located in the northwest of Jiangxi Province. This deposit is made up of the Shimensi deposit in the north, Dalingshang deposit in the center, and Shiweidong deposit in the south, with total reserves of more than 1 Mt @ 0.17–0.19% WO_3 (Jiang et al., 2015; Mao et al., 2015; Xiang et al., 2013b). The strata in the mining region are Neoproterozoic dark gray phyllite and slate intercalated with meta-sandstone of the Shuangqiaoshan Group. These meta-sedimentary rocks are discretely distributed, and intruded by the Jiuling biotite granitoid (Li et al., 2016). The Neoproterozoic Jiuling granitoid is classified as medium- to coarse-grained quartz-phyric granodiorites (Li et al., 2003; Wang et al., 2013b; Zhao et al., 2013; Zhong et al., 2005), which was later intruded by multiple phases of Mesozoic granitoids (Huang and Jiang, 2014; Mao et al., 2015; Wang et al., 2015; Xiang et al., 2013a). These Mesozoic phases consist of porphyritic two-mica granite, fine-grained muscovite granite, porphyritic two-mica granite, fine-grained two-mica granite, and granite porphyry dykes, which are all S-type with low ε_{Nd} values and high $^{87}Sr/^{86}Sr_0$ values (Huang and Jiang, 2014; Mao et al., 2015). An EW-striking ductile shear zone intersected by the NNE-trending fault mainly acted as an ore-controlling structure (Jiang et al., 2015; Li et al., 2016; Xiang et al., 2013a). Besides, several NW- and NE-trending faults are extensively developed filled with wolframite-scheelite quartz veins (Fig. 18a). Stockwork fractures and breccias are densely developed at the contact between the Mesozoic granite and the Neoproterozoic granite (Fig. 18b). Three ore styles are exhibited, including veinlets-disseminated (~95% of the total reserve), breccia (~4%) and wolframite-scheelite quartz vein (~1%) (Mao et al., 2013b), with wolframite, scheelite and molybdenite as the major ore minerals and cassiterite, pyrite, chalcopyrite and sphalerite in a minor amount. Re-Os dating on molybdenite gives a mineralization age at around 140 Ma (Feng et al., 2012c; Mao et al., 2013b).

5. Deposits in the Xiangzhong basin, Qin-Hang belt, and coastal area

In addition to the Nanling Range and the Yangtze River regions, there are other regions with significant Mesozoic W mineralization, such as the Xiangzhong basin, and areas along the Qin-Hang belt and along the coastal areas.

5.1. Xiangzhong basin

The Xiangzhong basin in central Hunan Province on the eastern margin of the Yangtze Block was dominated by a prolonged period of sedimentation from the Neoproterozoic to early Mesozoic. During the late Triassic, the Indosinian orogeny produced numerous granitic plutons in the region (Shu et al., 2009; Wang et al., 2012b), and abundant low-temperature Sb-Au deposits, including the Zazixi, Xitianshan and Banxi deposits, are thought to be related to the granitic magmatism (Fig. 19) (Hu et al., 2016). Although direct relationships with the granitic intrusions have not yet been established, it has been postulated that deep-seated intrusions triggered circulation of probably meteoric fluids to leach ore-forming materials from the host rocks to form these Sb-Au deposits (Hu et al., 2016).

Tungsten is often a by-product in these deposits, and is being mined in the Zazixi deposit. Stibnite and/or gold-bearing minerals often occur in quartz veins that cut Sinian to Triassic phyllite, slate, siltstone and sandstone. The mineral assemblage is simple, mainly composed of stibnite, scheelite, native gold, pyrite, and less commonly, arsenopyrite. Quartz, sericite and calcite are the dominant gangue minerals. Alteration is weak due to the low temperature of the ore-forming fluids and is chiefly silicification and sericitiza-

Table 2
U-Th-Pb isotope compositions of zircon from the Baoshan W deposit.

	Th	U	Th/U	U-Pb ratios				Age (Ma)			
	ppm	ppm		$^{207}Pb/^{235}U$	1sigma	$^{206}Pb/^{238}U$	1sigma	$^{207}Pb/^{235}U$	1sigma	$^{206}Pb/^{238}U$	1sigma
XLS13-01	86	62	1.38	0.13635	0.00156	0.01992	0.00019	129.8	1.4	127.2	1.2
XLS13-02	34	118	0.29	0.13544	0.00100	0.01991	0.00013	129.0	0.9	127.1	0.8
XLS13-03	95	51	1.86	0.13746	0.00145	0.01991	0.00019	130.8	1.3	127.1	1.2
XLS13-06	64	94	0.68	0.13646	0.00091	0.01990	0.00013	129.9	0.8	127.0	0.8
XLS13-08	66	90	0.73	0.13852	0.00208	0.01994	0.00028	131.7	1.9	127.3	1.8
XLS13-10	34	124	0.27	0.15463	0.00138	0.01990	0.00012	146.0	1.2	127.1	0.8
XLS13-13	40	112	0.36	0.15227	0.00162	0.01991	0.00017	143.9	1.4	127.1	1.0
XLS13-14	55	102	0.54	0.13579	0.00176	0.01998	0.00025	129.3	1.6	127.5	1.6
XLS13-15	58	99	0.59	0.14331	0.00131	0.01991	0.00018	136.0	1.2	127.1	1.1
XLS13-16	54	104	0.52	0.13512	0.00108	0.01993	0.00015	128.7	1.0	127.2	1.0
XLS13-18	64	91	0.71	0.13381	0.00159	0.01995	0.00024	127.5	1.4	127.3	1.5
XLS13-20	63	95	0.67	0.13458	0.00102	0.01998	0.00014	128.2	0.9	127.5	0.9
XLS13-22	56	101	0.56	0.14473	0.00096	0.01991	0.00011	137.3	0.8	127.1	0.7
XLS13-23	81	73	1.11	0.14452	0.00130	0.01997	0.00012	137.1	1.2	127.4	0.7
XLS13-27	43	107	0.40	0.16416	0.00174	0.01996	0.00023	154.3	1.5	127.4	1.5
XLS13-29	71	85	0.84	0.14028	0.00209	0.01993	0.00027	133.3	1.9	127.2	1.7
XLS13-30	85	65	1.31	0.13595	0.00164	0.01994	0.00020	129.4	1.5	127.3	1.3

tion. A Sm-Nd isochron age of 227.3 ± 6.2 Ma from scheelite (Wang et al., 2012b) indicates that the W mineralization in the Xiangzhong basin took place during the late Triassic, earlier than in most others parts of South China.

5.2. Qin-Hang belt

The "Qin-Hang belt" refers to a tectonic belt extending from Qinzhou in Guangxi Province to Hangzhou in Zhejiang Province. It is a NE-trending belt superimposed on the Neoproterozoic suture zone which separates the Yangtze and Cathaysia Blocks. Sedimentary rocks within the belt include red beds, sandstones, siltstones, mudstones, conglomerates, breccias, tuffs and ignimbrites (Gilder et al., 1991; Goodell et al., 1991). Widespread I-, S- and A-type granites and bimodal volcanic rocks were formed in the belt between 135 and 75 Ma (Gilder et al., 1991; Goodell et al., 1991; Jiang et al., 2011; Qi et al., 2016; Sun et al., 2015; Wong et al., 2009; Wu et al., 2016; Yang et al., 2013), during the peak of extension between the Late-Middle Jurassic and the Middle-Late Cretaceous (Goodell et al., 1991). Along the Qin-Hang belt there are a number of Mesozoic W deposits, including the Late Triassic Limu deposit, the Late Jurassic Hukeng, Xiatongling and Xushan deposits and the Late Cretaceous Damingshan deposit.

The Limu deposit in Guangxi Province is a Triassic Nb-Ta-W-Sn polymetallic deposit associated with the Triassic medium- to fine-grained, muscovite granite. Tungsten mineralization occurs in steeply dipping, wolframite- and scheelite-bearing quartz veins above the granitic intrusion. W-Sn bearing quartz veins are developed above pegmatite-aplite dykes and the alkali feldspar granite (Zhu et al., 2001), indicating the explusion of ore-forming, hydrothermal fluids from the granite and upward transport of the ore-forming materials.

In central Jiangxi Province, there are also a number of large W deposits, including the Hukeng, Xiatongling and Xushan bodies. These deposits formed in the late Jurassic between 147 and 152 Ma (Li et al., 2011a, 2011b; Liu et al., 2008b). In general, these deposits are of the quartz-vein type associated with granitic intrusions. Major ore minerals include wolframite, scheelite and pyrite, whereas quartz, muscovite and K-feldspar are the major gangue minerals. Intense greisenization is widespread in the granitic intrusions, which also contribute to the mineralization. At the Xushan deposit, mineralization occurs mainly in greisen at depth but changes to skarn- and vein-type at shallower levels (Wang and Long, 2010). These mineralized veins have shallow to moderate dips in contrast to the steeply dipping veins in W deposits elsewhere in Southeast China. These veins are composed of scheelite instead of wolframite (Wang and Long, 2010). In Xiaotongling, mineralization mainly occurs in networks of quartz veinlets that are concentrated at the contact zone (Li et al., 2011a).

The Damingshan deposit in Guangxi Province was formed at 95 ± 1 Ma (Li et al., 2008b) and consists of moderately dipping, scheelite-dominant, quartz veins (Li et al., 2008b; Wang et al., 2010a). In this deposit, Mo dominates at deep levels, W prevails in the middle, and Cu, Pb-Zn in the uppermost levels. Three styles of mineralization are recognized in this deposit; porphyry-type mineralization in the granitic stock, ore-bearing veins and vein networks in the Cambrian and Devonian host strata and stratiform ore layers up to 1500 m long and 30 m thick in the Lower Devonian sandstone and shale.

5.3. Coastal area

The Middle to Late Jurrassic magmatism in South China is largely restricted to the coastal areas in Fujian and Zhejiang Provinces. S-, I- and A-type granites are very common and are associated with bimodal volcanic rocks(Chen et al., 2004, 2008a, 2008b; Li et al., 2007; Zhou et al., 2006). The Lianhuashan porphyry deposit is one of the largest in this region and is hosted in the granite porphyry as networking veinlets and at both endo- and exo-contacts with the Jurassic sandstone. Intense greisenization occurred due to circulation of high-temperature hydrothermal fluids. Subsequently, hydrothermal fluids of lower temperature led to the quartz-sulfide mineralization stage and the latest carbonate stage (Li, 1995; Man et al., 1983).

The Needle Hill deposit in Hong Kong is another major W deposit in the region. Although Hong Kong is only a small place in terms of area, quite a number of metal deposits occur throughout the territory, including the Needle Hill W-(Mo) deposit, the Lin Ma Hang Pb-Ag deposit in the northeast and the Ma On Shan Fe deposit in the east (Fig. 20a). The Needle Hill deposit possesses a total reserve of about 330,000 t of probable ores with an average grade of 0.48% WO_3 according to an evaluation in 1977 (Roberts and Strange, 1991). The deposit is composed of a series of NW-striking, steeply dipping fissure veins, eleven of which have been mined (Fig. 20b) (Roberts and Strange, 1991). The linear extents of these veins are mostly about 150 m but a few of them can reach up to 450 m, and all are less than 0.5 m wide. The deposit is hosted within, and very likely closely associated with, the medium- to fine-grained Sha Tin fractionated, I-type granite-monzogranite and the fine-grained biotite Needle Hill A-type monzogranite.

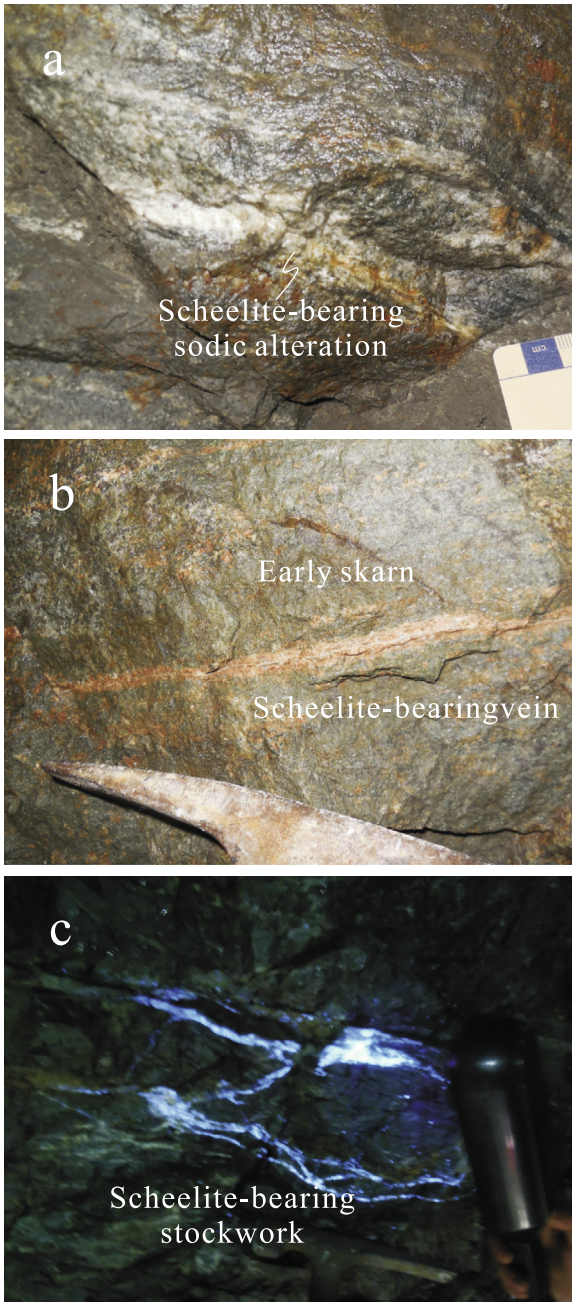

Fig. 17. (a) Ore-bearing sodic alteration between granite and skarns; (b) Ore-bearing pyroxene-garnet skarns; (c) Scheelite-enriched veins, in the Xianglushan deposit.

Results from TIMS U-Pb dating suggest that these two granitic pluton formed around 146 Ma (Davis et al., 1997; Sewell and Campbell, 1997; Sewell et al., 2012). The Needle Hill granite and the Sha Tin granite have $^{87}Sr/^{86}Sr_0$ ratios of 0.70773 and 0.70613–0.70802, and ε_{Nd} values of −6.3 and −4.4, respectively (Darbyshire and Sewell, 1997). Mineralization can be divided into vein-type, including pegmatite veins and quartz veins, and greisen type (Davis, 1958, 1961). In the pegmatite veins, molybdenite and subordinate wolframite are usually associated with coarse-grained K-feldspar, muscovite and quartz (Fig. 21a), whereas in the quartz veins, wolframite dominates over molybdenite (Fig. 21b). Ore minerals are wolframite and molybdenite with minor amounts of cassiterite and scheelite, whereas the major gangue minerals include quartz, K-feldspar and muscovite. Intense greisenization, together with minor chloritization, sericitization and epidotization, has affected the granitic rocks in contact with the veins.

6. Genetic types of W deposits in South China

Most of the W deposits in South China are closely related to granites. According to their geological, geochemical, and mineralogical features they are classified into three types: (1) greisen and quartz-vein type (Table 3); (2) skarn type (Table 4); and (3) porphyry type (Table 5). The spatial distributions of these W deposits relative to the associated plutons are shown in Fig. 22. The most popular model suggests that the perluminous and metaluminous granitic magmas were derived from partial melting of the crust with input from mafic materials. After formation, the magmas are thought to have undergone strong differentiation and enrichment in W and other rare metals with abundant volatiles in the apical parts of magma chambers. Hydrofracturing resulted in the release of hydrothermal fluids into the country rocks. Greisen, quartz-vein, and porphyry-type deposits are likely to form when the fluids encounter granitic, clastic, and/or metamorphic country rocks, but skarn(-greisen) type deposits would form preferentially where the host rocks are carbonates. These types are summarized and discussed below.

6.1. Greisen and quartz-vein type

Greisen and quartz-vein type W deposits account for about 40% of the total W reserves in China (Sheng et al., 2015), and represent one of the most typical types of mineralization, especially in the Nanling region. Wolframite is typically the main ore mineral. These deposits most commonly occur in the endo- and exo-contacts of highly fractionated granites. On the basis of mineral exploration data for southern Jiangxi and northern Guangdong Provinces, local field geologists have proposed a "five-floor model" to describe the greisen and quartz-vein deposits in this region (Fig. 23) (Giuliani et al., 1988; Mao et al., 2013a; Wu and Mei, 1982; Xu et al., 2008). Greisen-type, disseminated W mineralization occurs in the apical portions of hydrothermally altered granite plutons with quartz-muscovite replacement. In some cases, barren potassic and/or sodic alteration zones may underlie the greisen zone. Greisens are usually associated with mineralized veins and breccias. The thickness of the veins ranges from meter-width lodes to millimeter-width veinlets, extending into the metaclastic wall rocks. These veins are mainly filled with quartz and wolframite with well-developed silicic, potassic, sodic, or greisen alteration envelopes.

The genesis of the greisen and quartz-vein W deposits is closely related to the evolution of the associated granites. Numerous studies have shown that the highly fractionated granites associated with W mineralization have much higher W concentrations than others (Blevin and Chappell, 1992; Candela and Bouton, 1990; Mahood and Hildreth, 1983; Newberry and Swanson, 1986). Manning and Henderson (1984) show that W can be strongly partitioned from melts to fluids, and transported principally as polytungstate complexes and/or chloride and phosphate complexes. The molar volume of vapor and fluid exsolved from melts increases substantially as pressure decreases, which provides considerable mechanical energy for fracturing of the country rocks when the magma is emplaced at a shallow level (Burnham, 1979, 1980, 1985). Quartz exhibits retrograde solubility in the fluids at pressures of <800 bars, and the change from lithostatic to hydrostatic pressure is a likely cause of crystallization of abundant quartz in those fractures (Redmond et al., 2004; Rusk and Reed, 2002). Subsequently, almost all dissolved W is precipitated between 350° and 300 °C (Eugster, 1985).

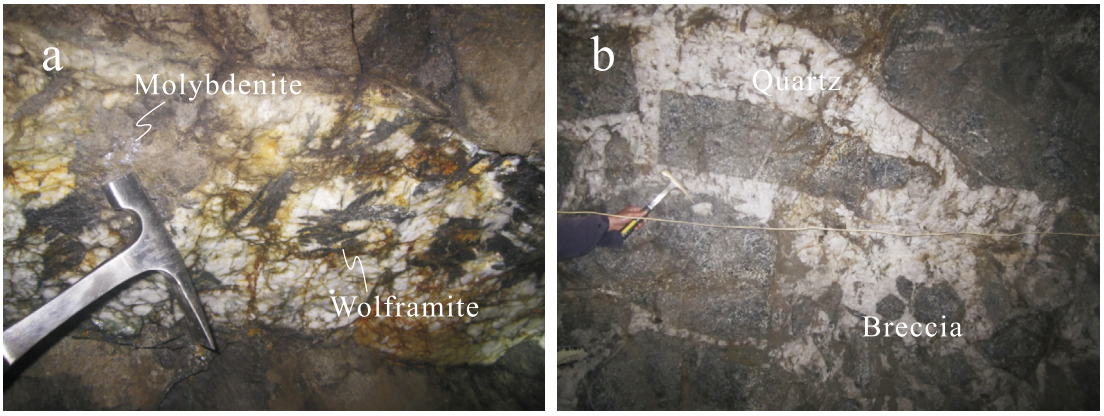

Fig. 18. (a) Wolframite-molybdenite-bearing lodes; (b) Quartz filling in interstices of breccias, in Dahutang deposit.

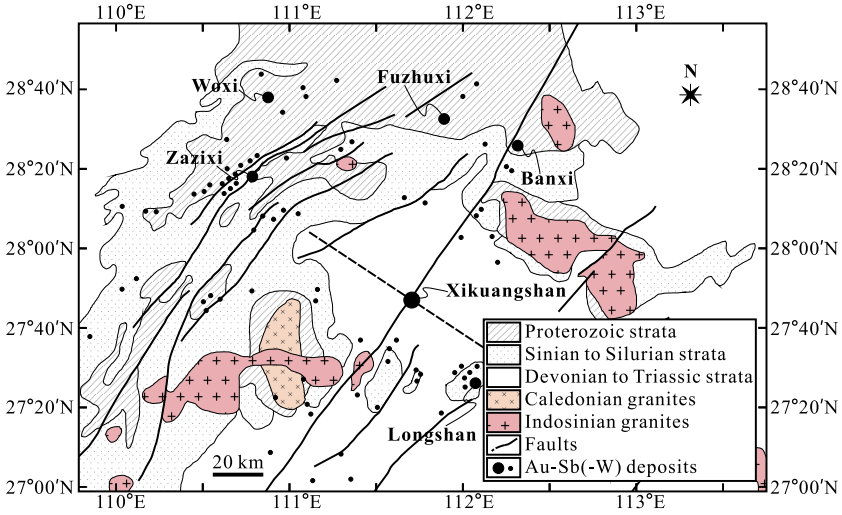

Fig. 19. Geological map of the Xiangzhong basin, modified after Peng et al. (2008).

Greisen and quartz veins are sometimes locally associated with disseminated ores, such as in the Dahutang deposit. This relationship is proposed to have resulted from H_2O saturation during the plutonic stage, which is experimentally documented for the disseminated mineralization and is an obvious prerequisite for the hydrothermal events (Černý et al., 2005). Tungsten mineralization can also be associated with Au-Sb veins and disseminated mineralization as shown by Thompson et al. (1999). Such mineralization is quite similar to that in the Xiangzhong basin, ash shown by the Zazixi deposit. Although the origin of the low-temperature Sb-Au-W deposits has long been controversial, recently stable isotope studies have shown that the ore-forming fluids might be magma-derived (see review by Hu et al., 2016).

6.2. Skarn type

Skarn W deposits are an important W sources because of their high grade ores. In China, they account for around 50% of the total W reserves (Sheng et al., 2015). Tungsten skarn ores are dominated by scheelite and associated with coarse-grained and equigranular granites surrounded by large, high-temperature, metamorphic and metasomatic aureoles, which are indicative of a deep environment (Einaudi et al., 1981; Meinert et al., 2005; Newberry, 1998).

Tungsten skarns are generally subdivided into reduced (W-Sn-F) and oxidized (W-Mo-Cu) types on the basis of skarn mineralogy (ferrous vs ferric), host rock compositions (carbonaceous vs hematitic), and relative formation depth, which are considered to reflect the wall rock and/or granite redox state (Aleksandrov, 1998; Einaudi et al., 1981; Keith et al., 1989; Kwak and White, 1982; Meinert et al., 2005; Newberry et al., 1991; Newberry, 1998). To be specific, oxidized W skarns are characterized by pyrite, diopsitic pyroxene, andraditic garnet, and Mo-enriched scheelite, whereas the reduced counterparts contain primarily pyrrhotite, hedenbergitic pyroxene, early garnet with high almandine component and late subcalcic garnet, and low Mo but commonly high Au contents (Einaudi et al., 1981; Johnson and Keith, 1991; Meinert et al., 2005; Newberry, 1983; Shimazaki, 1977). Generally, oxidized W skarns tend to have smaller reserves than reduced W skarns, and in both systems, the highest ore grades are typically associated with hydrous minerals that formed during retrograde alteration (Einaudi et al., 1981; Meinert et al., 2005). However, as described before, it is difficult to divide skarn W deposits simply into these two categories. For example, at the Shizhuyuan deposit in the Nanling region, the presence of andraditic garnet, pyroxene, pyrite, and Mo-rich scheelite, suggest an oxidized environment, whereas high W contents with highly-enriched Sn-Bi-Mo-F contents and typical stockwork features are characteristic of reduced W-Sn-F types (Liu et al., 1998; Lu et al., 2003). Moreover, at the Xianglushan deposit in the Yangtze River region, these deposits have hedenbergite, Mo-depleted scheelite and pyrrhotite similar to typical reduced W skarns, but also contain abundant fluorite (Tian and Yuan, 2008; Wu et al., 2014; Zhang et al., 2008b). Hence, Newberry (1998) fur-

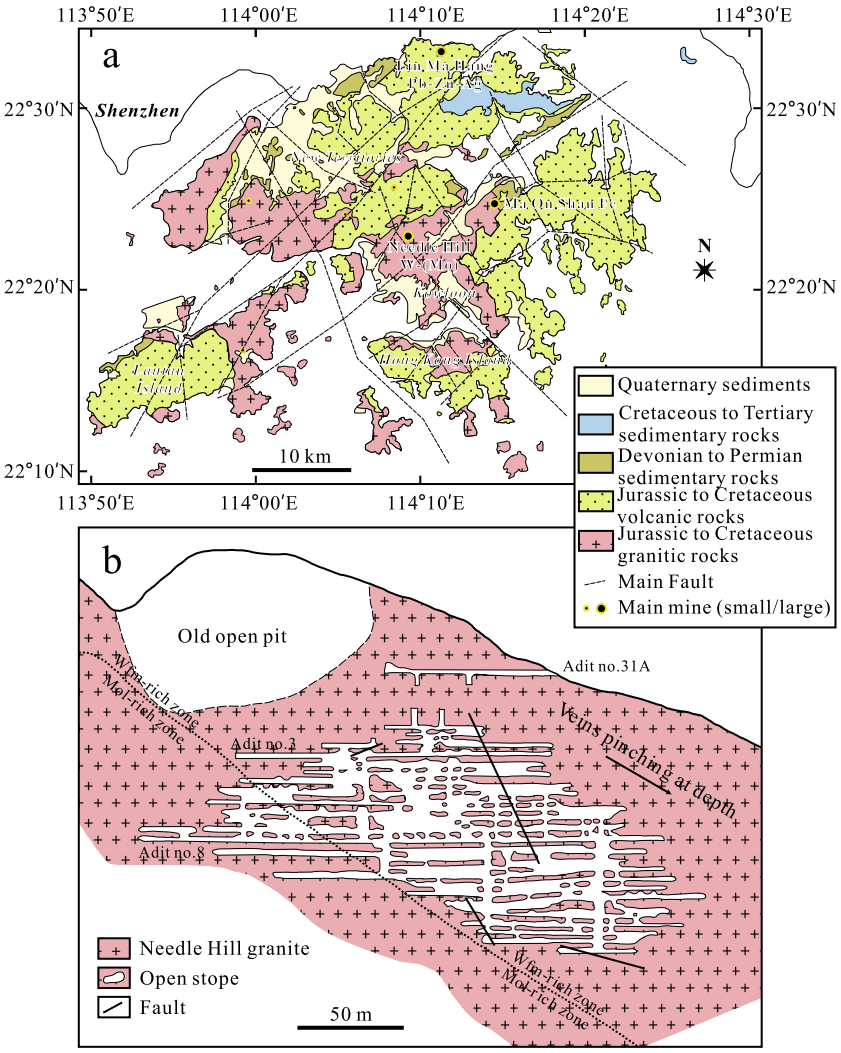

Fig. 20. (a) Simplified geological map of Hong Kong; (b) Sketch showing the mining in Needle Hill, Hong Kong.

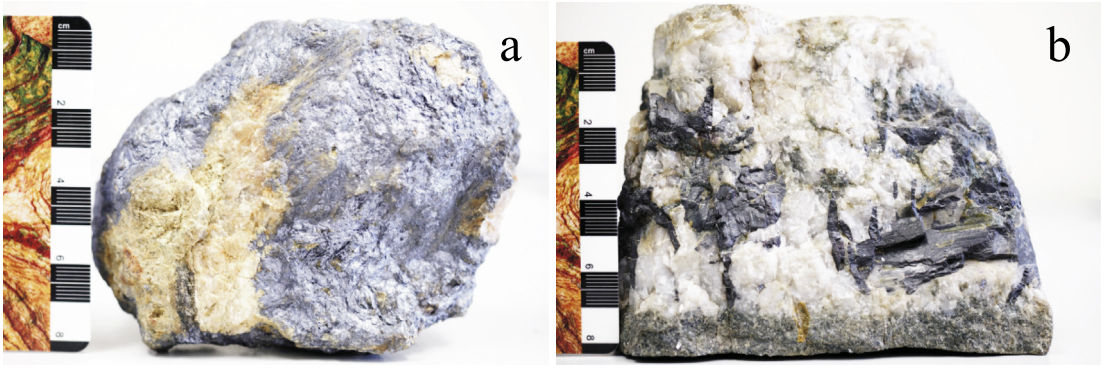

Fig. 21. (a) Molybdenite-enriched ores; (b) Wolframite-enriched ores, in Needle Hill deposit.

ther classified these into two types: intermediate Mo-rich type, such as in the Shizhuyuan deposit, and intermediate Mo-poor type, such as in the Xianglushan deposit.

6.3. Porphyry type

Porphyry W deposits are relatively small compared to Cu, Mo, Au, and Sn porphyry types, and thus are not an important producer of W (Cooke et al., 2005; Seedorff et al., 2005; Sillitoe, 2010). In China, reserves of this type of deposit account for less than 8% of the total (Sheng et al., 2015).

Porphyry W deposits are genetically related to hypahyssal, strongly peraluminous, porphyritic granites (Seedorff et al., 2005). The main ore minerals are wolframite and scheelite with lesser molybdentite, which are present in veinlets and as disseminations in large volumes of hydrothermally altered rocks (Seedorff

Table 3
Characteristics of representative greisen and quartz-vein W deposits in South China.

Name	Metal	Reserve (t)/ Grade (%)	Ore minerals	Gangue minerals	Alteration	Host rock	Associated intrusions	Method/Age (Ma)/ Reference
Anqiantan (Jiangxi)	Quartz-vein W-Bi	–	Scheelite, wolframite, bismuthinite, pyrite	Quartz, muscovite	Silicification	Sinian and Devonian meta-sedimentary rocks	Medium- to fine-grained porphyritic biotite granite	Re-Os: 154.4 ± 1.6 (Liu et al., 2010)
Baiyunxian (Hunan)	Quartz-vein Sn-W-Pb-Zn	–	Wolframite, scheelite, bismuthinite, molybdenite, cassiterite, chalcopyrite, pyrite	Quartz, fluorite, beryl, calcite,muscovite, chlorite	Greisenization, sericitization, chloritization, silification	Sinian meta-sandstone, slate and middle Devonian siltstone and limestone	Medium- to fine-grained biotite granite	Re-Os: 169.6 ± 2.7 (Wang et al., 2009)
Baxiannao (Jiangxi)	Quartz-vein W–Sn	WO_3 100,000; Sn 100,000/ WO_3 0.37; Sn 0.35	Wolframite, cassiterite, chalcopyrite, galena, sphalerite, arsenopyrite, pyrite	Quartz, feldspar, fluorite, chlorite, zinnwaldite	Greisenization, silicification, chloritization, carbonization	Neoproterozoic metasandstone and slate	Fine-grained porphyritic biotite granite	Re-Os: 157.9 ± 1.5 (Feng et al., 2012a)
Da'ao (Hunan)	Quartz-vein Greisen W	–/WO_3 0.04–0.1; Sn 0.1–1.5	Cassiterite, wolframite, pyrite, chalcopyrite, sphalerite	Quartz, K-feldspar, muscovite, topaz	Greisenization, topazization, albitization, fluoritization	Sinian to Cambrian meta-sedimentary rocks	Medium- to fine-grained two-mica monzonite	Re-Os: 151.3 ± 2.4 (Fu et al., 2007)
Dahutang (Jiangxi)	Quartz-vein W-Cu-Mo	WO_3 1.1M; Cu 500,000; Mo 802,000/WO_3 0.152; Cu 0.12; Mo 0.098	Wolframite, scheelite, molybdenite, cassiterite, pyrite, chalcopyrite, sphalerite	Quartz, biotite, muscovite, K-feldspar albite, chlorite, fluorite, calcite	Greisenization, K-feldspar alteration, silicification, carbonatization, chloritization, fluoritization	Neoproterozoic biotite granodiorite	Porphyritic biotite granite and fine-grained biotite granite	Re-Os: 140.9 ± 3.6 Re-Os: 143.7 ± 1.2 (Feng et al., 2012c) Re-Os: 139.18 ± 0.97 (Mao et al., 2013b)
Dajinshan (Guangdong)	Quartz-vein W–Sn	WO_3 + Sn 52,700/WO_3 0.44; Sn 0.05	Cassiterite, wolframite, pyrite, arsenopyrite, bornite, molybdenite, bismuthinite, pyrrhotite	Quartz, mica, feldspar, tourmaline	Greisenization, silicification	Devonian-Triassic clastic rock, carbonate rock and chert	Medium- to fine-grained biotite granite and porphyritic biotite granite	Re-Os: 80.07 ± 1.19 Re-Os: 84.93 ± 1.42 (Yu et al., 2012b)
Dajishan (Jiangxi)	Quartz-vein W-Mo	WO_3 160,000/ WO_3 2.04	Wolframite, scheelite, molybdenite, arsenopyrite, pyrite, chalcopyrite, bismuthinite, pyrrhotite	Quartz, muscovite, microcline, tourmaline, fluorite, calcite	Greisenization, silicification	Camrian metamorposed sandstone and intercalated slate	Porphyritic biotite granite, medium to fine-grained two-mica granite, fine-grained muscovite granite	K-Ar: 158–153 (Jiang et al., 2004) Ar-Ar: 144.04 ± 0.73 Ar-Ar: 147.17 ± 0.57 (Zhang et al., 2006b)
Damingshan (Guangxi)	Quartz-vein W-Cu	WO_3 160,200/ WO_3 0.05–1.0	Wolframite, chalcopyrite, molybdenite, pytite, bismuthinite	Quartz, mica	Silification, greisenization	Cambrian and Devonian clastic rock	Muscovite granite	Re-Os: 95.4 ± 0.97 (Li et al., 2008b)
Guimeishan (Jiangxi)	Quartz-vein skarn W	WO_3 53,000/ WO_3 0.73 (Quartz-vein), 1.5 (Skarn)	Wolframite, scheelite, chalcopyrite, pyrite, bismuthinite, cassiterite	Quartz, muscovite, diopside, garnet, epidote, idocrase, fluorite, calcite	Greisenization, sericitization, silicification, tourmalization, chloritization	Cambrian slate, quartzite and marble	Coarse- to medium-grained biotite granite	Re-Os: 153.7 ± 1.5 (Feng et al., 2012d)
Hongling (Guangdong)	Quartz-vein Greisen W-Sn	–/WO_3 1.85 (quartz-vein), 0.13 (greisen-type)	Wolframite, scheelite, molybdenite, bismuthinite, chalcopyrite, pyrite, sphalerite, arsenopyrite, beryl	Quartz, K-feldspar, muscovite, fluorite, topaz, chlorite, tourmaline, calcite	Greisenization, fluoritization, chloritization, potassic alteration	Fine-grained muscovite granite	Fine-grained muscovite granite	Re-Os: 159.1 ± 1.5 (Wang et al., 2010b)
Hongshuizhai (Jiangxi)	Quartz-vein Greisen W-Sn	–	Wolframite, cassiterite, molybdenite, chalcopyrite	Quartz, muscovite, fluorite, topaz chlorite	Greisenization, silicification, chloritization, potassic alteration	Sinian sandstone and slate	Medium- to fine-grained porphyritic biotite granite	Re-Os: 157 ± 3.3 (Feng et al., 2011b)
Hukeng (Jiangxi)	Quartz-vein W	WO_3 154,475/ WO_3 1.5	Wolframite, sphalerite, bismuthinite, pyrite	Quartz, feldspar, muscovite, fluorite, tourmaline	Silicification, chloritization, fluoritization, tourmalization	Neoprotenzoic meta-clastic rocks	Medium- to fine-grained muscovite granite	Ar-Ar: 147.2 ± 1.4 Re-Os: 150.2 ± 2.2 (Liu et al., 2008b)

(*continued on next page*)

Table 3 (*continued*)

Name	Metal	Reserve (t)/ Grade (%)	Ore minerals	Gangue minerals	Alteration	Host rock	Associated intrusions	Method/Age (Ma)/ Reference
Huameiao (Jiangxi)	Quartz-vein W	WO_3 67,400/ WO_3 1.334	Wolframite, scheelite, molybdenite, bismuthinite, chalcopyrite, pyrite, sphalerite, galena, pyrrhotite, beryl	Quartz, K-feldspar, muscovite, biotite, lepidolite, fluorite, calcite, tourmaline, chlorite	Silicification, biotitization, tourmalinization, chloritization, carbonization	Middle Sinian metamorphosed sandstone	Medium- to fine-grained biotite granite	Re-Os: 158.5 ± 3.3 (Feng et al., 2015b)
Huangsha (Jiangxi)	Quartz-vein W-Cu, Zn, Bi, Mo, Sn	WO_3 126,900/–	Wolframite, molybdenite, cassiterite, galena, sphalerite	Quartz, muscovite, K-feldspar	Greisenization, silicification, potassic alteration	Cambrian metamorphosed sandstone and slate	Coarse-grained porphyritic tourmaline biotite granite and medium-grained two mica granite	Re-Os: 153 ± 3.0 (Huang et al., 2011)
Jiulongnao (Jiangxi)	Quartz-vein W-Sn	WO_3 19,800/–	Wolframite, cassiterite, molybdenite, chalcopyrite	Quartz, muscovite, fluorite, topaz chlorite	Greisenization, silicification, chloritization, potassic alteration	Sinian sandstone and slate	Medium-grained porphyritic biotite granite	Re-Os: 151.5 ± 1.1 (Feng et al., 2011a)
Jubankeng (Guangdong)	Quartz-vein W-Sn	WO_3 129,600; Sn 26,900/WO_3 0.33, Sn 0.127	Wolframite, cassiterite, chalcopyrite, sphalerite, galena, pyrite, molybdenite	Quartz, topaz, chlorite, malachite, triplite, trilithionite, protolithionite	Silicification, topazization, tourmalinization, chloritization	Cambrian to middle Devonian meta-sedimentary quartzites, slates and interlayered limestone, siltstones and cherts	–	Ar-Ar: 139.2 ± 1.5 (Fu et al., 2009) Ar-Ar: 137.93 ± 1.44 Ar-Ar: 138.07 ± 1.52 (Qi et al., 2012)
Keshuling (Jiangxi)	Quartz-vein W	WO_3 > 40,000/–	Wolframite, cassiterite, sphalerite	Feldspar, quartz, muscovite, fluorite	Greisenization, silicification	Fine-grained porphyritic two-mica monzonite	Fine-grained porphyritic two-mica monzonite	U-Pb:~223 Ma (Wang Haoyang, personal communication)
Liguifu (Guangxi)	Quartz-vein Greisen W-Sn-Mo	WO_3 11,370; Sn 4013; Mo 8328/ WO_3 0.557; Sn 0.221; Mo 0.303	Molybdenite, wolframite, cassiterite, sphalerite, chalcopyrite, scheelite, pyrite	Quartz, K-feldspar, biotite, muscovite, fluorite, calcite	Silicification, greisenization, potassic alteration	Fine-grained porphyritic two-mica monzonite	Fine-grained porphyritic two-mica monzonite	Re-Os: 211.9 ± 6.4 (Zou et al., 2009)
Limu (Guangxi)	Quartz-vein Nb–Ta–W–Sn	WO_3 4642; Sn 2219/WO_3 0.26–0.34	Cassiterite, ildefonsite, columbite-tantalite, wolframite, huebnerite, scheelite	Feldspar, quartz, muscovite, topaz, fluorite	Greisenization, silicification, fluoritization	Cambrian epimetamorphic rocks, Devonian sandstone and carbonate, and lower carboniferous limestone	Medium- to fine-grained muscovite granite	Ar-Ar: 214.1 ± 1.9 (Yang et al., 2009)
Maoping (Jiangxi)	Quartze-vein W–Sn	WO_3 108,800; Sn 51,100/WO_3 0.130; Sn 0.116	Wolframite, cassiterite, molybdenite, chalcopyrite, sphalerite	Quartz, topaz, zinnwaldite, muscovite	Greisenization, silification,	Lower-Middle Cambrian metasandstone, metasiltite and slate	Porphyritic granite and fine-grained muscovite granite	Re-Os: 158–141 (Zeng et al., 2009) Re-Os: 150.2 ± 2.0 Re-Os: 155.3 ± 2.8 (Feng et al., 2011a)
Meiziwo (Guangdong)	Quartz-vein W-Sn	–/WO_3 1.1; Sn 0.05; Cu 0.06	Wolframite, scheelite, cassiterite, chalcopyrite, pyrite, molybdenite	Quartz, feldspar, beryl, fluorite, tourmaline, muscovite	Greisenization, tourmalization, silicification	Cambrian to middle Devonian meta-sedimentary quartzites, slates and interlayered limestone, siltstones and cherts	Biotite granite	Re-Os: 157.7 ± 2.8 (Qi et al., 2012)
Muziyuan (Jiangxi)	Quartz-vein W	WO_3 6123/WO_3 1.720	Wolframite, cassiterite, molybdenite, beryl, chalcopyrite, pyrite, scheelite, galena	Quartz, muscovite, topaz, fluorite	Greisenization, chloritization, potassic alteration	Middle-Upper Cambrian metasandstone and slate	Fine-grained biotite granite	Re-Os: 151 ± 8.5 (Zhang et al., 2009)
Needle Hill (Hong Kong)	Quartz-vein W-(Mo)	WO_3 330,000 (probable ore)/ WO_3 0.48	Wolframite, molybdenite, cassiterite, scheelite	Quartz, K-feldspar, muscovite, biotite	Greisenization, silicification	Medium- to fine-grained biotite granite	Medium- to fine-grained biotite granite	U-Pb:<146 (Davis et al., 1997)
Niuling (Jiangxi)	Quartz-vein W-Sn	WO_3 29,122; Sn 11,227/ WO_3 1.27; Sn 0.53	Wolframite, scheelite, cassiterite, molybdenite, chalcopyrite	Quartz, feldspar, fluorite, muscovite, calcite	Greisenization, silicification, potash feldspathization, carbonization	Cambrian metamorphosed sandstone and slate	Medium- to fine-grained biotite granite	Re-Os: 154.9 ± 4.1 (Feng et al., 2011a)

Pangushan (Jiangxi)	Quartz-vein W-Bi-(Te)	WO_3 111,800/ -	Wolframite, scheelite, molybdenite, bismuthinite, pyrite, chalcopyrite	Quartz, muscovite, sericite, biotite	Greisenization, silicification, sericitization, carbonization	Devonian clastic rocks	Medium- to fine-grained biotite granite and two mica granite	Re-Os: 157.8 ± 0.8 (Zeng et al., 2011)
Piaotang (Jiangxi)	Quartz-vein W-Sn, Mo	WO_3 69,858/ WO_3 0.201	Wolframite, cassiterite, molybdenite, chalcopyrite, galena, sphalerite, beryl	Quartz, muscovite, topaz, fluorite, calcite, zinnwaldite	Greisenization, silicification, topazization	Middle-Upper Cambrian metasandstone and slate	Fine-grained porphyritic granite and medium- to fine-grained porphyritic biotite granite	K-Ar: 156–154 (Mu et al., 1988) Ar-Ar: 154 (Chen et al., 2006) Ar-Ar: 159 (Liu et al., 2008c) Ar-Ar: 152 ± 1.9 (Zhang et al., 2009)
Shanhu (Guangxi)	Quartz-vein W-Sn	WO_3 63,802; Sn 18,819/–	Wolframite, cassiterite, sphalerite, chalcopyrite, pyrite, arsenopyrite	Quartz, fluorite, muscovite, topaz, calcite, tourmaline	Sericitization, fluoritization, topazization, chloritization	Cambrian quartz arenite and sandstone, Devonian sandstone and shale	Medium- to fine-grained porphyritic granite	Ar-Ar: 100.8 ± 0.7 Ar-Ar: 102.7 ± 1.7 (Xiao et al., 2011)
Shigushan (Guangdong)	Quartz-vein W-Bi	–	Wolframite, bismuthinite, sphalerite, pyrite, chalcopyrite, molybdenite, arsenopyrite	Quartz, fluorite, muscovite, tourmaline	Silification, greisenization	Middle Cambrian clastic rocks	Granite stock	Re-Os: 154.2 ± 2.7 (Fu et al., 2008)
Shirenzheng (Guangdong)	Quartz-vein W	–	Wolframite, cassiterite, chalcopyrite, molybdenite, bismuthinite	Quartz, fluorite, muscovite, tourmaline	Silicification, tourmalization	Devonian meta-sandstone and slate	Granite stock	Re-Os: 159.1 ± 2.2 (Fu et al., 2008)
Taoxikeng (Jiangxi)	Quartz-vein W	WO_3 120,627/ WO_3 1.5	Wolframite, cassiterite, scheelite, chalcopyrite, pyrite, arsenopyrite, sphalerite, molybdenite, bismuthinite	Quartz, calcite, muscovite, topaz, fluorite, tourmaline, pyrophyllite, chlorite	Silicification, greisenization, chloritization	Sinian - Early Paleozoic clastic rocks	Biotite monzogranite	Re-Os: 154.4 ± 3.8 (Chen et al., 2006) Ar-Ar: 153.4 ± 1.3 Re-Os: 154.4 ± 3.8 (Guo et al., 2011)
Wazishan (Anhui)	Quartz-vein W-Mo	–/WO_3 ~0.1; Mo ~0.08	Wolframite, scheelite, molybdenite, chalcopyrite, bornite, pyrite	Quartz, sericite, chlorite, epidote	Silicification, sericitization, chloritization	Silurian sandstone and siltstone	Biotite granodiorite and biotite monzonite	–
Xiatongling (Jiangxi)	Quartz-vein W-Mo, Bi, Be	–	Wolframite, scheelite, molybdenite, bismuthinite, beryl	Quartz, orthoclase, muscovite, fluorite	Silicification, greisenization, potassic alteration	Sinian metamorphosed sandstone and slate	Granite porphyry	Re-Os: 152.0 ± 3.3 (Li et al., 2011a)
Xianetang (Jiangxi)	Quartz-vein W-Sn	–/WO_3 0.404, Sn 03587	Wolframite, scheelite, cassiterite, arsenopyrite, chalcopyrite	Quartz, K-feldspar, muscovite	Silicification, sericitization	Sinian slate and quartzite	Medium- to fine-grained porphyritic two mica granite	Ar-Ar: 231.4 ± 2.4 (Liu et al., 2008c)
Xihuashan (Jiangxi)	Quartz-vein W	WO_3 121,000/ WO_3 0.63–1.6	Wolframite, scheelite, molybdenite, bismuthinite, cassiterite, pyrite, chalcopyrite	Quartz, sericite, muscovite, calcite, fluorite	Silification, greisenization, fluoritization, carbonization	Cambrian metasandstone and metamudstone	Porphyritic granite and equigranular granite	K-Ar 150–149 (Mu et al., 1988) Sm-Nd 139.2 ± 2.8 (Li et al., 1992) Re-Os 157 ± 2.5 (Wang et al., 2011b) Rb-Sr 139.8 ± 4.5 Ar-Ar 152.8 ± 1.6 Re-Os 157.8 ± 0.9 (Hu et al., 2012)
Yaolanzhai (Jiangxi)	Quartz-vein Greisen W-Sn	WO_3 10,346; Sn 6194/WO_3 0.12; Sn 0.04	Wolframite. Scheelite, cassiterite, molybdenite, bismuthinite, sphalerite, pyrite, chalcopyrite	Quartz, feldspar, fluorite, muscovite, chlorite and epidote	Silicification, fluoritization, chloritization	Cambrian meta-arenite intercalated with slate and metapelite	Medium- to fine-grained porphyritic two-mica granite and fine-grained porphyritic muscovite granite	Re-Os 155.8 ± 2.8 (Feng et al., 2011a)
Yuntoujie (Guangxi)	Quartz-vein W-Mo	WO_3 10,000/–	Wolframite, scheelite, molybdenite, chalcopyrite, sphalerite, pyrite	Quartz, muscovite, albite, tourmaline	Greisenization, tourmalinization	Muscovite granite	Muscovite granite	Re-Os: 216.8 ± 7.5 (Wu et al., 2012)

(*continued on next page*)

Table 3 (*continued*)

Name	Metal	Reserve (t)/ Grade (%)	Ore minerals	Gangue minerals	Alteration	Host rock	Associated intrusions	Method/Age (Ma)/ Reference
Zazixi (Hunan)	Quartz-vein W-Sb	–	Scheelite, stibnite	Quartz, calcite	Silicification	Sinian meta-clastic and meta-volcanic rocks	Lamprophyre (?)	Sm-Nd: 227.3 ± 6.2 (Wang et al., 2012b)
Zhangdongkeng (Jiangxi)	Quartz-vein W	–	Wolframite, cassiterite, molybdenite, chalcopyrite	Quartz, muscovite, fluorite, topaz chlorite	Greisenization, silicification, chloritization, potassic alteration	Middle-Upper Cambrian metasandstone and slate	Medium- to fine-grained porphyritic biotite granite	Re-Os: 150.9 ± 5.3 (Feng et al., 2011a)
Zhangdou (Jiangxi)	Quartz-vein W	WO_3 40,400/–	Wolframite, scheelite, cassiterite, molybdenite, chalcopyrite	Quartz, feldspar, fluorite, muscovite, calcite	Greisenization, silicification, potash feldspathization, carbonization	Cambrian metamorphosed sandstone and slate	Medium- to fine-grained biotite granite	Re-Os: 149.1 ± 7.1 (Feng et al., 2011a)
Zhangjiadi (Jiangxi)	Quartz-vein and Greisen type W-Mo	–/WO_3 ~0.1, Mo ~0.3	Wolframite, molybdenite, chalcopyrite, cassiterite, pyrite, sphalerite, bismuthinite	Quartz, K-feldspar, fluorite, biotite, sericite, chlorite	Silicification, greisenization, chloritization	Sinian meta-clastic rocks	Medium- to fine-grained porphyritic biotite granite	Re-Os: 158.4 ± 3.1 (Quartz-vein) Re-Os: 161.9 ± 3.3 (Greisen type) (Feng et al., 2015a)

et al., 2005). Hydrothermal alteration can be a good exploration guide because alteration mineral assemblages both within the ore zones and surrounding adjacent rocks may be different. Typical porphyry W deposits in South China, such as the Yangchuling deposit in the Yangtze River region, show typical alteration sequences from early, high-temperature (potassic alteration) biotite ± K-feldspar assembalges to sericitic alteration (muscovite ± chlorite assemblages) to low-temperature advanced and intermediate argillic alteration (clay-bearing assemblages). This sequence is consistent with progressively greater acidity and higher fluid-to-rock ratios of fluids, prior to their eventual neutralization. The advanced argillic alteration occurred relatively late and was superimposed on ores and potassic alteration assemblages. In contrast, the sodic-calcic alteration (Na plagioclase-actinolite assemblages) and the propylitic alteration (albite-epi dote-chlorite-carbonate assemblages) formed from fluids with low acidity and are commonly barren. These alteration styles are generally related to volatile addition (e.g., propylitic alteration), hydrolysis (e.g., sericitic, advanced argillic, and intermediate argillic alteration), alkali exchange (e.g., potassic and sodic-calcic alteration), and addition of silica (e.g., silicic alteration) (Seedorff et al., 2005). Ore-forming fluids of porphyry W deposits show lower oxidation states (reducing), sulfidation states, and total sulfur contents than porphyries of other types, and typically lack anhydrite, possibly reflecting a dominance of reduced sulfur species over oxidized species throughout the evolutionary path (Burnham, 1980; Seedorff et al., 2005). Although porphyry W deposits are relatively rare around the world, the Yangchuling deposit is similar to porphyry W deposits at Mount Pleasant, New Brunswick (Kooiman et al., 1986), which are classified as rhyolitic porphyry W-Mo type by Seedorff et al. (2005).

7. Ages of W deposits in South China

Four episodes of Mesozoic W mineralization occurred in South China (Fig. 24). The first was from 230 to 210 Ma during the Late Triassic. These deposits are mainly located in the southern and western parts of South China, including deposits in the Xiangzhong Basin (e.g., Zazixi), the Nanling region (e.g., Keshuling and Limu) and near the Naupaijiang Basin (e.g., Nanyangtian). The second episode, from the Middle Jurassic (ca.170 Ma) to very Early Cretaceous (ca. 140 Ma) produced the deposits in the interior of South China, including those in the Nanling region and the Yangtze River region, showing a NNE-younging trend (Fig. 2). Specifically, in southern Jiangxi Province, there are areas of extremely intensive W mineralization with ages ranging from ca.165 to 150 Ma. The third period of W mineralization is poorly constrained from 136 to 120 Ma, with deposits across South China, such as the Xianglushan deposit in the Yangtze River region, the Tiemuli deposit in the Nanling region, and the Needle Hill and Lianhuashan deposits in the coastal area. The last episode is dominatedly in the southern and southwestern parts of South China with ages ranging from 100 to 80 Ma (e.g., Damingshan and Dajishan). Although the last period is not the main W mineralization stage, these deposits are associated with the large-scale Cretaceous Sn deposits in the southwestern part of South China. The episodes of W mineralization are roughly coincident with those of other metals (e.g., Sn, Fe, Cu, Pb-Zn, Ag and Au), which together show mineralization peaks in the Late Triassic, Mid-Late Jurassic, and Cretaceous (e.g., Hu and Zhou, 2012; Mao et al., 2011a, 2013a).

8. An integrated geodynamic model

After decades of work, numerous models have been proposed to explain the Mesozoic geodynamic evolution of South China. The

Table 4
Charateristics of representitative skarn W deposits in South China.

Name	Metal	Reserve (t)/Grade (%)	Ore minerals	Gangue minerals	Alteration	Host rock	Associated intrusions	Method/Age(Ma)/ Reference
Baizhangyan (Anhui)	Skarn-porphyry W-Mo	WO_3 20,000; Mo 10,000/–	Scheelite, molybdenite, pyrite	Garnet, diopside, quartz, epidote, tremolite, vesuvianite, hornblende	Silicification, chloritization	Sinian limestone	Monzonite and fine-grained granite	Re-Os: 134.1 ± 2.2 (Song et al., 2012)
Baoshan (Jiangxi)	Skarn W	WO_3 40,500/–	Scheelite, molybdenite, galena, sphalerite, pyrite, pyrrhotite, chalcopyrite	Tremolite, diopside, garnet, talc, sericite, chlorite	Skarnization	Devonian carbonate rocks	Medium-grained biotite granite	Re-Os: 164.2 ± 2.6 (This study) Re-Os: 162.9 ± 5.1 (Feng et al., 2012b)
Dawujian (Anhui)	Skarn W–Mo	–/WO_3 0.2	Scheelite, molybdenite, galena, sphalerite, pyrite, pyrrhotite, chalcopyrite	Dolomite, calcite, tremolite, diopside, talc, sericite, chlorite	Silicification, sericitization, chloritization, marbleization	Sinian meta-volcanic rock and mudstone	Granodiorite porphyry	Re-Os: 144.4 ± 1.5 (Li et al., 2015)
Gaojiabang (Anhui)	Skarn-porphyry W-Mo, Au	WO_3 62,000; Mo 5400; Au 3.79/–	Scheelite, molybdenite, magnetite, pyrrhotite, pyrite, chalcopyrite	Garnet, diopside, wollastonite, idocrase, tremolite, epidote, chlorite, quartz, sericite, calcite	Silicification, sericitization, potassic alteration, chloritization	Cambrian carbonaeous shale interlayered with marble and limestone	Fine-grained porphyritic granodiorite	Re-Os: 146.1 ± 4.8 (Fan, 2015)
Huangshaping (Hunan)	Skarn W-Mo-Cu-Pb-Zn	WO_3 152,900; Mo 43,200; Pb 761,300; Zn 15291M/WO_3 0.2; Mo 0.2; Pb 3.55; Zn 7.13	Scheelite, molybdenite, bismuthinite, native bismuth, galena, sphalerite, chalcopyrite, cassiterite	Quartz, calcite, sericite, chlorite, fluorite, garnet, diopside, tremolite	Silicification, fluoritization, chloritization, carbonization	Carboniferous limestone and sandstone	Granite porphyry	Re-Os: 154.8 ± 1.9 (Yao et al., 2007) Re-Os: 153.8 ± 4.8 (Ma et al., 2007) Re-Os: 159.4 ± 3.3 Re-Os: 157.5 ± 2.4 Re-Os: 157.6 ± 2.3 (Lei et al., 2010)
Jiaoli (Jiangxi)	Skarn W-Ag, Pb-Zn	WO_3 > 50,000; Ag > 1000; Pb + Zn > 300,000/WO_3 0.34; Ag 69.5 ppm; Pb 1.17; Zn 0.75	Scheelite, galena, sphalerite, pyrrhotite, pyrite, chalcopyrite	Grossular, andradite, diopside, fluorite, quartz, calcite, chlorite, epidote	Silicification, fluoritization, sericitization, chloritization, carbonization	Upper Cambrian clastic rocks intercalated with carbonate	Medium- to fine-grained porphyritic granodiorite	Re-Os: 170.6 ± 4.6 (Feng et al., 2012b)
Matou (Anhui)	Skarn-porphyry Cu–Mo (±W)	Mo 60,000/–	Molybdenite, chalcopyrite, pyrite, scheelite, pyrrhotite	Quartz, biotite, amphibole, chlorite, sericite, kaolinite	Silicification, sericitization,	Silurian silty slate and shale	Granodiorite porphyry	Re-Os: 149.2 ± 3.2 (Yang et al., 2014)
Nanyangtian (Yunnan)	Skarn W	WO_3 34,245/ WO_3 0.59	Scheelite, pyrrhotite, pyrite, chalcopyrite	Quartz, feldspar, muscovite, garnet, pyroxene, fluorite, tourmaline	Silicification, fluoritization, tourmalinization	Schist, gneiss, hornblende leptynite	Granite porphyry	Re-Os: 214.1 ± 4.3 (Feng et al., 2011c)
Shangfang (Fujian)	Skarn Quartz-vein W-Mo	WO_3 ~50,000/–	Scheelite, Molybdenite, pyrite, chalcopyrite, galena, sphalerite	Quartz, tourmaline, chlorite, sericite, albite, garnet, diopside, epidote, fluorite, calcite, muscovite	Greisenization, chloritization, silicification, fluoritization	Sinian schists, gneiss and amphibolite	Porphyritic biotite syenite	Re-Os: 158.1 ± 5.4 (Chen et al., 2013a)
Shizhuyuan (Hunan)	Skarn W–Sn–Mo–Bi	WO_3 800,000; Sn 486,000; Mo 200,000; Bi 100,000/ WO_3 0.35; Sn 0.36; Mo 0.07; Bi 0.17	Scheelite, wolframite, molybdenite, bismuthinite, cassiterite	Garnet, pyroxene, quartz, muscovite, biotite, fluorite, topaz, chlorite	Greisenization, sericitization, chloritization, silification, chloritization, carbonatization	Devonian limestone	Porphyritic biotite granite, equigranular biotite granite, granite porphyry	Re-Os: 151.0 ± 3.5 (Li et al., 1996) Sm-Nd: 149 ± 2 (Li et al., 2004a) Ar-Ar: 153.7 ± 0.9 (Wang et al., 2016a)
Tiemuli (Jiangxi)	Skarn W-Fe	–	Scheelite, magnetite, pyrite, pyrrhotite, arsenopyrite	Garnet, epidote, wollastonite	Silicification, chloritization, carbonization, sericitization	Upper Cambrian meta-sandstone and slate	Medium- to fine-grained biotite granite and porphyritic biotite granite	Re-Os: ~138 (Lu Lin, personal communication)

(*continued on next page*)

Table 4 (*continued*)

Name	Metal	Reserve (t)/Grade (%)	Ore minerals	Gangue minerals	Alteration	Host rock	Associated intrusions	Method/Age(Ma)/ Reference
Xianghuapu (Hunan)	Skarn W	–	Scheelite, galena, sphalerite, chalcopyrite, cassiterite, wolframite	Fluorite, calcite, dolomite, quartz, muscovite	Marbleization, fluoritization, silification, chloritization	Middle Devonian dolomite and limestone	Biotite granite	Ar-Ar: 161.3 ± 1.1 (Yuan et al., 2007)
Xianglushan (Jiangxi)	Skarn W-Pb-Zn	WO_3 210,000/ -	Scheelite, galena, sphalerite, pyrite, pyrrhotite	Tremolite, diopside, garnet, talc, sericite, chlorite	Greisenization, silicification, fluoritization, chloritization, epidotization	Cambrian limestone and dolomite	Biotite granite	U-Pb: 127.2 ± 0.7 (This study) Sm-Nd: 121 ± 11 Rb-Sr: 128 ± 3 (Zhang et al., 2008b)
Xintianling (Hunan)	Skarn W-Mo	WO_3 300,000/ WO_3 0.4	Scheelite, molybdenite, bismuthinite, galena, sphalerite, pyrrhotite, pyrite, chalcopyrite, bornite, arsenopyrite	Garnet, diopside, vesuvianite, wollastonite, tremolite, actinolite, quartz, fluorite, calcite, chlorite, epidote	Marbleization, silicification, sericitization, chloritization, epidotization	Lower Carboniferous limestone	Biotite monzonite and fine-grained biotite granite of the Qitianling batholith	Ar-Ar: 157.1 ± 0.3 (Mao et al., 2004) Rb-Sr: 157.4 ± 3.2 (Cai et al., 2008) Re-Os: 161.7 ± 9.3 (Yuan et al., 2012)
Xitian (Hunan)	Skarn Sn-W	Sn 586,000; WO_3 46,300/Sn 0.26–0.36; WO_3 0.28–0.63	Cassiterite, scheelite, pyrite, chalcopyrite, marmatite	Garnet, diopside, sericite, calcite, quartz, fluorite	Greisenization, fluoritization, silicification, marbleization	Devonian carbonate rocks	Medium-grained porphyritic biotite granite and fine-grained biotite granite	Re-Os: 150 ± 2.7 (Liu et al., 2008a) Ar-Ar: 155.6 ± 1.3 Ar-Ar: 157.2 ± 1.4 (Ma et al., 2008) Rb-Sr: 153 ± 12 (Fu et al., 2012)
Xushan (Jiangxi)	Skarn Quartz-vein W-Cu	–	Scheelite, Wolframite, Chalcopyrite	Quartz, muscovite, calcite, diopside, garnet, tourmaline	Albitization, greisenization, silicification, carbonization, tourmalization	Sinian metamorphosed sandstone and slate	Biotite granite	Rb-Sr: 147.1 ± 3.4 (Li et al., 2011b)
Yaogangxian (Hunan)	Skarn Quartz-vein W-Mo	WO_3 236,000/WO_3 1.27	Wolframite, molybdenite, arsenopyrite, cassiterite, chalcopyrite, pyrite, bournonite, bismuthinite	Quartz, muscovite, feldspar, fluorite, calcite	Silicification, fluoritization, sericitization, chloritization, carbonization	Cambrian metasandstone and slate, Devonian limestone	Two-mica granite	Re-Os: 154.9 ± 2.6 Ar-Ar: 153.0 ± 1.1 Ar-Ar: 155.1 ± 1.1 (Peng et al., 2006)
Yaoling (Guangdong)	Skarn Quartz-vein Greisen W	–/WO_3 1.35 (quartz-vein), 0.43 (skarn), 0.34 (greisen-type)	Wolframite, scheelite, cassiterite, chalcopyrite, pyrite, arsenopyrite, galena, sphalerite	Quartz, tourmaline, fluorite, muscovite	Silicification, chloritization, sericitization, greisenization, tourmalization	Cambrian to middle Devonian meta-sedimentary quartzites, slates and interlayered limestone, siltstones and cherts	Baijizhai biotite granite	Re-Os: 159.5 ± 2.8 (Qi et al., 2012)
Zhuxi (Jiangxi)	Skarn W-Cu	WO_3 1M/–	Scheelite, pyrrhotite, molybdenite, sphalerite, chalcopyrite, arsenopyrite, stibnite	Garnet, diopside, tremolite, wollastonite, quartz, chlorite, calcite	Silicification, chloritization, carbonization	Sinian phyllite, meta-sandstone, slate and Middle Carboniferous to Triassic limestone, dolomite	Biotite granite and granite porphyry	Re-Os: 145.1 ± 1.5 (Li, 2014) Sm-Nd: 144 ± 5 (Hu, 2015)

Table 5
Charateristics of representitative porphyry W deposits in South China.

Name	Metal	Reserve (t)/Grade (%)	Ore minerals	Gangue minerals	Alteration	Host rock	Associated intrusions	Method/Age(Ma)/Reference
Dabaoshan (Guangdong)	Porphyry Cu–W–Mo	WO_3 45,000; Mo 52,000; Cu 313,000; Pb 20,000; Zn 52,000; Fe 11M/WO_3 0.3; Mo 0.07; Cu 0.86; Pb 1.77; Zn 4.44; Fe 48.21	Molybdenite, pyrite, chalcopyrite, sphalerite, wolframite, magnetite, hematie, cassiterite	Diopside, garnet, quartz, sericite, muscovite	Greisenization, silicification, sericitization, potassic alteration	Devonian carbonate rocks	Dacite porphyry, granodiorite porphyry	Re-Os: 163.9 ± 1.3 (Wang et al., 2011c)
Lianhuashan (Guangdong)	Porphyry W	WO_3 33,831/WO_3 0.04	Wolframite, scheelite, pyrite	Muscovite, quartz, andalusite, sericite	Greisenization, silification,	Early Jurassic sandstone, shale, and felsic volcanic rock	Biotite granite, quartz porphyry	K-Ar: 129.4 ± 1.2 (Bai et al., 1983)
Qimen (Dongyuan)	Porphyry W-Mo	WO_3 94,500/–	Scheelite, chalcopyrite, pyrite, galena, molybdenite, bismuthinite, sphalerite	Quartz, muscovite, chlorite, sericite	Silicification, potassic alteration, sericitization, chloritization	Neoproterozoic phyllite, slate and meta-siltstone	Granodiorite porphyry	Re-Os: 146.4 ± 2.3 (Zhou et al., 2011)
Xingluokeng (Fujian)	Porphyry Quartz-vein W-Mo	WO_3 304,300/Mo 0.02; WO_3 0.23	Scheelite, Wolframite, Molybdenite	Lepidolite, apatite, feldspar, fluorite, calcite, quartz, muscovite	Potassic alteration, greisenization, sericitization, albitization, chloritization, silicification	Neoprotenzoic metamorphic rocks	Biotite porphyritic granite	Rb-Sr: 147.5 ± 2.9 Re-Os: 156.3 ± 4.8 (Zhang et al., 2008a)
Yangchuling (Jiangxi)	Porphyry W-Mo	–	Scheelite, molybdenite, pyrite, pyrrhotite, chalcopyrite	Quartz, K-feldspar, muscovite, sericite, chlorite, calcite	Potassic alteration, silicification, sericitization, carbonization	Monzonite and hornfel	Monzonite	K-Ar: 134.0 ± 4.7 (Man et al., 1988)
Zhongjia (Fujian)	Porphyry Sn-W	–	Cassiterite, wolframite, chalcopyrite, molybdenite, pyrite, bismuthinite, pyrrhotite	Quartz, chlorite, topaz, fluorite, sericite, biotite	Greisenization, chloritization, topazization	Cambrian to Ordovician meta-sandstone	Biotite granite and quartz porphyry	Re-Os: 193–196 (Zhang et al., 2003)

majority of these models suggest that South China was affected by collision of the South China and Indochina Blocks in the Triassic, whereas subduction of the paleo-Pacific plate dominated in the Jurassic (Cai and Zhang, 2009; Charvet et al., 1994; Chen et al., 2004, 2008a, 2008b; Chu et al., 2012; Cui et al., 2013; Li et al., 2014a, 2007, 2014b, 2012d, 2014c; Li and Li, 2007; Liu et al., 2012a, 2012b; Mao et al., 2013a; Sun et al., 2007; Sun et al., 2012; Wang et al., 2011a, 2013c; Zhou and Li, 2000; Zhou et al., 2006). Many of these models also try to link the widespread Mesozoic magmatism with the known orogenies (e.g., Li and Li, 2007; Zhou et al., 2006). For example, the flat-slab subduction model (Li et al., 2012c; Li and Li, 2007) suggests that the flat-slab subduction of the paleo-Pacific plate led to orogeny in the Triassic and that subsequent slab break-off and rollback caused the vast magmatism from the interior to the coastal area of South China. Zhou and Li (2000) and Zhou et al. (2006) proposed the gradual rollback of a low-angle paleo-Pacific plate to explain the regional extension and magmatism in South China during the Mesozoic. Mao et al. (2013a) postulated a tear-off of the subducting slab in Middle Jurassic (ca. 170–160 Ma) and a shift of the subduction of the paleo-Pacific plate from a NW-direction to parallel with the Eurasia continental margin at 134–80 Ma to explain the vast metallogenesis in South China during these periods. Other proposals include post-orogeny extension (Chen et al., 2008b), Basin and Range-like continental rifting and extension in a continental, back arc basin with fault-induced remelting (Gilder et al., 1991; Li, 2000), an intraplate lithospheric event such as closure of an oceanic basin (Hsü et al., 1990; Li, 1998) and continental thinning by a mantle plume (Deng et al., 2004).

However, most proposed models lack detailed descriptions and a rationale interpretation for the transformation from the Triassic Indosinian domain to the Jurassic Pacific domain. Moreover, many of these models fail to explain the vast metallogenesis, especially W mineralization, in the Mesozoic of South China. Here, we present our geodynamic model of the region after integrating previous work and emphasizing the relationship between the ridge subduction and the vast metallogenesis in the region.

8.1. Triassic

Collision between the South China and North China Blocks along the Qinling-Dabie Orogenic Belt, and between the South China and the Indochina Blocks along the Song-Ma Suture formed an amalgamated block between 258 and 220 Ma (Cai and Zhang, 2009; Carter et al., 2001; Qiu et al., 2016b; Zhou et al., 2006). The widespread orogeny resulted in NNE-SSW shortening accommodated by NE-SW strike-slip shear zones and ~S- and N-verging folds (Cai and Zhang, 2009; Lepvrier et al., 2004; Li et al., 2016, 2006; Qiu et al., 2016a; Wang et al., 2013c). The corresponding abundant Triassic granites of peraluminous affinity with highly aluminous minerals, such as muscovite, garnet and tourmaline, are classified as S-type (Sun et al., 2005; Zhou et al., 2006) or minor A-type (e.g., Gao et al., 2014; Li et al., 2012b; Sun et al., 2011) granites resulting from crustal melting. Furthermore, the Early to Middle Triassic gneissic or mylonitized granitoids are interpreted as syn-collisional plutons in a compressional setting produced by the closure of the paleo-Tethys ocean (Zhou et al., 2006). The Middle to Late Triassic granitoids are interpreted as late-collisional plutons in a locally extensional environment after the Early Triassic collisions (Zhou et al., 2006). However, Li and Li (2007) argued that the ages of the Permian to Triassic NW-verging thrusts, metamorphism, and synorogenic magmatism all have a similar trend of younging toward the interior of the South China Block, which is proposed to result from the northwestern-directed flat subduction of the paleo-Pacific plate. Furthermore, Calc-alkaline magmatism in the West Philippine Block (260–250 Ma) (Knittel et al., 2010),

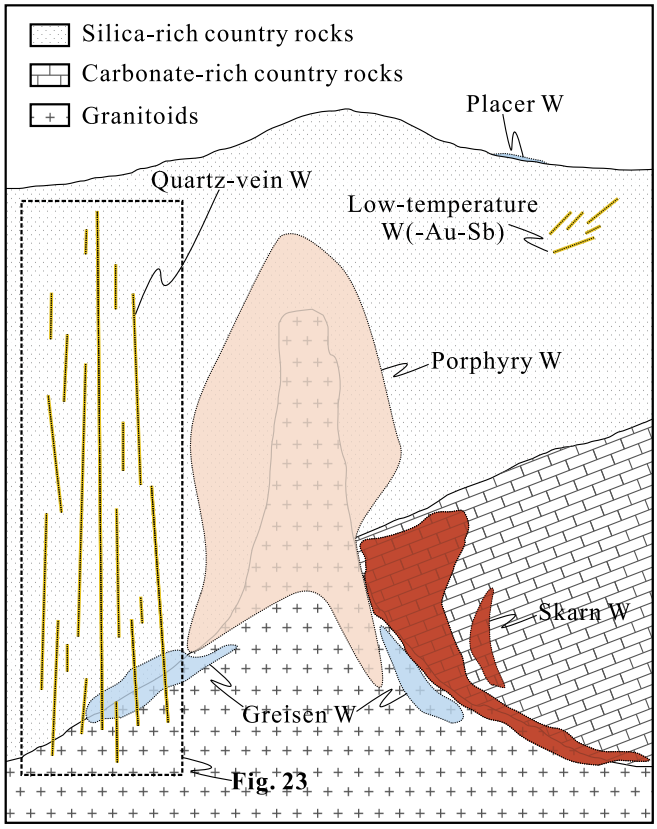

Fig. 22. Cartoon showing the positions of the different types of tungsten mineralization relative to the causative granites.

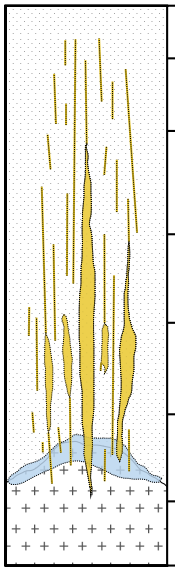

Types (thickness)	Mineral associations	Economic significance
Veinlets (1mm~1cm)	Cst+Wfm+Ms +Tur	Barren; vectors for ores
Thin veins (0.02~0.1m)	Wfm+Cst+Brl +Ccp+Py+Ms	High-grade
Thick veins (0.05~0.5m)	Wfm+Sch+Csl +Ccp+Py+Gn +Sp+Ms	Very high-grade
Lodes (0.2~2m)	Wfm+Ccp+Py +Gn+Mol	High-grade
Greisen and veins	Wfm+Sch+Ccp +Py+Gn+Mol	High-grade
Granitoids	-	Barren

Fig. 23. Simplified summary of the "Five-floor" model for the granite-related W(-Sn) deposits in the Nanling region, modified after Wu et al. (1987) and Xu et al. (2008).

and the Permian accretion of the Akiyoshi-Sawadani Complex with metamorphism in the South Kitakami Belt, Japan at ca. 260 – 230 Ma (Cawood et al., 2009; Ernst et al., 2007; Isozaki et al., 2010; Miyamoto and Yanagi, 1996; Suzuki and Adachi, 1994), are thought to record the initial subduction of the paleo-Pacific plate during the Permian (Li et al., 2016, 2006; Li and Li, 2007). Currently, it is still unsettled whether the paleo-Tethys tectonic

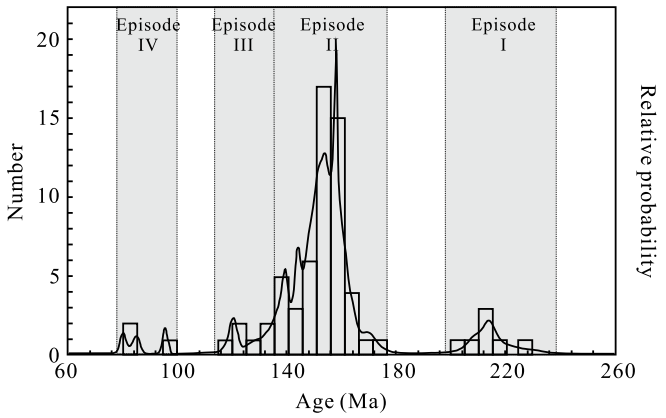

Fig. 24. Age distribution of the Mesozoic tungsten deposits in South China.

domain or the paleo-Pacific domain was responsible for the Triassic tectonism of the South China Block, and how and when the setting changed from the Tethyan regime to the Pacific regime. Because both NW- and NE-verging structures are present in the South China Block, we suspect a combined effect of flat subduction and collision dynamics in the paleo-Pacific and Tethys tectonic domains during the Triassic.

As the result of the gradual closure of paleo-Tethys ocean and initiation of flat subduction of the paleo-Pacific plate, a series of Triassic S-type granitoids were emplaced in locally extensional environments (Li and Li, 2007; Mao et al., 2013a; Zhou et al., 2006), which were responsible for the W polymetallic mineralization in the southwestern part of South China (e.g., the Nanyangtian, Liguifu, Yuntoujie, Gaoling, Exiantang, Limu, and Keshuling deposits). By the Late Triassic, the NE-trending slab front had propagated more than 1000 km inland (Li and Li, 2007), and reached the northwestern side of the Nanling region. Ahead of the slab front, deep-seated granitic magmas might have caused outward migration of mineralizing fluids in a regional thermal gradient, resulting in the formation of low-temperature W-Sb-Au deposits (e.g., Zazixi) in the Xiangzhong basin (Hu et al., 2016).

8.2. Jurassic

An E-W-trending Middle Jurassic bimodal volcanic belt, composed of alkaline and tholeiitic basalt, along with rhyolite and minor andesite, is recognized in southern Hunan, Jiangxi, and Fujian Provinces, indicating a rift environment (Mao et al., 2013a; Zhou et al., 2006). However, the Late Jurassic granitoids in the Nanling region are strongly differentiated, and their origin remains controversial (Mao et al., 2013a). On the basis enrichment of SiO_2 and Al_2O_3, coupled with depletion of mafic components, these granitoids are considered as S-type (Xu et al., 1982; Zhao et al., 2015b). However, some workers argue that they are A-type granitoids because of their enriched alkaline components (Jiang et al., 2008), or even highly differentiated I-type granitoids due to their lack of Al-rich minerals (Li and Li, 2007). An abundance of mafic enclaves in these granitoids suggests a mantle contributions (Zhu et al., 2005). A series of E-W-trending Middle Jurassic granitoids in this region show low t_{DM} and high ε_{Nd} (−4.0 to −8.0), implying crust-mantle interaction during lithospheric extension (Chen and Jahn, 1998; Gilder et al., 1996; Zhou et al., 2006). Accordingly, we propose that an E-W-trending mid-ocean ridge was subducted and then broke off under the Nanling region in the Middle Jurassic (Fig. 25a). This is consistent with the findings of Sun et al. (2007) and Ling et al. (2009) that the ridge between the Izanagi plate and the Pacific plate was subducted under the East

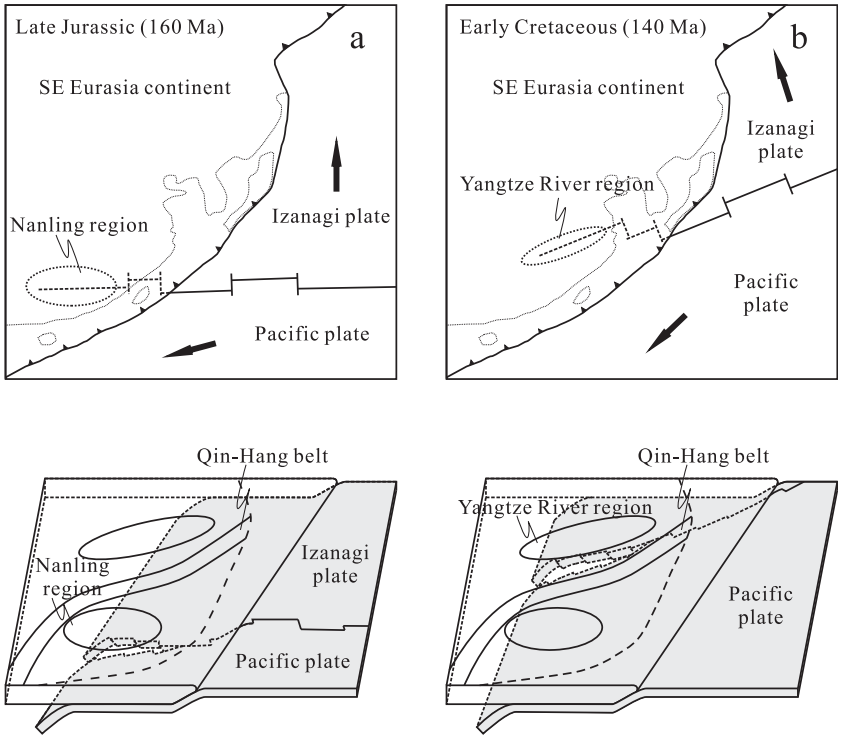

Fig. 25. Cartoons showing the MOR subduction underneath South China Block during Late Jurassic (a) and Early Cretaceous (b).

Eurasia continent. On the basis of the estimated northward drifting rate (~5 cm/yr) of the paleo-Pacific plate (Ling et al., 2009), the ridge would also roughly have been under the Nanling region during the Middle Jurassic, and under the Yangtze River region during the Early Cretaceous (Fig. 25b). Because E-W-trending structures dominate in the Nanling region and NE-directed structures occur in the Yangtze River region, we suggest that the subducting ridge segment was rorated anticlockwise from E-W to SW, during its NW-ward movement from the Nanling region to the Yangtze River region. In fact, the anticlockwise rotation of the paleo-Pacific plate is well recorded on the modern Pacific ocean floor (Fig. 26). The distribution and ages of island chains on the Pacific ocean floor indicate that the Pacific plate was drifting SW-ward from the Mid-Jurassic to the Early Cretaceous (Koppers et al., 2001; Sun et al., 2007). In additon, the magmatic anomalies in the modern Pacific ocean floor show that the Pacific plate was drifting anticlockwise during Middle to Late Jurassic (Ludden et al., 2006) (Fig. 26). From the Late Jurassic (ca. 160 Ma), the Southeast China Block rotated clockwise (Zhu et al., 1998). Accordingly, the northwest-ward and anticlockwise movement of the ridge segment between the Pacific plate and the Izanagi plate resulted in the large-scale, NE-younging magmatism between the Nanling region and the Yangtze River region, where it has obviously low t_{DM} and high ε_{Nd}, implying a continuous interaction of mantle and crustal material (Zhou et al., 2006).

In the Nanling region, we suspect that breakoff of the ridge segment occurred in the earliest Jurassic (ca. 190 Ma), because A-type granites, such as the Keshubei pluton in the eastern Nanling region appeared at that time (Li and Li, 2007). Upwelling of the asthenoshperic mantle resulted in bimodal volcanism in rift basins, with minor mafic components formed at the early stage (180–170 Ma). At a later stage, underplating basaltic magmas induced melting of the upper crust, resulting in the strongly differentiated granitoids. These granitoids originated from partial melting of the upper crust with mantle input, resulting in strong differentiation and gradual enrichment of W and other ore-forming elements in the fractionated hydrothermal fluids. Carbonate country rocks favored the development of skarn-greisen ore deposits proximal to the pluton-country rock contacts (e.g., Baoshan and Shizhuyuan). Where clastic and/or metamorphic rocks were the country rocks, wolframite-quartz vein-type ore deposits were preferentially formed (e.g., Xihuashan).

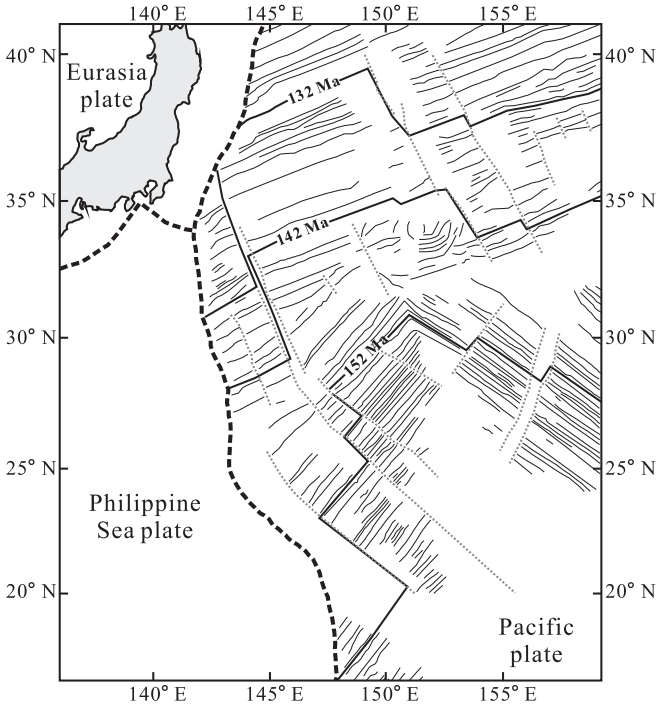

Fig. 26. Magnetic anomalies of the modern Pacific Ocean floor, modified after Ludden et al. (2006).

The NE-ward younging trend of the W deposits is exactly consistent with the movement of the ridge segment. As shown by the magnetic anomalies in the Pacific ocean floor (Ludden et al., 2006), the anticlockwise rotation primarily took place before ca. 150 Ma, which is also recorded by the triple junction migration on the Shatsky Rise (Mahoney et al., 2005). Hence, we suggest that rotation of the ridge segment took place under the eastern Nanling region, where there are widespread W deposits with ages of ca. 165–150 Ma.

8.3. Cretaceous

In the earliest Cretaceous (ca. 140 Ma), the mid-ocean ridge between the Pacific and Izanagi plates migrated to the Yangtze River region (Ling et al., 2009). The NE-trending slab window of the ridge is thought to have been under the southern part of the Yangtze River region, which has recently been defined as the North Yangtze Tungsten Belt (Mao et al., 2013b, 2015). Peraluminous granitoids were generated by partial melting of crustal materials due to upwelling asthenosphere through the slab window (Fig. 25b). In the northern part of the Yangtze River region, i.e. traditionally the Middle-Lower Yangtze River Valley Metallogenic Belt (Mao et al., 2011b), adakitic rocks and Cu-Au mineralization were derived from the partial melting of the Izanagi slab and thickened mafic continental crust, and the addition of various proportions of juvenile mantle compositions from ca. 145 to 135 Ma.

The post-136-Ma tectonic regime of South China is considered to be extensional, represented by the formation of widespread extensional basin systems (Li et al., 2012a, 2013, 2014a; Li, 2000; Zhou et al., 2006). Slab rollback or retreat of the subducted plate, as indicated by the oceanward migration of the subduction hinge (Fig. 27a), is proposed to be responsible for the extensional rifting (Li et al., 2014a; Li and Li, 2007). Li et al. (2014a) recognized three tectonic stages between 136 and 86 Ma. In the first stage (136–118 Ma) extension caused significant subsidence, triggered voluminous magmatism and generated widespread NE-trending extensional basins and dome structures (Li, 2000; Zhou and Li, 2000; Zhou et al., 2006). Here, we propose that the NW-SE-directed slab rollback of the Pacific plate. which started at ca. 136 Ma and the northwestward movement of the Izanagi plate, resulted in extensive asthenosphere upwelling through the resulting slab window to form the A-type granitoids in the Yangtze River region (Fig. 27a). During this stage, the late Early Cretaceous W mineralization took place across all of South China region and formed a large number of deposits, such as the Xianglushan, Tiemuli, Lianhuashan, and Machang bodies. During a short period in the Late Early Cretaceous (117–108 Ma), a tectonic inversion is proposed in response to the collision of the West Philippine Block with the East Eurasia continental margin (Fig. 27b), which led to cessation of extension-related magmatism (Charvet et al., 1994; Li et al., 2014a). During the Late Cretaceous (107–86 Ma), South China was controlled by WNW-ESE extension caused by the ESE-ward retreat and the subsequent WNW-ward subduction (Li et al., 2014a). The change of subduction direction of the Pacific plate from NW to WNW (Fig. 27b), could have resulted in intensive mantle-crust interaction in the southwestern part of South China, creating the ca. 100–80-Ma W deposits with large-scale Sn mineralization in this region.

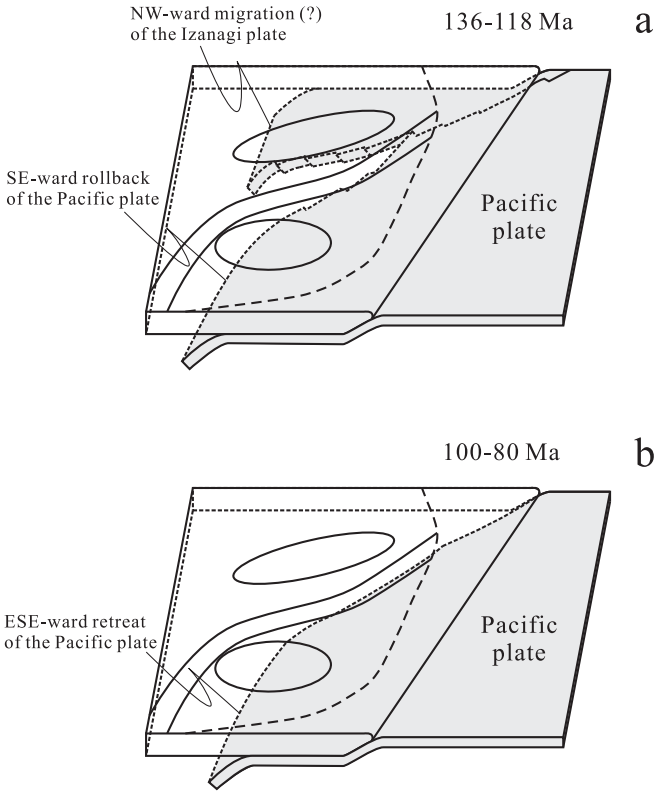

Fig. 27. Cartoons showing the slab rollback and retreat underneath South China Block during Cretaceous. (a) 136–118 Ma; (b) 100–80 Ma.

9. Conclusions

The W deposits in South China are dominated by skarn, greisen and quartz-vein, and porphyry types, all genetically related to highly fractionated granitoids. Four episodes of W mineralization events are recognized; 230–210 Ma, 170–140 Ma, 136–120 Ma, and 100–80 Ma, which were the result of the closure of the paleo-Tethys ocean and subduction of the paleo-Pacific plate. In the Late Triassic, both closure of paleo-Tethys and the subduction of the paleo-Pacific plate caused local extensional settings, which resulted in emplacement of peraluminous granitoids and formation of W deposits in the central and western parts of South China. In the Middle Jurassic, break-off along the subducted mid ocean ridge between the Pacific and Izanagi plates resulted in E-W-trending emplacement of highly fractionated granites in the Nanling region. The following anticlockwise rotation of the ridge segment and the paleo-Pacific plate created the widespread S-type intrusions and associated Middle Jurassic to Early Cretaceous W mineralization in the interior of South China with a NNE-younging trend from the Nanling region to the Yangtze River region. At ca. 136 Ma, rollback of the subducted Pacific plate started along the ridge segment, producing a slab window that resulted in weak W mineralization across South China. Finally, a change in the direction of slab retreat from NW-SE to WNW-ESE caused the intensive mineralization in the southwestern part of South China.

Acknowledgements

We express our sincere thanks to Prof. Paul T. Robinson, Prof. Wei Wang, Dr. Jianhua Li, and Dr. Yuanyuan Liu for their constructive suggestions and comments. Special thanks to Stephen Hui Geological Museum for providing samples. This study was financially supported by grants from the Special Fund for Public Welfare Professions from the Ministry of Land and Resources of the People's Republic of China (201411050), the National Key Research and Development Plan (2016YFC0600207), the Stephen Hui Trust Fund and the CRCG of HKU.

References

Aleksandrov, S.M., 1998. Geochemistry of Skarn and Ore Formation in Dolomites. VSP. 300 pp.

Bai, Y., Man, F., Ni, S., Li, T., 1983. K-Ar dating of Lianhuashan tungsten ore deposit. Geochimica 2, 133–139.

Barton, M.D., 1987. Lithophile-element mineralization associated with Late Cretaceous two-mica granites in the Great Basin. Geology 15 (4), 337–340.

Blevin, P.L., Chappell, B.W., 1992. The role of magma sources, oxidation states and fractionation in determining the granite metallogeny of eastern Australia. Transact. Roy. Soc. Edinburgh: Earth Sci. 83 (1–2), 305–316.

Bowman, J.R., Covert, J., Clark, A., Mathieson, G., 1985. The CanTung E Zone scheelite skarn orebody, Tungsten, Northwest Territories; oxygen, hydrogen, and carbon isotope studies. Econ. Geol. 80 (7), 1872–1895.

Burnham, C.W., 1979. Magmas and hydrothermal fluids. In: Barnes, H.L. (Ed.), Geochemistry of Hydrothermal Ore Deposits. John Wiley and Sons, New York, pp. 71–136.

Burnham, C.W., 1980. Late-stage processes of felsic magmatism. Soc. Min. Geol. Jpn. 8, 1–11.

Burnham, C.W., 1985. Energy release in subvolcanic environments; implications for breccia formation. Econ. Geol. 80 (6), 1515–1522.

Cai, J.-X., Zhang, K.-J., 2009. A new model for the Indochina and South China collision during the Late Permian to the Middle Triassic. Tectonophysics 467 (1), 35–43.

Cai, M., Han, F., He, L., Liu, G., Chen, K., Fu, J., 2008. He, Ar isotope characteristics and Rb-Sr dating of the Xintianling skarn scheelite deposit in southern Hunan, China. Acta Geosci. Sinica 29 (2), 167–173.

Cai, Y., 1984. A study of the genetic type of Xingluokeng tungsten (molybdenum) deposit, Fujian province. Miner. Depos. 3 (1), 28–36.

Candela, P.A., Bouton, S.L., 1990. The influence of oxygen fugacity on tungsten and molybdenum partitioning between silicate melts and ilmenite. Econ. Geol. 85 (3), 633–640.

Carter, A., Roques, D., Bristow, C., Kinny, P., 2001. Understanding Mesozoic accretion in Southeast Asia: significance of Triassic thermotectonism (Indosinian orogeny) in Vietnam. Geology 29 (3), 211–214.

Cawood, P.A., Kröner, A., Collins, W.J., Kusky, T.M., Mooney, W.D., Windley, B.F., 2009. Accretionary orogens through Earth history. Geol. Soc., Lond., Spec. Publ. 318 (1), 1–36.

Černý, P., Blevin, P., Cuney, M., London, D., 2005. Granite-related ore deposits. Soc. Econ. Geol. 100, 337–370.

Chang, Y.F., Liu, X.P., Wu, Y.C., 1991. The Copper–Iron Belt of the Lower and Middle Reaches of the Changjiang River. Geology Publication House, Beijing, pp. 71–76.

Charvet, J., Lapierre, H., Yu, Y., 1994. Geodynamic significance of the Mesozoic volcanism of southeastern China. J. SE Asian Earth Sci. 9 (4), 387–396.

Chen, B., Zhou, X., 2012. Ore-controlling factors and a metallogenic model for the Xianglushan tungsten-ore field in northern Jiangxi Province. Geol. Explor. 48 (3), 562–569.

Chen, C.-H., Lin, W., Lan, C.-Y., Lee, C.-Y., 2004. Geochemical, Sr and Nd isotopic characteristics and tectonic implications for three stages of igneous rock in the Late Yanshanian (Cretaceous) orogeny, SE China. Transact. Roy. Soc. Edinburgh-Earth Sci 95, 237–248.

Chen, C.-H., Lee, C.-Y., Lu, H.-Y., Hsieh, P.-S., 2008a. Generation of Late Cretaceous silicic rocks in SE China: age, major element and numerical simulation constraints. J. Asian Earth Sci. 31 (4), 479–498.

Chen, C.-H., Lee, C.-Y., Shinjo, R., 2008b. Was there Jurassic paleo-Pacific subduction in South China?: constraints from $^{40}Ar/^{39}Ar$ dating, elemental and Sr–Nd–Pb isotopic geochemistry of the Mesozoic basalts. Lithos 106 (1), 83–92.

Chen, G., 1990. Geology and genesis of the Xianglushan concealed scheelite deposit. Geol. Prospect. 6, 4.

Chen, G., Wan, H., Shu, L., Zhang, C., Kang, C., 2012a. An analysis on ore-controlling conditions and geological features of the Cu-W polymetallic ore deposit in the Zhuxi area of Jingdezhen, Jiangxi Province. Acta Petrol. Sinica 28 (12), 3901–3914.

Chen, G., Shu, L., Shu, L., Zhang, C., Ouyang, Y., 2016. Geological characteristics and mineralization setting of the Zhuxi tungsten (copper) polymetallic deposit in the Eastern Jiangnan Orogen. Sci. China Earth Sci. 59 (4), 803–823.

Chen, J.F., Jahn, B.M., 1998. Crustal evolution of southeastern China: Nd and Sr isotopic evidence. Tectonophysics 284 (1–2), 101–133.

Chen, L., Qin, K., Li, J., Xiao, B., Li, G., Zhao, J., Fan, X., 2012b. Fluid inclusions and hydrogen, oxygen, sulfur isotopes of Nuri Cu-W-Mo deposit in the southern Gangdese, Tibet. Resour. Geol. 62 (1), 42–62.

Chen, P., Hua, R., Zhang, B., Lu, J., Fan, C., 2002. Early Yanshanian post-orogenic granitoids in the Nanling region. Sci. China, Ser. D Earth Sci. 45 (8), 755–768.

Chen, R.-S., Li, J.-E., Cao, K., Qu, C.-Y., Li, Y.-J., 2013a. Zircon U-Pb and molybdenite Re-Os dating of the Shangfang tungsten deposit in northern Fujian provinceL Implications for regional mineralization. Earth Sci. – J. China Univ. Geosci. 38 (2), 289–304.

Chen, W.T., Zhou, M.-F., Zhao, X.-F., 2013b. Late Paleoproterozoic sedimentary and mafic rocks in the Hekou area, SW China: implication for the reconstruction of the Yangtze Block in Columbia. Precambr. Res. 231, 61–77.

Chen, Z., Wang, D., Qu, W., Chen, Y., Wang, P., Xu, J., Zhang, J., Xu, M., 2006. Geological characteristics and mineralization age of the Taoxikeng tungsten deposit in Chongyi County, southern Jiangxi Province, China. Geol. Bull. China 25 (4), 496–501.

Chu, Y., Faure, M., Lin, W., Wang, Q., 2012. Early Mesozoic tectonics of the South China block: insights from the Xuefengshan intracontinental orogen. J. Asian Earth Sci. 61, 199–220.

Cooke, D.R., Hollings, P., Walshe, J.L., 2005. Giant porphyry deposits: characteristics, distribution, and tectonic controls. Econ. Geol. 100 (5), 801–818.

Cui, J., Zhang, Y., Dong, S., Jahn, B.-M., Xu, X., Ma, L., 2013. Zircon U-Pb geochronology of the Mesozoic metamorphic rocks and granitoids in the coastal tectonic zone of SE China: constraints on the timing of Late Mesozoic orogeny. J. Asian Earth Sci. 62, 237–252.

Darbyshire, D.P.F., Sewell, R.J., 1997. Nd and Sr isotope geochemistry of plutonic rocks from Hong Kong: implications for granite petrogenesis, regional structure and crustal evolution. Chem. Geol. 143 (1), 81–93.

Davis, D.W., Sewell, R.J., Campbell, S.D.G., 1997. U-Pb dating of Mesozoic igneous rocks from Hong Kong. J. Geol. Soc. 154 (6), 1067–1076.

Davis, S.G., 1958. Tungsten mineralization in Hong Kong and the New Territories. Econ. Geol. 53 (4), 481–488.

Davis, S.G., 1961. Mineralogy and genesis of the wolframite ore deposits, Needle Hill Mine, New Territories, Hong Kong. Econ. Geol. 56 (7), 1238–1249.

Deng, J.F., Mo, X.X., Zhao, H.L., Wu, Z.X., Luo, Z.H., Su, S.G., 2004. A new model for the dynamic evolution of Chinese lithosphere:'continental roots–plume tectonics'. Earth Sci. Rev. 65 (3), 223–275.

Di, Y., Wu, G., Zhang, D., Song, B., Zang, W., Zhang, Z., Li, J., 2005. SHRIMP U-Pb zircon geochronology of the Xiaotongguanshan and Shatanjiao intrusions and its petrological implications in the Tongling area, Anhui. Acta Geol. Sinica 79 (6), 795–802.

Dick, L.A., Hodgson, C.J., 1982. The MacTung W-Cu (Zn) contact metasomatic and related deposits of the northeastern Canadian Cordillera. Econ. Geol. 77 (4), 845–867.

Einaudi, M.T., Meinert, L.D., Newberry, R.J., 1981. Skarn deposits. Econ. Geol. 75, 317–391.

Ernst, W.G., Tsujimori, T., Zhang, R., Liou, J.G., 2007. Permo-Triassic collision, subduction-zone metamorphism, and tectonic exhumation along the East Asian continental margin. Annu. Rev. Earth Planet. Sci. 35, 73–110.

Eugster, H.P., 1985. Granites and hydrothermal ore deposits: a geochemical framework. Mineral. Mag. 49 (350), 7–23.

Fan, Y., 2015. Study on Tungsten-Molybdenum Mineralization in Qingyang Area. Hefei University of Technology, Hefei University of Technology, Anhui province. 125 pp.

Feng, C., Huang, F., Qu, W., Zeng, Z., Ding, M., 2011a. Molybdenite Re-Os isotopic dating on different types of tungsten deposits in southeast of Jiulongnao orefield and its geological significances. China Tungsten Ind. 26 (4), 6–11.

Feng, C., Huang, F., Zeng, Z., Qu, W., Ding, M., 2011b. Isotopic chronology of Jiulongnao granite and Hongshuizhai greisens-type tungsten deposit in South Jiangxi Province. J. Jilin Univ. (Earth Science Edition) 41, 112–121.

Feng, C., Wang, S., Zeng, Z., Zhang, D., Li, D., She, H., 2012a. Fluid inclusion and chronology studies of Baxiannao mineralized fractured zone-type tungsten polymetallic deposit, southern Jiangxi Province, China. Acta Geol. Sinica 28 (1), 52–64.

Feng, C., Zeng, Z., Wang, S., Liang, J., Ding, M., 2012b. SHRIMP zircon U-Pb and molybdenite Re-Os dating of the skarn-type tungsten deposits in Southern Jiangxi Province, China, and geological implications: examplified by the Jiaoli and Baoshan tungsten polymetallic deposits. Geotectonica et Metallogenia 36 (3), 337–349.

Feng, C., Zhang, D., Xiang, X., Li, D., Qu, H., Liu, J., Xiao, Y., 2012c. Re-Os isotopic dating of molybdenite from the Dahutang tungsten deposit in northwestern Jiangxi Province and its geological implication. Acta Petrol. Sinica 28 (12), 3858–3868.

Feng, C., Zhang, D., Zeng, Z., Wang, S., 2012d. Chronology of the tungsten deposits in southern Jiangxi Province, and episodes and zonation of the regional W-Sn mineralization–evidence from high-precision zircon U-Pb, molybdenite Re-Os and muscovite Ar-Ar ages. Acta Geol. Sinica 86 (3), 555–567.

Feng, C., Li, C., Li, D., Zhou, A., Li, H., 2013. Ore-controlling structure and 40Ar/39Ar geochronology of Kekekaerde tungsten-tin deposit in Qimantage area, Xinjiang. Miner. Depos. 32 (1), 207–216.

Feng, C., Zeng, Z., Qu, W., Liu, J., Li, H., 2015a. A geochronological study of granite and related mineralization of the Zhangjiadi molybdenite-tungsten deposit in Xingguo County, southern Jiangxi Province, China, and its geological significance. Acta Geol. Sinica 31 (3), 709–724.

Feng, C., Zhao, Z., Qu, W., Zeng, Z., 2015b. Temporal consistency between granite evolution and tungsten mineralization in Huamei'ao, southern Jiangxi Province, China: Evidence from precise zircon U-Pb, molybdenite Re–Os, and muscovite $^{40}Ar–^{39}Ar$ isotope geochronology. Ore Geol. Rev. 65, 1005–1020.

Feng, J.R., Mao, J.W., Pei, R.F., Li, C., 2011c. Ore-forming fluids and metallogenesis of Nanyangtian tungsten deposit in Laojunshan, southeastern Yunnan Province. Miner. Depos. 30 (3), 403–419.

Fu, J., Li, H., Qu, W., Yang, X., Wei, J., Liu, G., Ma, L., 2007. Re-Os isotope dating of the Da' ao tungsten- tin deposit in the Jiuyi Mountains, southern Hunan Province. Geol. China 34 (4), 651–656.

Fu, J., Li, H., Qu, W., Ma, L., Yang, X., Wei, J., Liu, G., 2008. Determination of mineralization epoch of quartz-vein type tungsten deposit in Shixing region, northern Guangdong and its geological significance. Geotectonica et Metallogenia 32 (1), 57–62.

Fu, J., Li, X., Cheng, S., Xu, D., Ma, L., Chen, X., 2009. Metallogenic ages of tungsten–tin polymetallic deposits in Lianping area, northern Guangdong Province. Geol. China 36, 1331–1339.

Fu, J., Cheng, S., Lu, Y., Wu, S., Ma, L., Chen, X., 2012. Geochronology of the greisen-quartz-vein type tungsten-tin deposit and its host granite in Xitian, Hunan province. Geol. Explor. 48 (2), 313–320.
Gao, L., Chen, J., Ding, X., Liu, Y., Zhang, C., Zhang, H., Liu, Y., Pang, W., Zhang, Y., 2011. Zircon SHRIMP U-Pb dating of the tuff bed of Lengjiaxi and Banxi groups, northeastern Hunan: constraints on the Wuling Movement. Geol. Bull. China 30 (7), 1001–1008.
Gao, P., Zhao, Z.-F., Zheng, Y.-F., 2014. Petrogenesis of Triassic granites from the Nanling Range in South China: implications for geochemical diversity in granites. Lithos 210, 40–56.
Gilder, S.A., Keller, G.R., Luo, M., Goodell, P.C., 1991. Eastern Asia and the western Pacific timing and spatial distribution of rifting in China. Tectonophysics 197 (2), 225–243.
Gilder, S.A., Gill, J., Coe, R.S., Zhao, X., Liu, Z., Wang, G., Yuan, K., Liu, W., Kuang, G., Wu, H., 1996. Isotopic and paleomagnetic constraints on the Mesozoic tectonic evolution of south China. J. Geophys. Res.: Solid Earth 101 (B7), 16137–16154.
Giuliani, G., Li, Y.D., Sheng, T.F., 1988. Fluid inclusion study of Xihuashan tungsten deposit in the southern Jiangxi province, China. Miner. Depos. 23 (1), 24–33.
Goodell, P.C., Gilder, S.A., Fang, X., 1991. A preliminary description of the Gan-Hang failed rift, southeastern China. Tectonophysics 197 (2–4), 245–255.
Guo, C., 2010. Study on Mineralization-Related Mesozoic Granitoids in Chongyi-Shangyou Counties, South Jiangxi and, Comparison to Corresponding Granitoids in the Nanling Region, South China. Chinese Academy of Geological Sciences, Chinese Academy of Geological Sciences. 249 pp.
Guo, C., Mao, J., Bierlein, F., Chen, Z., Chen, Y., Li, C., Zeng, Z., 2011. SHRIMP U-Pb (zircon), Ar–Ar (muscovite) and Re–Os (molybdenite) isotopic dating of the Taoxikeng tungsten deposit, South China Block. Ore Geol. Rev. 43 (1), 26–39.
Guo, C., Chen, Y., Zeng, Z., Lou, F., 2012. Petrogenesis of the Xihuashan granites in southeastern China: Constraints from geochemistry and in-situ analyses of zircon U Pb Hf O isotopes. Lithos 148, 209–227.
Hsü, K.J., Li, J., Chen, H., Wang, Q., Sun, S., Şengör, A., 1990. Tectonics of South China: key to understanding West Pacific geology. Tectonophysics 183 (1–4), 9–39.
Hu, R.Z., Wei, W.F., Bi, X.W., Peng, J.T., Qi, Y.Q., Wu, L.Y., Chen, Y.W., 2012. Molybdenite Re–Os and muscovite $^{40}Ar/^{39}Ar$ dating of the Xihuashan tungsten deposit, central Nanling district, South China. Lithos 150, 111–118.
Hu, R.Z., Zhou, M.F., 2012. Multiple Mesozoic mineralization events in South China-an introduction to the thematic issue. Miner. Depos. 47 (6), 579–588.
Hu, R.Z., Fu, S.L., Huang, Y., Zhou, M.F., Fu, S.H., Zhao, C.H., Wang, Y.J., Bi, X.W., Xiao, J. F., 2016. The giant South China Mesozoic low-temperature metallogenic domain: reviews and a new geodynamic model. J. Asian Earth Sci. 137, 9–34.
Hu, Z., 2015. The Formation Conditions and Metallogenic Regularity of Zhuxi Tungsten Polymetallic Deposit in Northeast of Jiangxi Province. Chengdu University of Technology, Chengdu University of Technology, p. 207.
Hua, R.M., Chen, P.R., Zhang, W.L., Lu, J.J., 2005. Three major metallogenic events in Mesozoic in South China. Miner. Depos. 24 (2), 99–107.
Huang, F., Feng, C., Chen, Y., Ying, L., Chen, Z., Zeng, Z., Qu, W., 2011. Isotopic chronological study of the Huangsha-Tieshanlong quartz vein-type tungsten deposit and timescale of molybdenum mineralization in southern Jiangxi Province, China. Acta Geol. Sinica 85 (6), 1434–1447.
Huang, L.C., Jiang, S.Y., 2014. Highly fractionated S-type granites from the giant Dahutang tungsten deposit in Jiangnan Orogen, Southeast China: geochronology, petrogenesis and their relationship with W-mineralization. Lithos 202, 207–226.
Isozaki, Y., Aoki, K., Nakama, T., Yanai, S., 2010. New insight into a subduction-related orogen: a reappraisal of the geotectonic framework and evolution of the Japanese Islands. Gondwana Res. 18 (1), 82–105.
Jiang, G.H., Hu, R.Z., Xie, G.Q., Zhao, J.H., Tang, Q.L., 2004. K-Ar ages of plutonism and mineralization at the Dajishan tungsten deposit, Jiangxi Province, China. Acta Minal. Sinica 24, 253–256.
Jiang, S.-H., Bagas, L., Hu, P., Han, N., Chen, C.-L., Liu, Y., Kang, H., 2016. Zircon U-Pb ages and Sr–Nd–Hf isotopes of the highly fractionated granite with tetrad REE patterns in the Shamai tungsten deposit in eastern Inner Mongolia, China: implications for the timing of mineralization and ore genesis. Lithos 261, 322–339.
Jiang, S.-Y., Zhao, K.-D., Jiang, Y.-H., Dai, B.-Z., 2008. Characteristics and genesis of Mesozoic A-type granites and associated mineral deposits in the southern Hunan and northern Guangxi provinces along the Shi-Hang belt, South China. Geol. J. China Univ. 14 (4), 496–509.
Jiang, S.-Y., Peng, N., Huang, L.-C., Xu, Y., Zhan, G., Dan, X., 2015. Geological characteristic and ore genesis of the giant tungsten deposits from the Dahutang ore-concentrated district in northern Jiangxi Province. Acta Geol. Sinica 31 (3), 639–655.
Jiang, Y.-H., Zhao, P., Zhou, Q., Liao, S.-Y., Jin, G.-D., 2011. Petrogenesis and tectonic implications of Early Cretaceous S-and A-type granites in the northwest of the Gan-Hang rift, SE China. Lithos 121 (1), 55–73.
Johnson, V.Y., Keith, J.D., 1991. Petrology and geochemistry of the Springer scheelite skarn deposit, Mill City, Nevada. Geol. Depos. Great Basin 2, 553–576.
Keith, J.D., van Middelaar, W., Clark, A.H., Hodgson, C.J., 1989. Granitoid textures, compositions, and volatile fugacities associated with the formation of tungsten-dominated skarn deposits. In: Whitney, J.A., Naldrett, A.J. (Eds.), Ore Deposition Associated with Magmas, Reviews in Economic Geology. Society of Economic Geologists Inc., Littleton, pp. 235–250.
Klepper, M.R., 1947. The Sangdong tungsten deposit, southern Korea. Econ. Geol. 42 (5), 465–477.
Knittel, U., Hung, C.-H., Yang, T.F., Iizuka, Y., 2010. Permian arc magmatism in Mindoro, the Philippines: an early Indosinian event in the Palawan Continental Terrane. Tectonophysics 493 (1), 113–117.
Kooiman, G.J.A., McLeod, M.J., Sinclair, W.D., 1986. Porphyry tungsten-molybdenum orebodies, polymetallic veins and replacement bodies, and tin-bearing greisen zones in the Fire Tower Zone, Mount Pleasant, New Brunswick. Econ. Geol. 81 (6), 1356–1373.
Koppers, A.A.P., Morgan, J.P., Morgan, J.W., Staudigel, H., 2001. Testing the fixed hotspot hypothesis using $^{40}Ar/^{39}Ar$ age progressions along seamount trails. Earth Planet. Sci. Lett. 185 (3), 237–252.
Kwak, T.A.P., 1978. The conditions of formation of the King Island scheelite contact skarn, King Island, Tasmania, Australia. Am. J. Sci. 278 (7), 969–999.
Kwak, T.A.P., Tan, T.H., 1981. The importance of $CaCl_2$ in fluid composition trends; evidence from the King Island (Dolphin) skarn deposit. Econ. Geol. 76 (4), 955–960.
Kwak, T.A.P., White, A.J.R., 1982. Contrasting W-Mo-Cu and W-Sn-F skarn types and related granitoids. Min. Geol. 32 (174), 339–351.
Le Bel, L., Li, Y.-D., Sheng, J.-F., 1984. Granitic evolution of the Xihuashan-Dangping (Jiangxi, China) tungsten-bearing system. Tschermaks Mineralogische und Petrographische Mitteilungen 33 (3), 149–167.
Lei, Z., Chen, F., Chen, Z., Xu, Y., Gong, S., Li, h., Mei, Y., Qu, W., Wang, D., 2010. Petrogenetic and metallogenic age determination of the Huangshaping lead-zinc polymetallic deposit and its geological significance. Acta Geosci. Sinica 31 (4), 532–540.
Lepvrier, C., Maluski, H., van Tich, V., Leyreloup, A., Thi, P.T., van Vuong, N., 2004. The early Triassic Indosinian orogeny in Vietnam (Truong Son Belt and Kontum Massif); implications for the geodynamic evolution of Indochina. Tectonophysics 393 (1), 87–118.
Li, B., Zhang, Z., Wu, M., Zhou, T., Zhao, W., 2015. LA-ICP-MS zircon U-Pb age and molybdenite Re-Os dating of the Dawujian W-Mo polymetallic deposit, Ningguo, Anhui Province. Geol. Bull. China 34 (2–3), 569–578.
Li, G., Hua, R., Huang, X., Wei, X., Qu, W., Wang, X., 2011a. Re-Os isotopic age of molybdenite from Xiatongling tungsten deposit, cantral Jiangxi province, and its geological implications. Miner. Depos. 30 (6), 1075–1084.
Li, G., Hua, R., Wei, X., Wang, X., Huang, X., 2011b. Rb-Sr isochron age of single-grain muscovite in the Xushan W-Cu deposit, central Jiangxi, and its geological significance. Earth Sci. – J. China Univ. Geosci. 36 (2), 282–288.
Li, H., Liu, J., Du, G., Wei, L., 1992. A chronological study on endogenic metallogenic deposit: An example from Xihuashan tungsten deposit. Chin. Sci. Bull. 12, 1109–1112.
Li, H., Mao, J., Sun, Y., Zou, X., He, H., Du, A., 1996. Re-Os isotopic chronology of molybdenites in the Shizhuyuan polymetallic tungsten deposit, Southern Hunan. Geol. Rev. 42 (3), 261–267.
Li, J.-W., Zhao, X.-F., Zhou, M.-F., Vasconcelos, P., Ma, C.-Q., Deng, X.-D., de Souza, Z.S., Zhao, Y.-X., Wu, G., 2008a. Origin of the Tongshankou porphyry–skarn Cu–Mo deposit, eastern Yangtze craton, Eastern China: geochronological, geochemical, and Sr–Nd–Hf isotopic constraints. Miner. Deposita 43 (3), 315–336.
Li, J.-W., Zhao, X.-F., Zhou, M.-F., Ma, C.-Q., de Souza, Z.S., Vasconcelos, P., 2009a. Late Mesozoic magmatism from the Daye region, eastern China: U-Pb ages, petrogenesis, and geodynamic implications. Contrib. Miner. Petrol. 157 (3), 383–409.
Li, J., Zhang, Y., Dong, S., Li, H., 2012a. Late Mesozoic-Early Cenozoic deformation history of the Yuanma Basin, central South China. Tectonophysics 570, 163–183.
Li, J., Zhang, Y., Dong, S., Su, J., Li, Y., Cui, J., Shi, W., 2013. The Hengshan low-angle normal fault zone: Structural and geochronological constraints on the Late Mesozoic crustal extension in South China. Tectonophysics 606, 97–115.
Li, J., Zhang, Y., Dong, S., Johnston, S.T., 2014a. Cretaceous tectonic evolution of South China: a preliminary synthesis. Earth Sci. Rev. 134, 98–136.
Li, J., Dong, S., Zhang, Y., Zhao, G., Johnston, S.T., Cui, J., Xin, Y., 2016. New insights into Phanerozoic tectonics of south China: Part 1, polyphase deformation in the Jiuling and Lianyunshan domains of the central Jiangnan Orogen. J. Geophys. Res.: Solid Earth 121 (4), 3048–3080.
Li, S., Wang, D., Liang, T., Qu, W., Ying, L., 2008b. Metal logenic epochs of the Damingshan tungsten deposit in Guangxi and its prospecting potential. Acta Geol. Sinica 82 (7), 873–879.
Li, W.Y., Ma, C.Q., Liu, Y.Y., Robinson, P.T., 2012b. Discovery of the Indosinian aluminum A-type granite in Zhejiang Province and its geological significance. Sci. China Earth Sci. 55 (1), 13–25.
Li, X.-H., 2000. Cretaceous magmatism and lithospheric extension in Southeast China. J. Asian Earth Sci. 18 (3), 293–305.
Li, X.-H., Li, Z.-X., Ge, W., Zhou, H., Li, W., Liu, Y., Wingate, M.T., 2003. Neoproterozoic granitoids in South China: crustal melting above a mantle plume at ca. 825 Ma? Precambr. Res. 122 (1), 45–83.
Li, X.-H., Liu, D., Sun, M., Li, W.-X., Liang, X.-R., Liu, Y., 2004a. Precise Sm–Nd and U-Pb isotopic dating of the supergiant Shizhuyuan polymetallic deposit and its host granite, SE China. Geol. Mag. 141 (02), 225–231.
Li, X.-H., Li, Z.-X., Li, W.-X., Liu, Y., Yuan, C., Wei, G.-J., Qi, C.-S., 2007. U-Pb zircon, geochemical and Sr-Nd-Hf isotopic constraints on age and origin of Jurassic I- and A-type granites from central Guangdong, SE China: a major igneous event in response to foundering of a subducted flat-slab? Lithos 96 (1–2), 186–204.
Li, X.-H., Li, W.-X., Li, Z.-X., Lo, C.-H., Wang, J., Ye, M.-F., Yang, Y.-H., 2009b. Amalgamation between the Yangtze and Cathaysia Blocks in South China: constraints from SHRIMP U-Pb zircon ages, geochemistry and Nd-Hf isotopes of the Shuangxiwu volcanic rocks. Precambr. Res. 174 (1–2), 117–128.

Li, X.-H., Li, W.-X., Wang, X.-C., Li, Q.-L., Liu, Y., Tang, G.-Q., Gao, Y.-Y., Wu, F.-Y., 2010a. SIMS U-Pb zircon geochronology of porphyry Cu–Au–(Mo) deposits in the Yangtze River Metallogenic Belt, eastern China: magmatic response to early Cretaceous lithospheric extension. Lithos 119 (3), 427–438.
Li, X.-H., Li, Z.-X., He, B., Li, W.-X., Li, Q.-L., Gao, Y., Wang, X.-C., 2012c. The Early Permian active continental margin and crustal growth of the Cathaysia Block: in situ U-Pb, Lu–Hf and O isotope analyses of detrital zircons. Chem. Geol. 328, 195–207.
Li, X.H., Li, Z.X., Li, W.X., Wang, Y., 2006. Initiation of the Indosinian Orogeny in South China: evidence for a Permian magmatic arc on Hainan Island. J. Geol. 114 (3), 341–353.
Li, Y., Mao, J., Guo, B., Shao, Y., Fei, H., Hu, H., 2004b. Re-Os dating of molybdenite from the Nannihu Mo(-W) orefield in the east Qinling and its geodynamic significance. Acta Geol. Sinica 78 (2), 463–470.
Li, Y., 2014. A Study of the Metallogenesis of the Zhuxi W-(Cu) Polymetallic Deposit, Jiangxi Province. China University of Geosciences (Beijing), China University of Geosciences (Beijing) (in Chinese with English abstract).
Li, Y.H.M., Zhou, M.-F., Lai, K.W., Chan, L.S., Chen, W.T., 2014b. Geochemical and geochronological constraints on Late Jurassic volcanic rocks at Tuen Mun, Hong Kong, with implications for the Palaeo-Pacific subduction. Int. Geol. Rev. 56 (4), 408–429.
Li, Z.-X., 1998. Tectonic history of the major east Asian lithospheric blocks since the mid-Proterozoic—a synthesis. In: Flower, M.F.J., Chung, S.-L., Lo, C.-H., Lee, T.-Y. (Eds.), Mantle Dynamics and Plate Interactions in East Asia, Geodynamics. American Geophysical Union, Washington, pp. 221–243.
Li, Z.-X., Li, X.-H., 2007. Formation of the 1300-km-wide intracontinental orogen and postorogenic magmatic province in Mesozoic South China: a flat-slab subduction model. Geology 35 (2), 179–182.
Li, Z.-X., Li, X.-H., Li, W.-X., Ding, S., 2008c. Was Cathaysia part of Proterozoic Laurentia?–new data from Hainan Island, south China. Terra Nova 20 (2), 154–164.
Li, Z.-X., Li, X.-H., Wartho, J.-A., Clark, C., Li, W.-X., Zhang, C.-L., Bao, C., 2010b. Magmatic and metamorphic events during the early Paleozoic Wuyi-Yunkai orogeny, southeastern South China: New age constraints and pressure-temperature conditions. Geol. Soc. Am. Bull. 122 (5–6), 772–793.
Li, Z.-X., Li, X.-H., Chung, S.-L., Lo, C.-H., Xu, X., Li, W.-X., 2012d. Magmatic switch-on and switch-off along the South China continental margin since the Permian: Transition from an Andean-type to a Western Pacific-type plate boundary. Tectonophysics 532, 271–290.
Li, Z., 1995. A study of rock-forming and ore-forming temperatures of the Lianhuashan tungsten deposit, Guangdong Province. Miner. Depos. 14, 260–271.
Li, Z., Qiu, J.-S., Yang, X.-M., 2014c. A review of the geochronology and geochemistry of Late Yanshanian (Cretaceous) plutons along the Fujian coastal area of southeastern China: implications for magma evolution related to slab break-off and rollback in the Cretaceous. Earth Sci. Rev. 128, 232–248.
Ling, M.-X., Wang, F.-Y., Ding, X., Hu, Y.-H., Zhou, J.-B., Zartman, R.E., Yang, X.-Y., Sun, W., 2009. Cretaceous ridge subduction along the lower Yangtze River belt, eastern China. Econ. Geol. 104 (2), 303–321.
Liu, C., Deng, J., Kong, W., Xu, L., Zhao, G., Luo, Z., Li, N., 2011. LA-ICP-MS zircon U-Pb geochronology of the fine-grained granite and molybdenite Re-Os dating in the Wurinitu molybdenum deposit, Inner Mongolia, China. Acta Geol. Sinica 85 (5), 1057–1066.
Liu, G., Wu, S., Du, A., Fu, J., Yang, X., Tang, Z., Wei, J., 2008a. Metallogenic ages of the Xitian tungsten-tin deposit, eastern Hunan province. Geotectonica et Metallogenia 32 (1), 63–71.
Liu, J., Ye, H., Xie, G., Yang, G., Zhang, W., 2008b. Re-Os dating of molybdenite from the Hukeng tungsten deposit in the Wugongshan area, Jiangxi province, and its geological significance. Acta Geol. Sinica 82 (11), 1576–1583.
Liu, L., Xu, X., Zou, H., 2012a. Episodic eruptions of the Late Mesozoic volcanic sequences in southeastern Zhejiang, SE China: petrogenesis and implications for the geodynamics of paleo-Pacific subduction. Lithos 154, 166–180.
Liu, Q., Yu, J.-H., Wang, Q., Su, B., Zhou, M.-F., Xu, H., Cui, X., 2012b. Ages and geochemistry of granites in the Pingtan-Dongshan Metamorphic Belt, Coastal South China: new constraints on Late Mesozoic magmatic evolution. Lithos 150, 268–286.
Liu, R., Zhou, H., Zhang, L., Zhong, Z., Zeng, W., Xiang, H., Jin, S., Lu, X., Li, C., 2009. Paleoproterozoic reworking of ancient crust in the Cathaysia Block, South China: Evidence from zircon trace elements, U-Pb and Lu-Hf isotopes. Chin. Sci. Bull. 54 (9), 1543–1554.
Liu, S., Wang, D., Chen, Y., Li, J., Ying, L., Xu, J., Zeng, Z., 2008c. $^{40}Ar/^{39}Ar$ ages of muscovite from different types tungsten-bearing quartz veins in the Chong-Yu-You concentrated mineral area in Gannan region and its geological significance. Acta Geol. Sinica 82 (7), 932–940.
Liu, S., Chen, Y., Fan, S., Xu, J., Qu, W., Ying, L., 2010. The second ore-prospecting space in the eastern and central parts of the Nanling metallogenic belt: evidence from isotopic chronology. Geol. China 37 (4), 1034–1049.
Liu, Y., Dai, T., Lu, H., Xu, Y., Wang, C., Kang, W., 1997. $^{40}Ar–^{39}Ar$ and Sm–Nd isotopic ages for the Qianlishan granite and its mineralization. Sci. China (Ser. D) 27, 425–430.
Liu, Y., Lu, H., Wang, C., Xu, Y., Kang, W., Zeng, T., 1998. On the ore-forming conditions and ore-forming model of the superlarge multimetal deposit in Shizhuyuan. Sci. China, Ser. D Earth Sci. 41 (5), 502–512.
Liu, Z., Liu, S., Chen, Y., Wang, C., Wan, H., Chen, G., Li, S., Liang, L., 2014. LA-ICP-MS zircon U-Pb isotopic dating of lamprophyre located Zhuxi copper-tungsten mine of Jiangxi Province and its geological significance. Rock Miner. Anal. 33 (55), 758–766.
Long, W.G., Ding, S.J., Ma, D.Q., Liu, Y.H., Mo, W.M., 2005. Formation and evolution of the Precambrian basement in Hainan island. Earth Sci.-J. China Univ. Geosci. 30 (4), 421–429.
Lu, H.-Z., Liu, Y., Wang, C., Xu, Y., Li, H., 2003. Mineralization and fluid inclusion study of the Shizhuyuan W-Sn-Bi-Mo-F skarn deposit, Hunan Province, China. Econ. Geol. 98 (5), 955–974.
Ludden, J.N., Plank, T., Larson, R., Escutia, C., 2006. Leg 185 synthesis: sampling the oldest crust in the ocean basins to understand Earth's geodynamic and geochemical fluxes. In: Proceedings of the Ocean Drilling Program - Scientific Results, p. 35.
Ma, L., Lu, Y., Qu, W., Fu, J., 2007. Re-Os isotopic chronology of molybdenites in Huangshaping lead-zinc deposit, southeast Hunan, and its geological implications. Miner. Depos. 26 (4), 425–431.
Ma, L., Fu, J., Wu, S., Xu, D., Yang, X., 2008. $^{40}Ar/^{39}Ar$ isotopic dating of the Longshang tin- polymetallic deposit, Xitian orefield, eastern Hunan. Geol. China 35 (4), 706–713.
Mahoney, J.J., Duncan, R.A., Tejada, M.L.G., Sager, W.W., Bralower, T.J., 2005. Jurassic-Cretaceous boundary age and mid-ocean-ridge–type mantle source for Shatsky Rise. Geology 33 (3), 185–188.
Mahood, G., Hildreth, W., 1983. Large partition coefficients for trace elements in high-silica rhyolites. Geochim. Cosmochim. Acta 47 (1), 11–30.
Man, F.S., Bai, Y.Z., Ni, S.B., Li, T., 1983. Preliminary isotope studies of the Lianhuashan tungsten ore deposit. Miner. Depos. 2, 35–42.
Man, F.S., Wang, X.S., 1988. Study on the isotopic geochronology of Yangchuling porphyry type of tungsten and molybdenum deposit. Miner. Resour. Geol. 2 (1), 61–67.
Manning, D.A.C., Henderson, P., 1984. The behaviour of tungsten in granitic melt-vapour systems. Contrib. Miner. Petrol. 86 (3), 286–293.
Mao, J.W., Li, H.Y., Pei, R.F., Raimbaull, L., Guy, B., 1995. Geology and geochemistry of the Qianlishan granite stock and its relationship to polymetallic tungsten mineralization. Miner. Depos. 14 (12–25).
Mao, J.W., Guy, B., Raimbaull, L., Shimazaki, H., 1996. Manganese skarn in the Shizhuyuan polymetallic tungsten deposit, Hunan, China. Resour. Geol. 46, 1–11.
Mao, J.W., Li, H.Y., Song, X.X., Rui, B., Xu, Y., Wang, D.H., Lan, X.M., Zhang, K.J., 1998. Geology and Geochemistry of the Shizhuyuan W-Sn-Mo-Bi Polymetallic Deposit, Hunan, China. Geological Pulishing House, Beijing. 215 pp.
Mao, J.W., Li, X.F., Lehmann, B., Chen, W., Lan, X.M., Wei, S.L., 2004. $^{40}Ar–^{39}Ar$ dating of tin ores and related granite in Furong tin orefield, Hunan Province, and its geodynamic significance. Miner. Depos. 22, 164–175.
Mao, J.W., Wang, Y.T., Lehmann, B., Yu, J.J., Du, A.D., Mei, Y.X., Li, Y.F., Zang, W.S., Stein, H.J., Zhou, T.F., 2006. Molybdenite Re–Os and albite $^{40}Ar/^{39}Ar$ dating of Cu–Au–Mo and magnetite porphyry systems in the Yangtze River valley and metallogenic implications. Ore Geol. Rev. 29 (3), 307–324.
Mao, J.W., Pirajno, F., Cook, N., 2011a. Mesozoic metallogeny in East China and corresponding geodynamic settings—an introduction to the special issue. Ore Geol. Rev. 43 (1), 1–7.
Mao, J.W., Xie, G.Q., Duan, C., Pirajno, F., Ishiyama, D., Chen, Y.C., 2011b. A tectono-genetic model for porphyry-skarn-stratabound Cu-Au-Mo-Fe and magnetite-apatite deposits along the Middle-Lower Yangtze River Valley, Eastern China. Ore Geol. Rev. 43 (1), 294–314.
Mao, J.W., Cheng, Y.B., Chen, M.H., Pirajno, F., 2013a. Major types and time-space distribution of Mesozoic ore deposits in South China and their geodynamic settings. Miner. Depos. 48 (3), 267–294.
Mao, Z.H., Cheng, Y.B., Liu, J.J., Yuan, S.D., Wu, S.H., Xiang, X.K., Luo, X.H., 2013b. Geology and molybdenite Re-Os age of the Dahutang granite-related veinlets-disseminated tungsten ore field in the Jiangxin Province, China. Ore Geol. Rev. 53, 422–433.
Mao, Z.H., Liu, J.J., Mao, J.W., Deng, J., Zhang, F., Meng, X.Y., Xiong, B.K., Xiang, X.K., Luo, X.H., 2015. Geochronology and geochemistry of granitoids related to the giant Dahutang tungsten deposit, middle Yangtze River region, China: implications for petrogenesis, geodynamic setting, and mineralization. Gondwana Res. 28 (2), 816–836.
Maruéjol, P., Cuney, M., Turpin, L., 1990. Magmatic and hydrothermal REE fractionation in the Xihuashan granites (SE China). Contrib. Miner. Petrol. 104 (6), 668–680.
McKee, E.H., Rytuba, J.J., Xu, K., 1987. Geochronology of the Xihuashan composite granitic body and tungsten mineralization, Jiangxi province, south China. Econ. Geol. 82 (1), 218–223.
Meinert, L.D., Dipple, G.M., Nicolescu, S., 2005. World skarn deposits. Econ. Geol. 100, 299–336.
Miyamoto, T., Yanagi, T., 1996. U-Pb dating of detrital zircons from the Sangun metamorphic rocks, Kyushu, Southwest Japan: an evidence for 1.9–2.0 Ga granite emplacement in the provenance. Geochem. J. 30 (5), 261–271.
Mu, Z., Huang, F., Lu, D., 1988. Potassium-argon ages of some tungsten-bearing granites in South China. Acta Petrol. Mineral. 7 (2), 109–118.
Newberry, R.J., 1983. The formation of subcalcic garnet in scheelite-bearing skarns. Can. Mineral. 21, 529–544.
Newberry, R.J., Swanson, S.E., 1986. Scheelite skarn granitoids: an evaluation of the roles of magmatic source and process. Ore Geol. Rev. 1 (1), 57–81.
Newberry, R.J., Einaudi, M.T., Eastman, H.S., 1991. Zoning and genesis of the Darwin Pb-Zn-Ag skarn deposit, California; a reinterpretation based on new data. Econ. Geol. 86 (5), 960–982.

Newberry, R.J., 1998. W-and Sn-skarn deposits: a 1998 status report. In: Lentz, D.R. (Ed.), Mineralized Intrusion-Related Skarn Systems. Mineralogical Association of Canada, Ottawa, pp. 289–335.
Nie, F.J., Jiang, S.H., 2011. Geological setting and origin of Mo–W–Cu deposits in the Honggor-Shamai district, Inner Mongolia, North China. Resour. Geol. 61 (4), 344–355.
Pan, Y., Dong, P., 1999. The Lower Changjiang (Yangzi/Yangtze River) metallogenic belt, east central China: intrusion-and wall rock-hosted Cu–Fe–Au, Mo, Zn, Pb, Ag deposits. Ore Geol. Rev. 15 (4), 177–242.
Peng, J.T., Zhou, M.-F., Hu, R.Z., Shen, N.P., Yuan, S.D., Bi, X.W., Du, A.D., Qu, W.J., 2006. Precise molybdenite Re–Os and mica Ar–Ar dating of the Mesozoic Yaogangxian tungsten deposit, central Nanling district, South China. Miner. Deposita 41 (7), 661–669.
Peng, J.T., Zhang, D.L., Hu, R.Z., Wu, M.J., Lin, Y.X., 2008. Sm-Nd and Sr isotope geochemistry of hydrothermal scheelite from the Zhazixi W-Sb Deposit, Western Hunan. Acta Geol. Sinica 82, 1514–1521.
Qi, H.-W., Hu, R.-Z., Wang, X.-F., Qu, W.-J., Bi, X.-W., Peng, J.-T., 2012. Molybdenite Re–Os and muscovite $^{40}Ar/^{39}Ar$ dating of quartz vein-type W-Sn polymetallic deposits in Northern Guangdong, South China. Miner. Depos. 47 (6), 607–622.
Qi, Y., Hu, R., Liu, S., Coulson, I.M., Qi, H., Tian, J., Zhu, J., 2016. Petrogenesis and geodynamic setting of Early Cretaceous mafic–ultramafic intrusions, South China: a case study from the Gan-Hang tectonic belt. Lithos 258, 149–162.
Qiu, L., Yan, D.-P., Tang, S.-L., Wang, Q., Yang, W.-X., Tang, X., Wang, J., 2016a. Mesozoic geology of southwestern China: Indosinian foreland overthrusting and subsequent deformation. J. Asian Earth Sci. 122, 91–105.
Qiu, L., Yan, D.-P., Yang, W.-X., Wang, J., Tang, X., Ariser, S., 2016b. Early to Middle Triassic sedimentary records in the Youjiang Basin, South China: Implications for Indosinian orogenesis. J. Asian Earth Sci. http://dx.doi.org/10.1016/j.jseaes.2016.09.020.
Qiu, Y.M., Gao, S., McNaughton, N.J., Groves, D.I., Ling, W., 2000. First evidence of >3.2 Ga continental crust in the Yangtze craton of south China and its implications for Archean crustal evolution and Phanerozoic tectonics. Geology 28 (1), 11–14.
Redmond, P.B., Einaudi, M.T., Inan, E.E., Landtwing, M.R., Heinrich, C.A., 2004. Copper deposition by fluid cooling in intrusion-centered systems: new insights from the Bingham porphyry ore deposit, Utah. Geology 32 (3), 217–220.
Roberts, K.J., Strange, P.J., 1991. The geology and exploitation of the Needle Hill wolframite deposit. Geol. Soc. Hong Kong Newslett. 9 (4), 29–40.
Rusk, B., Reed, M., 2002. Scanning electron microscope–cathodoluminescence analysis of quartz reveals complex growth histories in veins from the Butte porphyry copper deposit, Montana. Geology 30 (8), 727–730.
Seedorff, E., Dilles, J.H., Proffett, J.M., Einaudi, M.T., Zurcher, L., Stavast, W.J.A., Johnson, D.A., Barton, M.D., 2005. Porphyry deposits: characteristics and origin of hypogene features. Econ. Geol. 29, 251–298. 100th anniversary.
Sewell, R.J., Campbell, S.D.G., 1997. Geochemistry of coeval Mesozoic plutonic and volcanic suites in Hong Kong. J. Geol. Soc. 154 (6), 1053–1066.
Sewell, R.J., Davis, D.W., Campbell, S.D.G., 2012. High precision U-Pb zircon ages for Mesozoic igneous rocks from Hong Kong. J. Asian Earth Sci. 43 (1), 164–175.
Shao, J., Li, X., Yang, H., 2011. Zircon SHRIMP U-Pb dating of granite in the Cuihongshan polymetallic deposit and its geological implications. Acta Geosci. Sinica 32 (2), 163–170.
Shen, W.-Z., Xu, S.-J., Wang, Y.-X., 1994. Study on the Nd-Sr isotope of the Xihuashan granite. Chin. Sci. Bull. 39 (8), 653–657.
Sheng, J., Liu, L., Wang, D., Chen, Z., Ying, L., Huang, F., Wang, J., Zeng, L., 2015. A preliminary review of metallogenic regularity of tungsten deposits in China. Acta Geol. Sinica 89 (4), 1359–1374.
Shimazaki, H., 1977. Grossular-spessartine-almandine garnets from some Japanese scheelite skarns. Cnad. Mineral. 15, 74–80.
Shu, L.-S., Faure, M., Yu, J.-H., Jahn, B.-M., 2011. Geochronological and geochemical features of the Cathaysia block (South China): new evidence for the Neoproterozoic breakup of Rodinia. Precambr. Res. 187 (3), 263–276.
Shu, L.S., Zhou, X.M., Deng, P., Wang, B., Jiang, S.-Y., Yu, J.H., Zhao, X.X., 2009. Mesozoic tectonic evolution of the Southeast China Block: new insights from basin analysis. J. Asian Earth Sci. 34 (3), 376–391.
Sillitoe, R.H., 2010. Porphyry copper systems. Econ. Geol. 105 (1), 3–41.
Song, G.X., Qin, K.Z., Li, G.M., Liu, T.B., Li, J.X., Li, X.H., Chang, Z.S., 2012. Geochronologic and isotope geochemical constraints on magmatism and associated W-Mo mineralization of the Jitoushan W-Mo deposit, middle-lower Yangtze Valley. Int. Geol. Rev. 54 (13), 1532–1547.
Sun, F., Xu, X., Zou, H., Xia, Y., 2015. Petrogenesis and magmatic evolution of ~130 Ma A-type granites in Southeast China. J. Asian Earth Sci. 98, 209–224.
Sun, T., Zhou, X., Chen, P., Li, H., Zhou, H., Wang, Z., Shen, W., 2005. Strongly peraluminous granites of Mesozoic in Eastern Nanling Range, southern China: petrogenesis and implications for tectonics. Sci. China, Ser. D Earth Sci. 48 (2), 165–174.
Sun, T., 2006. A new map showing the distribution of granites in South China and its explanatory notes. Geol. Bull. China 25 (3), 332–335.
Sun, W.-D., Xie, Z., Chen, J., Zhang, X., Chai, Z., Du, A., Zhao, J., Zhang, C., Zhou, T., 2003. Os-Os dating of copper and molybdenum deposits along the middle and lower reaches of the Yangtze River, China. Econ. Geol. 98 (1), 175–180.
Sun, W.-D., Ding, X., Hu, Y.-H., Li, X.-H., 2007. The golden transformation of the Cretaceous plate subduction in the west Pacific. Earth Planet. Sci. Lett. 262 (3), 533–542.
Sun, W.-D., Yang, X.-Y., Fan, W.-M., Wu, F.-Y., 2012. Mesozoic large scale magmatism and mineralization in South China: preface. Lithos 150, 1–5.
Sun, W.-H., Zhou, M.-F., Yan, D.-P., Li, J.-W., Ma, Y.-X., 2008. Provenance and tectonic setting of the Neoproterozoic Yanbian Group, western Yangtze Block (SW China). Precambr. Res. 167 (1), 213–236.
Sun, Y., Ma, C., Liu, Y., She, Z., 2011. Geochronological and geochemical constraints on the petrogenesis of late Triassic aluminous A-type granites in southeast China. J. Asian Earth Sci. 42 (6), 1117–1131.
Suzuki, K., Adachi, M., 1994. Middle Precambrian detrital monazite and zircon from the Hida gneiss on Oki-Dogo Island, Japan: their origin and implications for the correlation of basement gneiss of Southwest Japan and Korea. Tectonophysics 235 (3), 277–292.
Tang, J.X., Wang, C.H., Qu, W.J., Du, A.D., Ying, L.J., Gao, Y.M., 2009. Re–Os isotopic dating of molybdenite from the Yulong porphyry copper–molybdenum deposit in Tibet and its metallogenic significance. Rock Miner. Anal. 28 (6), 215–218.
Thompson, J.F.H., Sillitoe, R.H., Baker, T., Lang, J.R., Mortensen, J.K., 1999. Intrusion-related gold deposits associated with tungsten-tin provinces. Miner. Deposita 34 (4), 323–334.
Tian, B.-S., Yuan, B.-Y., 2008. Geological characteristics and prospecting criteria of Xianglushan tungsten deposit, northwestern Jiangxi Province. Geol. J. China Univ. 14 (1), 114–119.
Wan, Y., Liu, D., Xu, M., Zhuang, J., Song, B., Shi, Y., Du, L., 2007. SHRIMP U-Pb zircon geochronology and geochemistry of metavolcanic and metasedimentary rocks in Northwestern Fujian, Cathaysia block, China: tectonic implications and the need to redefine lithostratigraphic units. Gondwana Res. 12 (1), 166–183.
Wang, C., Luo, S., Xu, Y., Sun, Y., Xie, C., Zhang, Z., Xu, W., Ren, X., 1987. Geology of the Shizhuyuan Tungsten-Polymetallic Deposit. Geological Publishing House. 174 pp.
Wang, D.-H., Tang, J.-X., Ying, L.-J., Chen, Z.-H., Xu, J.-X., Zhang, J.-J., Li, S.-R., Zeng, Z.-L., 2010a. Application of "Five levels+ Basement" model for prospecting deposits into depth. J. Jilin Univ. (Earth Science Edition) 40 (4), 733–738.
Wang, F.-Y., Ling, M.-X., Ding, X., Hu, Y.-H., Zhou, J.-B., Yang, X.-Y., Liang, H.-Y., Fan, W.-M., Sun, W., 2011a. Mesozoic large magmatic events and mineralization in SE China: oblique subduction of the Pacific plate. Int. Geol. Rev. 53 (5–6), 704–726.
Wang, F.Y., Li, C.Y., Ling, M.X., Zhang, H., Sun, Y.L., Sun, W., 2011b. Geochronology of the Xihuashan tungsten deposit in southeastern China: constraints from Re–Os and U-Pb dating. Resour. Geol. 61 (4), 414–423.
Wang, H., Feng, C., Li, D., Xiang, X., Zhou, J., 2015. Sources of granitoids and ore-forming materials of Dahutang tungsten deposit in northern Jiangxi province: constraints from mineralogy and isotopic tracing. Acta Geol. Sinica 31 (3), 725–739.
Wang, J., Li, Z.-X., 2003. History of Neoproterozoic rift basins in South China: implications for Rodinia break-up. Precambr. Res. 122 (1), 141–158.
Wang, L., Hu, M., Yang, Z., Qu, W., Xia, J., Chen, K., 2011c. U-Pb and Re–Os geochronology and geodynamic setting of the Dabaoshan polymetallic deposit, northern Guangdong Province, South China. Ore Geol. Rev. 43 (1), 40–49.
Wang, M., Bai, X.-J., Yun, J.-B., Zhao, L.-H., Li, Y.-L., Wang, Z.-Y., Pu, Z.-P., Qiu, H.-N., 2016a. $^{40}Ar/^{39}Ar$ dating of mineralization of Shizhuyuan polymetallic deposit. Geochimica 45 (1), 41–51.
Wang, R.C., Fontan, F., Chen, X.M., Hu, H., Liu, C.S., Xu, S.J., de Parseval, P., 2003. Accessory minerals in the Xihuashan Y-enriched granitic complex, southern China: a record of magmatic and hydrothermal stages of evolution. Canad. Mineral. 41 (3), 727–748.
Wang, W., Zhou, M.-F., Yan, D.-P., Li, L., Malpas, J., 2013a. Detrital zircon record of Neoproterozoic active-margin sedimentation in the eastern Jiangnan Orogen, South China. Precambr. Res. 235, 1–19.
Wang, W., Zhou, M.-F., 2014. Provenance and tectonic setting of the Paleo-to Mesoproterozoic Dongchuan Group in the southwestern Yangtze Block, South China: implication for the breakup of the supercontinent Columbia. Tectonophysics 610, 110–127.
Wang, W., Cawood, P.A., Zhou, M.-F., Zhao, J.-H., 2016b. Paleoproterozoic magmatic and metamorphic events link Yangtze to northwest Laurentia in the Nuna supercontinent. Earth Planet. Sci. Lett. 433, 269–279.
Wang, X.-F., Qi, H.-W., Hu, R.-Z., Qu, W., Peng, J.-T., Bi, X.-W., 2010b. Re-Os isotopic chronology of molybdenites from Hongling tungsten deposit of Guangdong Province and its geological significance. Miner. Depos. 29 (3), 415–426.
Wang, X.-L., Zhao, G., Zhou, J.-C., Liu, Y., Hu, J., 2008. Geochronology and Hf isotopes of zircon from volcanic rocks of the Shuangqiaoshan Group, South China: implications for the Neoproterozoic tectonic evolution of the eastern Jiangnan orogen. Gondwana Res. 14 (3), 355–367.
Wang, X.-L., Shu, L.-S., Xing, G.-F., Zhou, J.-C., Tang, M., Shu, X.-J., Qi, L., Hu, Y.-H., 2012a. Post-orogenic extension in the eastern part of the Jiangnan orogen: evidence from ca 800–760 Ma volcanic rocks. Precambr. Res. 222, 404–423.
Wang, X.-L., Zhou, J.-C., Wan, Y.-S., Kitajima, K., Wang, D., Bonamici, C., Qiu, J.-S., Sun, T., 2013b. Magmatic evolution and crustal recycling for Neoproterozoic strongly peraluminous granitoids from southern China: Hf and O isotopes in zircon. Earth Planet. Sci. Lett. 366, 71–82.
Wang, X., Long, X., 2010. Tectonic superimposition and metallogenic tectonic evolution model of XuShan tungsten deposit, Fengcheng, Jiangxi Province. West-China Explor. Eng. 22 (12), 5.
Wang, Y.B., Liu, D., Zeng, P., Yang, Z., Tian, S., 2004. SHRIMP U-Pb geochronology of pyroxene diorite in the Chaoshan gold deposit and its geological significance. Acta Geosci. Sinica 25 (3), 423–428.
Wang, Y.J., Fan, W., Zhang, G., Zhang, Y., 2013c. Phanerozoic tectonics of the South China Block: key observations and controversies. Gondwana Res. 23 (4), 1273–1305.

Wang, Y.L., Pei, R., Li, J., Wang, H., Liu, X., 2009. Geochemical characteristics of granites from the Jiangjunzhai tungsten deposit of southeast Hunan Province and its Re-Os isotopic dating. Rock Miner. Anal. 2009 (28), 3.
Wang, Y.L., Chen, Y., Wang, D., Xu, J., Chen, Z., 2012b. Scheelite Sm-Nd dating of the Zhazixi W-Sb deposit in Hunan and its geological significance. Geol. China 39 (5), 1339–1344.
Wei, W., Hu, R., Bi, X., Peng, J., Su, W., Song, S., Shi, S., 2012. Infrared microthermometric and stable isotopic study of fluid inclusions in wolframite at the Xihuashan tungsten deposit, Jiangxi province, China. Mineral. Depos. 47 (6), 589–605.
Wong, J., Sun, M., Xing, G., Li, X.-H., Zhao, G., Wong, K., Yuan, C., Xia, X., Li, L., Wu, F., 2009. Geochemical and zircon U-Pb and Hf isotopic study of the Baijuhuajian metaluminous A-type granite: extension at 125–100 Ma and its tectonic significance for South China. Lithos 112 (3), 289–305.
Wu, J., Liang, H., Huang, W., Wang, C., Sun, W., Sun, Y., Li, J., Mo, J., Wang, X., 2012. Indosinian isotope ages of plutons and deposits in southwestern Miaoershan-Yuechengling, northeastern Guangxi and implications on Indosinian mineralization in South China. Chin. Sci. Bull. 57 (9), 1024–1035.
Wu, L.-Y., Hu, R.-Z., Peng, J.-T., Bi, X.-W., Jiang, G.-H., Chen, H.-W., Wang, Q.-Y., Liu, Y.-Y., 2011. He and Ar isotopic compositions and genetic implications for the giant Shizhuyuan W-Sn–Bi–Mo deposit, Hunan Province, South China. Int. Geol. Rev. 53 (5–6), 677–690.
Wu, Q., Cao, J., Kong, H., Shao, Y., Li, H., Xi, X., Deng, X., 2016. Petrogenesis and tectonic setting of the early Mesozoic Xitian granitic pluton in the middle Qin-Hang Belt, South China: Constraints from zircon U-Pb ages and bulk-rock trace element and Sr–Nd–Pb isotopic compositions. J. Asian Earth Sci. 128, 130–148.
Wu, S.H., Wang, X.D., Xiong, B.K., 2014. Fluid inclusion studies of the Xianglushan skarn tungsten deposit, Jiangxi Province, China. Acta Petrol. Sinica 30 (1), 178–188.
Wu, Y., Mei, Y.W., 1982. Multi-Phase Intrusion and Multi-Phase Mineralization in Xihuashan Tungsten Ore Field, Tungsten Geology Symposium, Jiangxi, China. ESCAP-RMRDC, Bandung, pp. 437–449.
Wu, Y.L., Mei, Y.W., Liu, P.C., Cai, C.L., Lu, T.Y., 1987. Geology of the Xihuashan Tungsten Ore Field. Geological Publishing House, Beijing, p. 317.
Xia, Y., Xu, X.-S., Zhu, K.-Y., 2012. Paleoproterozoic S-and A-type granites in southwestern Zhejiang: magmatism, metamorphism and implications for the crustal evolution of the Cathaysia basement. Precambr. Res. 216, 177–207.
Xiang, X., Chen, M., Zhan, G., Qian, Z., Li, H., Xu, J., 2013a. Metallogenic geological conditions of Shimensi tungsten-polymetallic deposit in north Jiangxi province. Contribut. Geol. Miner. Resour. Res. 27 (2), 143–155.
Xiang, X., Wang, P., Zhan, G., Sun, D., Zhong, B., Qian, Z., 2013b. Geological characteristics of Shimensi tungsten polymetallic deposit in northern Jiangxi province. Miner. Depos. 32 (6), 1171–1187.
Xiao, J., Wang, Y., Hong, Y., Zhou, Y., Xie, M., Wang, D., Guo, J., 2009. Geochemistry characteristics of Xihuashan tungsten granite and its relationship to tungsten metallogenesis. J. East China Shipbuild. Inst. Natur. Sci. Ed. 32, 22–31.
Xiao, R., Li, X., Feng, Z., Yang, F., Song, C., 2011. ^{40}Ar-^{39}Ar dating of muscovite from tungsten-quartz vein in Shanhu tungsten-tin deposit and its geological significance. Miner. Depos. 30 (3), 488–496.
Xie, G.Q., Mao, J.W., Li, R.L., Qu, W.J., Pirajno, F., Du, A.D., 2007. Re-Os molybdenite and Ar-Ar phlogopite dating of Cu-Fe-Au-Mo (W) deposits in southeastern Hubei, China. Mineral. Petrol. 90 (3–4), 249–270.
Xiong, X., Xu, W., Wen, C., 2015. Fluid characteristics and genesis of Xianglushan skam scheelite deposit in Xiushui, Jiangxi province. Miner. Depos. 34 (5), 1046–1056.
Xu, D.R., Ma, C., Li, P.C., Xia, B., Zhang, Y.Q., 2007. U-Pb SHRIMP-dating of zircon domains from metaclastic sedimentary rocks in Hainan Island, South China, and its geological significance. Acta Geol. Sinica 81 (3), 381–393.
Xu, J.-X., Zeng, Z.-L., Wang, D.-H., Chen, Z., Liu, S., Wang, C., Ying, L., 2008. A new type of tungsten deposit in Southern Jiangxi and the new model of "Five Floors+ Basement" for prospecting. Acta Geol. Sinica 82 (7), 880–887.
Xu, K.Q., Hu, S.X., Sun, M.Z., Ye, J., 1982. On the two genetic series of granites in south eastern China and their metallogenetic characteristics. Miner. Depos. 1 (2), 1–14.
Xu, X.S., Fan, Q.C., O'Reilly, S.Y., Jiang, S.Y., Griffin, W.L., Wang, R.C., Qiu, J.S., 2004. U-Pb dating of zircons from quartz diorite and its enclaves at Tongguanshan in Anhui and its petrogenetic implication. Chin. Sci. Bull. 49, 1883–1891.
Xu, Z., 1985. Genesis of Mesozoic volcanic rocks in eastern China as disscussed in the light of the characteristics of the structural stress field. Acta Geol. Sinica 2.
Yan, C., Shu, L., Santosh, M., Yao, J., Li, J., Li, C., 2015. The Precambrian tectonic evolution of the western Jiangnan Orogen and western Cathaysia Block: evidence from detrital zircon age spectra and geochemistry of clastic rocks. Precambr. Res. 268, 33–60.
Yan, D.P., Zhou, M.F., Song, H.L., Wang, X.W., Malpas, J., 2003. Origin and tectonic significance of a Mesozoic multi-layer over-thrust system within the Yangtze Block (South China). Tectonophysics 361 (3–4), 239–254.
Yang, F., Li, X., Feng, Z., Bai, Y., 2009. ^{40}Ar/^{39}Ar dating of muscovite from geisenized granite and geological significance in Limu tin deposit. J. Guilin Univ. Technol. 29 (1), 21–24.
Yang, G., Ge, L., Lu, Y., Zou, Y., Xing, J., Zhang, F., Yuan, S., 2014. Re-Os isotopic dating of molybdenite from the Matou iindgrenite deposit from Chizhou area in the south of Anhui province and its geological implications. J. Mineral. Petrol. 34 (1), 30–35.
Yang, J., Peng, J., Zhao, J., Fu, Y., Yang, C., Hong, Y., 2012. Petrogenesis of the Xihuashan granite in southern Jiangxi Province, South China: constraints from zircon U-Pb geochronology, geochemistry and Nd isotopes. Acta Geol. Sinica 86 (1), 131–152.
Yang, S.-Y., Jiang, S.-Y., Zhao, K.-D., Jiang, Y.-H., 2013. Petrogenesis and tectonic significance of Early Cretaceous high-Zr rhyolite in the Dazhou uranium district, Gan-Hang Belt, Southeast China. J. Asian Earth Sci. 74, 303–315.
Yao, J.M., Hua, R.M., Qu, W.J., Qi, H.W., Lin, J.F., Du, A.D., 2007. Re-Os isotope dating of molybdenites in the Huangshaping Pb-Zn-W-Mo polymetallic deposit, Hunan Province, South China and its geological significance. Sci. China, Ser. D Earth Sci. 50 (4), 519–526.
Yao, J.M., Mathur, R., Sun, W.D., Song, W., Chen, H.Y., Mutti, L., Xiang, X.K., Luo, X.H., 2016. Fractionation of Cu and Mo isotopes caused by vapor-liquid partitioning, evidence from the Dahutang W-Cu-Mo ore field. Geochem. Geophys. Geosyst. 17 (5), 1725–1739.
Yin, C., Lin, S., Davis, D.W., Zhao, G., Xiao, W., Li, L., He, Y., 2013. 2.1–1.85 Ga tectonic events in the Yangtze Block, South China: petrological and geochronological evidence from the Kongling Complex and implications for the reconstruction of supercontinent Columbia. Lithos 182, 200–210.
Yin, J., Kim, S.J., Lee, H.K., Itay, T., 2002. K-Ar ages of plutonism and mineralization at the Shizhuyuan W–Sn–Bi–Mo deposit, Hunan Province, China. J. Asian Earth Sci. 20 (2), 151–155.
Yin, J.W., Lee, H.K., Chio, K.K., Kim, S.J., 2000. Characteristics of garnet in Shizhuyuan skarn deposit, Hunan province. Earth Sci. – J. China Univ. Geosci. 25 (2), 163–171.
Yong, W.J., 1963. Geology and origin of Sangdong tungsten mine, Republic of Korea. Econ. Geol. 58 (8), 1285–1300.
Yu, J.H., Wang, L., O'reilly, S.Y., Griffin, W.L., Zhang, M., Li, C., Shu, L., 2009. A Paleoproterozoic orogeny recorded in a long-lived cratonic remnant (Wuyishan terrane), eastern Cathaysia Block, China. Precambr. Res. 174 (3), 347–363.
Yu, J.H., O'Reilly, S.Y., Zhou, M.F., Griffin, W.L., Wang, L.J., 2012a. U-Pb geochronology and Hf-Nd isotopic geochemistry of the Badu Complex, Southeastern China: implications for the Precambrian crustal evolution and paleogeography of the Cathaysia Block. Precambr. Res. 222, 424–449.
Yu, Z., Mao, J., Zhao, H., Chen, M., Luo, D., Guo, M., 2012b. Geological characteristics and ages of granites and related mineralization in the Dajinshan tungsten-tin polymetallic deposit, western Guangdong Province. Acta Geol. Sinica 28 (12), 3967–3979.
Yuan, S., Peng, J., Shen, N., Hu, R., Dai, Y., 2007. ^{40}Ar-^{39}Ar Isotopic Dating of the Xianghualing Sn-polymetallic Orefield in Southern Hunan, China and Its Geological Implications. Acta Geol. Sinica (English Edition) 81 (2), 278–286.
Yuan, S., Zhang, D., Shuang, Y., Du, A., Qu, W., 2012. Re-Os dating of molybdenite from the Xintianling giant tungsten-molybdenum deposit in southern Hunan Province, China and its geological implications. Acta Geol. Sinica 28 (1), 27–38.
Zaw, K., Peters, S.G., Cromie, P., Burrett, C., Hou, Z., 2007. Nature, diversity of deposit types and metallogenic relations of South China. Ore Geol. Rev. 31 (1), 3–47.
Zeng, Y., Zhu, Y., Liu, J., 2001. Carbonaceous material in S-type Xihuashan granite. Geochem. J. 35 (3), 145–153.
Zeng, Z., Zhang, Y., Zhu, X., Chen, Z., Wang, C., Qu, W., 2009. Re-Os isotopic dating of molybdenite from the Maoping tungsten-tin deposit in Chongyi County of Southern Jiangxi Province and its geological significance. Rock Miner. Anal. 28 (3), 209–214.
Zeng, Z., Zhang, Y., Chen, Z., Chen, Y., Zhu, X., Tong, Q., Zheng, B., Zhou, Y., 2011. Geological characteristics and metallogenic epoch of Pangushan W-Bi-(Te) ore deposit in Yudu County, Jiangxi Province. Miner. Depos. 30 (5), 949–958.
Zhang, D., Wu, G.-G., Wiu, J., Chen, X., 2003. Re-Os ages of the Zhongjia tin polymetallic deposit, southwestern Fujian, and their geological significance. J. Geomech. 9 (3), 261–267.
Zhang, J., 1983. Geochemical features of granites at Xingluokeng. Fujian Geol. 3, 33–45.
Zhang, J.J., Chen, Z., Wang, D., Chen, Z., Liu, S., Wang, C., 2008a. Geological characteristics and metallogenic epoch of the Xingluokeng tungsten deposit, Fujian province. Geotectonica et Metallogenia 32 (1), 92–97.
Zhang, J.J., Mei, Y.P., Wang, D.H., Li, H.Q., 2008b. Isochronology study on the Xianglushan scheelite deposit in North Jiangxi Province and its geological significance. Acta Geol. Sinica 82, 927–931.
Zhang, S.-B., Zheng, Y.-F., Wu, Y.-B., Zhao, Z.-F., Gao, S., Wu, F.-Y., 2006a. Zircon U-Pb age and Hf isotope evidence for 3.8 Ga crustal remnant and episodic reworking of Archean crust in South China. Earth Planet. Sci. Lett. 252 (1), 56–71.
Zhang, S.-B., Wu, R.-X., Zheng, Y.-F., 2012. Neoproterozoic continental accretion in South China: geochemical evidence from the Fuchuan ophiolite in the Jiangnan orogen. Precambr. Res. 220, 45–64.
Zhang, W., Hua, R., Wang, R., Chen, P., Li, H., 2006b. New dating of the Dajishan granite and related tungsten mineralization in southern Jiangxi. Acta Geol. Sinica 80 (7), 956–962.
Zhang, W., Hua, R., Wang, R., Li, H., Qu, W., Ji, J., 2009. New dating of the Piaotang granite and related tungsten mineralization in southern Jiangxi. Acta Geol. Sinica 83 (5), 659–670.
Zhang, Y., Liu, Y., 1993. Geological-geochemical characteristics and origin of the Xingluokeng W deposit. Geochemica (2), 10.
Zhang, Z., Mao, J., Yang, J., Wang, Z., Zhang, Z., 2002. Geology and genesis of Ta'ergou skarn-quartz vein type tungsten deposit in North Qilian Caledonian Orogen, Northwest China. Miner. Depos. 21 (2), 200–211.
Zhao, G., 2015. Jiangnan Orogen in South China: developing from divergent double subduction. Gondwana Res. 27 (3), 1173–1180.
Zhao, J.-H., Zhou, M.-F., Yan, D.-P., Zheng, J.-P., Li, J.-W., 2011. Reappraisal of the ages of Neoproterozoic strata in South China: No connection with the Grenvillian orogeny. Geology 39 (4), 299–302.

Zhao, J.-H., Zhou, M.-F., Zheng, J.-P., 2013. Constraints from zircon U-Pb ages, O and Hf isotopic compositions on the origin of Neoproterozoic peraluminous granitoids from the Jiangnan Fold Belt, South China. Contrib. Miner. Petrol. 166 (5), 1505–1519.

Zhao, L., Zhou, X., Zhai, M., Santosh, M., Geng, Y., 2015a. Zircon U-Th–Pb–Hf isotopes of the basement rocks in northeastern Cathaysia block, South China: implications for Phanerozoic multiple metamorphic reworking of a Paleoproterozoic terrane. Gondwana Res. 28 (1), 246–261.

Zhao, W.W., Zhou, M.-F., 2015. In-situ LA–ICP-MS trace elemental analyses of magnetite: the Mesozoic Tengtie skarn Fe deposit in the Nanling Range, South China. Ore Geol. Rev. 65, 872–883.

Zhao, X.-F., Zhou, M.-F., Li, J.-W., Sun, M., Gao, J.-F., Sun, W.-H., Yang, J.-H., 2010. Late Paleoproterozoic to early Mesoproterozoic Dongchuan Group in Yunnan, SW China: implications for tectonic evolution of the Yangtze Block. Precambr. Res. 182 (1), 57–69.

Zhao, Z.-F., Gao, P., Zheng, Y.-F., 2015b. The source of Mesozoic granitoids in South China: Integrated geochemical constraints from the Taoshan batholith in the Nanling Range. Chem. Geol. 395, 11–26.

Zheng, Y.F., Wu, R.X., Wu, Y.B., Zhang, S.B., Yuan, H.L., Wu, F.Y., 2008. Rift melting of juvenile arc-derived crust: Geochemical evidence from Neoproterozoic volcanic and granitic rocks in the Jiangnan Orogen, South China. Precambr. Res. 163 (3–4), 351–383.

Zhong, Y.-F., Ma, C.-Q., She, Z.-B., Lin, G.-C., Xu, H., Wang, R.-J., Yang, K.-G., Liu, Q., 2005. SHRIMP U-Pb zircon geochronology of the Jiuling granitic complex batholith in Jiangxi Province. Earth Sci. 30 (6), 685–691.

Zhou, M.-F., Yan, D.-P., Kennedy, A.K., Li, Y.-Q., Ding, J., 2002. SHRIMP U-Pb zircon geochronological and geochemical evidence for Neoproterozoic arc-magmatism along the western margin of the Yangtze Block, South China. Earth Planet. Sci. Lett. 196 (1–2), 51–67.

Zhou, M.-F., Zhao, X.-F., Chen, W.T., Li, X.-C., Wang, W., Yan, D.-P., Qiu, H.-N., 2014. Proterozoic Fe–Cu metallogeny and supercontinental cycles of the southwestern Yangtze Block, southern China and northern Vietnam. Earth Sci. Rev. 139, 59–82.

Zhou, T., Fan, Y., Yuan, F., Song, C., Zhang, L., Qian, C., Lu, S., Cooke, D.R., 2010. Temporal–spatial framework of magmatic intrusions in Luzong volcanic basin in East China and their constrain to mineralization. Acta Geol. Sinica 26, 2694–2714.

Zhou, T., Wang, S., Fan, Y., Yuan, F., Zhang, D., White, N.C., 2015. A review of the intracontinental porphyry deposits in the Middle-Lower Yangtze River Valley metallogenic belt, Eastern China. Ore Geol. Rev. 65, 433–456.

Zhou, X., Yu, X., Wang, D., Zhang, D., Li, C., Fu, J., Dong, H., 2011. Characteristics and geochronology of the W, Mo-bearing granodiorite porphyry in Dongyuan, southern Anhui. Geoscience 25 (2), 201–210.

Zhou, X.M., Li, W.X., 2000. Origin of Late Mesozoic igneous rocks in Southeastern China: implications for lithosphere subduction and underplating of mafic magmas. Tectonophysics 326 (3), 269–287.

Zhou, X.M., Sun, T., Shen, W.Z., Shu, L.S., Niu, Y.L., 2006. Petrogenesis of Mesozoic granitoids and volcanic rocks in South China: a response to tectonic evolution. Episodes 29 (1), 26–33.

Zhu, J.C., Li, R.K., Li, F.C., Xiong, X.L., Zhou, F.Y., Huang, X.L., 2001. Topaz–albite granites and rare-metal mineralization in the Limu district, Guangxi Province, southeast China. Miner. Depos. 36 (5), 393–405.

Zhu, J.C., Zhang, H., Xie, C.F., Zhang, P.H., Yang, C., 2005. Zircon SHRIMP U-Pb geochronology, petrology and geochemistry of the Zhujianshui granite, Qitianling pluton, southern Hunan Province. Geol. J. China Univ. 11 (3), 335–342.

Zhu, R., Yang, Z., Wu, H., Ma, X., Huang, B., Meng, Z., Fang, D., 1998. Paleomagnetic constraints on the tectonic history of the major blocks of China duing the Phanerozoic. Sci. China, Ser. D Earth Sci. 41 (2), 1–19.

Zou, X., Cui, S., Qu, W., Bai, Y., Chen, X., 2009. Re-Os isotope dating of the Liguifu tungsten-tin polymetallic deposit in Dupangling area, Guangxi. Geol. China 36 (4), 837–844.